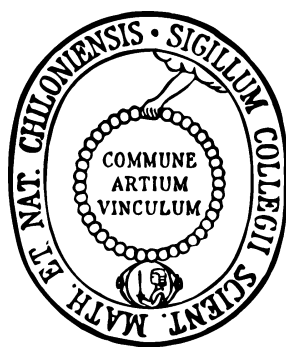


Molecular Characterisation of Antimicrobial Arsenal of *Dictyostelium discoideum*



Dissertation

Submitted for the Degree of
Doctor of Philosophy
Faculty of Mathematics and Natural Sciences
Christian-Albrechts University of Kiel

by

Ranjani Dhakshinamoorthy

from Kiel

Kiel, October 2012

Referee:

Prof. Dr. Matthias Leippe

Coreferee:

Prof. Dr. Eric Beitz

Date of the oral exam:

12. 12. 2012

Approved for printing:

12. 12. 2012

Prof. Dr. Wolfgang J. Duschl

The Dean

TABLE OF CONTENTS

TABLE OF CONTENTS.....	I
ABBREVIATIONS.....	VI
1 INTRODUCTION.....	1
1.1 Immune system.....	1
1.1.1 Cell surface PRRs.....	3
1.1.1.1 Plants and invertebrates.....	3
1.1.1.2 Vertebrates.....	3
1.1.2 Intracellular PRRs.....	4
1.1.2.1 Plants and invertebrates.....	4
1.1.2.2 Vertebrates.....	4
1.1.3 Other PRRs.....	5
1.2 Antimicrobial peptides (AMPs).....	5
1.2.1 Mode of actions.....	6
1.2.1.1 Transmembrane-pore formation.....	6
1.2.1.2 Intracellular killing.....	8
1.2.2 AMPs, the future antibiotics.....	8
1.3 <i>E. histolytica</i> : a model to study functions of AMPs.....	9
1.3.1 Amoebapores, the antimicrobial armament of <i>E. histolytica</i>	10
1.3.2 Structure of amoebapores.....	10
1.3.3 Functions of SAPLIPs.....	11
1.3.4 Mode of actions of SAPLIPs.....	12
1.4 Need for a versatile host model.....	13
1.4.1 Life cycle of <i>D. discoideum</i>	14
1.4.2 Evolution of <i>D. discoideum</i>	17
1.4.3 Immune effector proteins of <i>D. discoideum</i>	18
1.4.3.1 Amoebapore-like peptides of <i>D. discoideum</i>	18
1.4.3.2 Lysozymes.....	19
1.4.4 <i>D. discoideum</i> as a model organism.....	20
1.5 Objectives.....	22

2	MATERIALS.....	23
2.1	Chemicals.....	23
2.2	Protein marker.....	25
2.3	DNA ladder.....	25
2.4	Dyes and substrates.....	25
2.5	Antibodies.....	25
2.5.1	Primary antibodies.....	25
2.5.2	Secondary antibodies.....	26
2.6	Enzymes.....	26
2.7	Media.....	26
2.8	Microscope.....	27
2.9	Oligonucleotides.....	28
2.9.1	PCR primers for the gene targeting vector.....	28
2.9.2	PCR primers for screening the knock-out clones.....	29
2.9.3	Quantitative real-time PCR (qRT-PCR) primers.....	30
2.9.4	PCR primers for ApID-FLAG intracellular localisation.....	31
2.9.5	PCR primers for <i>apID</i> expression under <i>apID</i> promoter.....	31
2.9.6	PCR primers for <i>apID</i> expression under <i>act15</i> promoter.....	31
2.9.7	pDrive and TOPO vector primers for PCR and DNA sequencing.....	31
2.10	Instruments.....	31
2.10.1	Incubators/ Shakers.....	32
2.10.2	Centrifuges.....	33
2.10.3	Sterile air flow units.....	33
2.11	Accessories.....	33
3	METHODS.....	34
3.1	<i>D. discoideum</i> cultures.....	34
3.2	<i>D. discoideum</i> cell stock and culture preparation.....	34
3.3	<i>D. discoideum</i> spore stock preparation and reviving spore stocks.....	35
3.4	Bacterial stocks preparation and reviving frozen stocks.....	35
3.5	<i>D. discoideum</i> genomic DNA isolation.....	35

3.6	DNA manipulation reactions.....	37
3.6.1	Amplification of DNA fragments by polymerase chain reaction (PCR).....	37
3.6.2	PCR product purification.....	38
3.6.3	Small scale plasmid DNA isolation.....	38
3.6.4	Large scale plasmid DNA isolation.....	39
3.6.5	Restriction endonuclease digestions.....	39
3.6.6	Agarose gel electrophoresis.....	40
3.6.7	DNA extraction from agarose gels.....	40
3.7	DNA ligation.....	40
3.8	Bacterial transformation.....	41
3.8.1	Chemical competent cells preparation with <i>E. coli</i> DH5 α	41
3.8.2	Transformation.....	42
3.9	Colony PCR.....	42
3.10	DNA sequencing.....	42
3.11	Bioinformatics.....	43
3.12	Analytical tools.....	43
3.13	<i>D. discoideum</i> transfection.....	43
3.14	Gene targeting vector or KO vector construction.....	44
3.15	KO vector transfection.....	44
3.16	<i>D. discoideum</i> genomic DNA isolation.....	45
3.16.1	Method-I.....	45
3.16.2	Method-II.....	45
3.17	RNA isolation.....	46
3.18	First strand cDNA synthesis.....	46
3.19	Cell lysate preparation for western blotting.....	47
3.20	SDS-polyacrylamide gel electrophoresis (SDS-PAGE).....	47
3.21	Western blotting.....	48
3.22	Growth assays using 24-well plates.....	49
3.23	Phagocytosis and killing of <i>B. subtilis</i> (ATCC# 6051) and KpLM21.....	52
3.24	Analyses of <i>apID</i> ⁻ development.....	53
3.25	Spore formation efficiency (sfe).....	53

3.26	Spore viability assay.....	54
3.27	Pre-stalk and pre-spore patterns in <i>apID</i> ⁻ slugs.....	54
3.28	ApID expression analysis by qRT-PCR.....	56
3.28.1	ApID expression analysis in axenic <i>D. discoideum</i> cells.....	56
3.28.2	ApID expression during Ax2 development.....	57
3.28.3	ApID expression in xenic Ax2 cells.....	57
3.28.4	ApID expression in pre-stalk and pre-spore regions of Ax2 slugs.....	58
3.29	Examinaion of sentinel (S) cells in <i>apID</i> ⁻ slugs.....	58
3.30	<i>D. discoideum</i> slugs infection with bacteria.....	59
3.31	Immunofluorescence microscopy.....	59
4	RESULTS.....	62
4.1	Genes of interest.....	62
4.2	ApID gene ablation.....	63
4.3	Identification of <i>apID</i> ⁻ by PCR analyses.....	64
4.4	<i>ApID</i> ⁻ growth analyses on KpLM21 and <i>K</i> ⁻	66
4.5	Two-dimentional virulence array.....	68
4.6	<i>ApID</i> ⁻ plaques on KpLM21 and <i>K</i> ⁻	69
4.7	Colony morphologies of avirulent and virulent <i>K. pneumoniae</i> strains.....	70
4.8	Phagocytosis and killing assays.....	71
4.9	ApID expression in axenic <i>D. discoideum</i> cultures.....	73
4.10	ApID expression during Ax2 development.....	74
4.11	ApID regulation in xenic Ax2 cultures.....	75
4.12	<i>ApID</i> ⁻ development on non-nutrient agar plates.....	76
4.13	Pre-stalk and pre-spore slug patterns in <i>apID</i> ⁻	77
4.14	Spore viability and spore formation efficiency (sfe).....	78
4.15	Examination of sentinel (S) cells in <i>apID</i> ⁻	79
4.16	<i>D. discoideum</i> slugs infection with <i>K. pneumoniae</i>	80
4.17	KpGFP clumps in <i>D. discoideum</i> slugs.....	81
4.18	<i>D. discoideum</i> slugs infection with <i>E. coli</i> DsRed.....	82
4.19	Western blot analysis of ApID-FLAG protein.....	83

4.20	Development experiment with rescue strain [<i>aplD</i> ⁻ (+)].....	84
5	DISCUSSION.....	86
6.A	SUMMARY.....	102
6.B	ZUSAMMENFASSUNG.....	104
7	REFERENCES.....	107
8	APPENDIX.....	121
	8.1 Identification of KO clones by PCR.....	121
	8.2 Intracellular localisation of AplD-FLAG fusion protein.....	124
	DECLARATION.....	127
	ACKNOWLEDGEMENTS.....	128
	BIODATA.....	130

ABBREVIATIONS

Amp	Ampicillin
AP	Alkaline Phosphatase
apls	<u>a</u> moebap <u>o</u> re <u>l</u> ike peptide coding genes
Apls	<u>A</u> moebap <u>o</u> re <u>l</u> ike peptides
APS	Ammonium persulfate
ATCC	American Type Culture Collection
BCIP	5-Bromo-4-chloro-3-indolyl-phosphate
BLAST	Basic Local Alignment Search Tool
bp	Base pairs
BPB	Bromophenol blue
BSA	Bovine Serum Albumin
cDNA	Complementary DNA
CFU	Colony Forming Unit(s)
CHAPS	3-[(3-cholamidopropyl)-dimethylammonio]-1-propanesulfonate
cm	Centimetre
Ct	Cycle threshold
°C	Degree Celsius
dH ₂ O	Deionised water
DMSO	Dimethyl sulfoxide
DNA	Deoxyribonucleic acid
dNTP	Deoxyribonucleotide triphosphate
DTT	Dithiothreitol
∅	Diameter
EDTA	Ethylenediaminetetraacetic acid
EST	Expressed Sequence Tag
EtBr	Ethidium Bromide
EtOH	Ethanol
g	Gram
G	Gauge
GFP	Green Fluorescence Protein

x g	g-force = Relative Centrifugal Force (RCF)
>	Greater than
h	Hour
H+L	Heavy chain + Light chain
HRP	Horseradish peroxidase
I	Insert
Ig	Immunoglobulin
IPTG	Isopropyl- β -D-thiogalactopyranoside
kDa	Kilodalton
kg	Kilogram
KK2	Potassium di-hydrogen phosphate and Dipotassium phosphate buffer
KO	Knock-out
kV	Kilovolt
L	Litre
LB	Luria-Bertani
<	Less than
M	Molar
mA	Milliampere
MeOH	Methanol
μ F	Microfarad
mg	Milligram
μ g	Microgram
min	Minute
ml	Millilitre
mm	Millimetre
mM	Millimolar
ms	Millisecond
μ l	Microlitre
μ m	Micrometre
μ M	Micromolar
N	Normal
NBT	Nitro blue tetrazolium chloride
ng	Nanogram

NIH	National Institutes of Health
nm	Nanometre
#	Number
OD ₆₀₀	Optical Density at 600 nm
PAGE	Polyacrylamide-gel electrophoresis
PBS	Phosphate-Buffered Saline
PCR	Polymerase Chain Reaction
PVDF	Polyvinylidene fluoride
%	Percentage
qRT-PCR	Quantitative real-time PCR
RFP	Red fluorescence protein
RNA	Ribonucleic acid
rpm	Revolutions per minute
RT	Room temperature
SAPLIP	<u>S</u> ap <u>o</u> sin- <u>l</u> i <u>k</u> e <u>p</u> ro <u>t</u> ein
SB	Sørensen's buffer
SDS	Sodium Dodecyl Sulfate
s	Second
Sfe	Spore formation efficiency
SM	Standard Medium
SOC	Salt-Optimised Broth + carbon
Tab	Table
TAE	Tris-Acetate-EDTA
TBS	Tris-Buffered Saline
TBST	Tris-Buffered Saline + Tween 20
TE	Tris-EDTA
TEMED	N,N,N',N'-Tetramethylethylenediamine
TfB	Transformation buffer
U	Units
UV	Ultraviolet
V	Vector
v/v	Volume to volume
w/v	Weight per volume
X-Gal	5-Bromo-4-chloro-3-indolyl- β -D-galactopyranoside

1 Introduction

1.1 Immune system

All living organisms need a protection mechanism to protect themselves from foreign invaders. In higher organisms, such as vertebrates these protective functions are governed by innate and acquired immune systems.

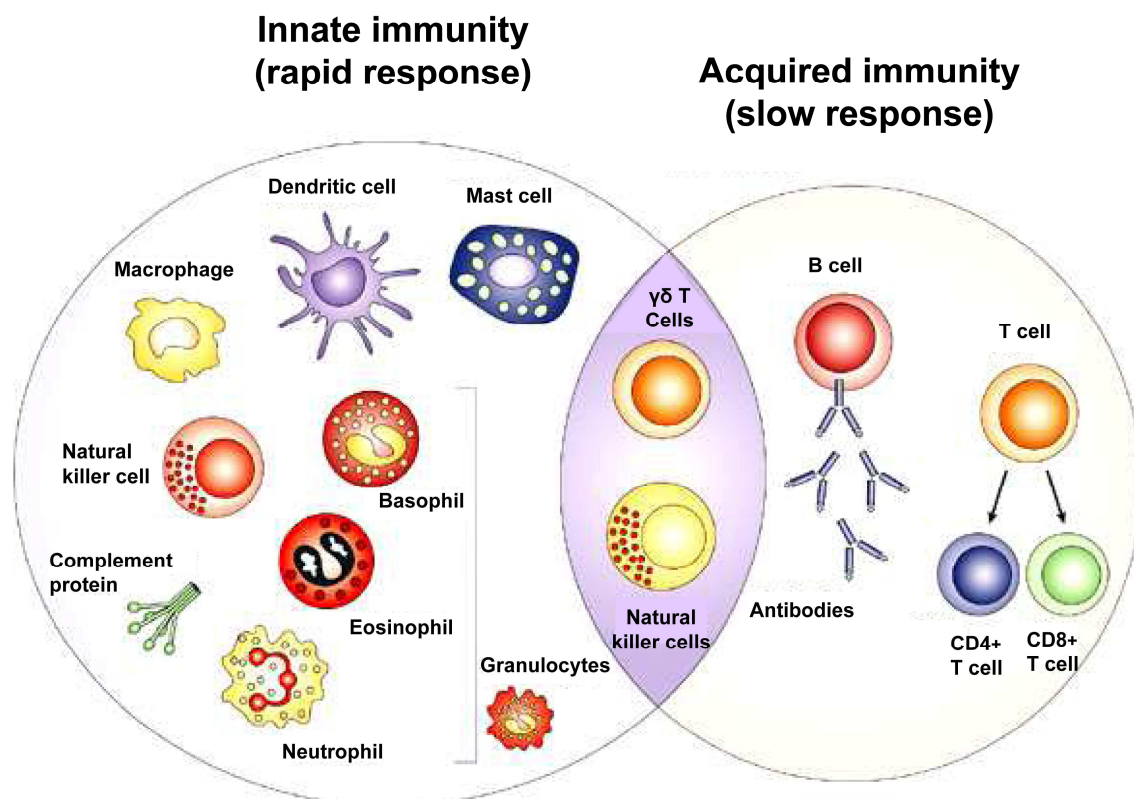


Fig. 1: Effector cells and effector molecules of innate and acquired immune system are represented. Innate immune system includes macrophages, dendritic cells, mast cells, granulocytes, and natural killer cells and their corresponding effector molecules comprise soluble factors such as complement proteins, antimicrobial peptides etc. Adaptive immune system constitutes T cells that activate phagocytes and natural killer cells and B cells, which produce antigen specific antibodies. The natural killer T cells and $\gamma\delta$ T cells remain as a part of both innate and acquired immunity (Dranoff, 2004).

In lower organisms, such as invertebrates the immune functions are fulfilled by the innate immune system, whereas vertebrates benefit from both, innate and acquired immunity (**Fig. 1**). The innate and acquired immune systems have their own advantages and disadvantages (**Tab. 1**). In every organism, innate immune

system serves as a primary defense mechanism against the foreign invaders or its pathogenic materials.

Tab 1:

Properties	Innate immunity	Acquired immunity
Time line	Ancient, evolved before the split of plant and animal kingdoms	Recent, present only in vertebrates.
Receptors	Limited and germline encoded	Gene encoded and clonal
Pathogen recognition	Non-specific, involves recognition of molecular structures and metabolic products for self, non-self discrimination (e.g. LPS, mannans, glycans etc.)	Recognise specific structures (e.g. peptides, proteins and carbohydrates). Is responsible for allergy, autoimmunity and graft rejections
Accomplishment	Very rapid in action, but retains no memory of the past infections	Slow, but retains the memory of the pathogen and the adaptor proteins used to remove pathogen
Effector cells	Non-clonal, includes macrophages, dendritic cells, mast cells, neutrophils, basophils, eosinophils and Natural killer cells	Clonal, T and B lymphocytes
Effector molecules	Respond by producing costimulatory molecules, such as cytokines, chemokines and antimicrobial peptides	Interleukins, antibodies and effector cytokines

The innate immune system is mediated by a limited number of germline encoded receptors, called the **pattern recognition receptors (PRRs)**. The PRRs recognise highly conserved structures, e.g., Lipopolysaccharides (LPS) of the bacterial cell wall or the biological materials released as a consequence of infection, e.g., uric acid, calcium efflux etc. (Janeway and Medzhitov 2002); (Thompson and Locarnini 2007); (Turvey and Broide 2010). The principle function of PRRs constitute opsonisation, induction of complements and coagulation cascades, phagocytosis, activation of proinflammatory signaling pathways, and activation of apoptosis pathway (Janeway and Medzhitov 2002). In general, the structures and the biological materials recognised by PRRs are called as **pathogen associated molecular patterns (PAMPs)**. The PRRs are classified into three groups, which include the cell surface receptors, e.g. Toll-like receptors (TLRs), the intracellular receptors, e.g. NOD-like receptors (NLRs), and the secretory receptors, which are present in the blood stream and body fluids, e.g., TLR5, Mannan-binding proteins (MBPs) (Medzhitov and Janeway 1997).

1.1.1 Cell surface PRRs

1.1.1.1 Plants and invertebrates

At first, *Drosophila* Toll was reported to be crucial for the dorso-ventral axis formation during embryogenesis (Belvin 1996; Hashimoto *et al.* 1988). *Drosophila* genome harbours eight Toll homologs. Later it was found that Toll is necessary for the flies to protect themselves from fungal infections (Lemaitre *et al.* 1996). The Toll receptor has an extracellular LRR-containing domain, a transmembrane region, and a cytosolic domain, which is homologous to human interleukin-1-receptor and therefore, called as Toll/interleukin-1-receptor (TIR) domain. Subsequently, any receptors with this TIR domain are called Toll-like receptors (TLRs). Additionally, both receptors induce the downstream effector genes through the transcription factor nuclear factor-kappa B (NF- κ B).

The analyses of promoter sequence of the genes encoding for antimicrobial peptides showed sequence specific for NF- κ B binding (Engström *et al.*, 1993.). The loss of function *Drosophila* mutant for the Toll receptor was highly susceptible to fungal infections, but not infected by Gram-negative bacteria. Toll pathway mediated stimulation of immune response in *Drosophila melanogaster* leads to production of antimicrobial peptides, mainly in the fat body. These antimicrobial peptides are pore-forming in function. In *Drosophila*, these antimicrobial peptides are classified into three types depending on the microbial targets. *Drosomycin* is antifungal peptide, dipterin is antibacterial towards Gram-negative bacteria and defensin is specific for Gram-positive bacteria (Hoffmann *et al.*, 1999). The mosquito *Anopheles gambiae* genome consists of ten Toll homologues. In plants, for example, the nucleotide-binding site (NBS)-LRR proteins, some of which possess the N-terminal TIR domain are involved in disease resistance functions towards viruses, bacteria, fungi, nematodes and insects (Nürnberg *et al.* 2004). In rice, *Oryza sativa* and *Arabidopsis thaliana* genome ~1% of the genome comprises these NBS-LRR genes.

1.1.1.2 Vertebrates

In vertebrates, TLRs can be classified into six major groups and each member recognises distinct PAMPs. The TLR2 family members recognise lipopeptides, TLR3 recognises double stranded RNA, TLR4 binds LPS, TLR5 binds flagellin, members of subfamilies TLR7, 8 and 9 bind nucleic acids and heme motifs, and the TLR1 family members form heterodimers with TLR2 (Thompson and

Locarnini 2007). In *Danio rerio*, there are at least 17 predicted TLRs. In humans, it has been proven that single nucleotide polymorphisms (SNPs) in the Toll gene affect cellular signaling, cytokine production and resistance to microbial infections (Hawn et al. 2003). For instance, SNP in the ligand binding domain of TLR5 affects flagellin signaling resulting in high susceptibility of the patient towards flagellated bacterium, *Legionella pneumophila*, which causes the Legionnaires disease.

1.1.2 Intracellular PRRs

1.1.2.1 Plants and invertebrates

A group of proteins involved in intracellular or cytoplasmic PAMPs recognition, called as nucleotide-binding oligomerisation (NOD) domain proteins (Inohara et al. 2001). The NOD proteins possess a N-terminal caspase activation and recruitment domains (CARD), a nucleotide binding domain, and a C-terminal LRR region (Bertin et al. 1999) (Inohara et al. 1999). The domain architecture of NOD proteins is comparable to that of the plant resistance (R) genes. In plants, the R genes play a vital role in detecting microbial infection, consequently induce hypersensitivity response. This helps the plant to inhibit intracellular replication of pathogens and the spread of infection (Hammond-Kosack and Jones 1997). The NOD-like receptors (NLRs) are distributed throughout the plant and animal kingdom. The invertebrate, sea urchin genome comprises about 203 putative NLRs (Sodergren et al., 2006).

1.1.2.2 Vertebrates

In mice there are at least 33 reported NLR genes and in human there are about 22 NLR family proteins. The NLRs are initially expressed in lymphocytes and antigen-presenting cells (e.g., Macrophages and dendritic cells), but also some non-immune cells do express NLRs (e.g. epithelial cells). The NLR proteins consist of N-terminal CARD, pyrin domain (PYD), baculovirus inhibitor repeat (BIR), central NOD domain and C-terminal LRR that are crucial for recognising PAMPs (Inohara et al., 2000) (Barth, Fraser, and Fisher 1998).

1.1.3 Other PRRs

Secretory pattern recognition molecules include e.g., Mannan-binding lectins and C-reactive protein (Fraser 1998); (Gewurz H et al., 1982), Macrophage scavenger receptor (MSR), a phagocytic PRR expressed on the macrophages. MSR has a broad range of pattern recognition, which includes polyanionic ligands, double-stranded RNA (dsRNA), LPS etc. The peptidoglycan recognition receptors (PGRPs) are involved in identification of peptidoglycan PAMPs. PGRP1 is highly expressed in polymorphonuclear leukocytes and is stored in tertiary (secretory) granules (Tydell et al. 2006).

1.2 Antimicrobial peptides (AMPs)

AMPs are one among the effector molecules of innate immune system. The characteristics, such as size, sequence, charge, conformation and structure, hydrophobicity, and amphipathicity influence the antimicrobial properties of the AMPs (K. A. Brogden 2005). Based on amino acid composition and structure AMPs are categorised into 4 groups, this includes anionic AMPs, cationic AMPs, cationic peptides that are enriched for specific amino acid residues, and anionic-and-cationic peptides (Boman 1995) (Hancock and Chapple 1997) (Gennaro and Zanetti 2000) (Vizioli and Salzet 2002). The anionic AMPs are small (700-900 Da) peptides present in many body secretions (Brogden, *et al.*, 1998). Many of them need zinc as cofactor for their antimicrobial function towards Gram-positive and Gram-negative bacteria, e.g., maximin H5 from amphibians and dermcidin from human.

The cationic peptides are short AMPs that consist of < 40 amino acid residues. Cationic peptides lack cysteine residues, but may possess some random structures. These peptides remain disordered in aqueous solution, but in the presence of trifluoroethanol, sodium dodecyl sulfate (SDS) micelles, phospholipids vesicles, liposomes or lipid A, most of the peptides adapt α -helical conformation. The extent of α -helix formation is directly proportional to the nature of antimicrobial activity, e.g., cecropin P1 from *Ascaris*, magainin from amphibians, Melittin from insects, and LL-37 from human (Gennaro and Zanetti 2000). Cationic peptides enriched in specific amino acids, these peptides are cationic in nature, but enriched in certain amino acid residues (Otvos 2002). For instance, abaecins from honeybees are rich in proline, Prophenins from pigs are rich in proline and phenylalanine,

Histatins from some higher primates and humans are rich in histidines. These cationic peptides are mostly linear, lack cysteine residues, but some may have extended coils.

Anionic and cationic peptides are peptides which consist of cysteine residues involved in intramolecular disulfide bonds. The anionic and cationic peptides group constitutes peptides with α -helices connected by intramolecular disulfide bonds, e.g., esculentin isolated from frog skin, which is a 46 amino acid, hydrophobic, and cationic peptide that forms an amphipathic α -helix (Wang et al. 1998) and amoebapores isolated from *E. histolytica* (M. Leippe 1997) (Hecht et al. 2004). Also, the peptides with β -strands, e.g., the β -defensins isolated from human and several other organisms are categorised under this anionic and cationic peptides group (Ganz 2003). In addition, this group includes peptides with both, α -helix and β -strands, e.g., drosomysin of *D. melanogaster*, an antifungal protein, which consists of 44 amino acid residues with α -helix and β -strands, whose structure is stabilised by intramolecular disulfide bonds (Fehlbaum et al. 1994). These anionic and cationic peptides also remain as a part of larger proteins, but their functions in such multiprotein complex is unknown, e.g., casocidin I from human casein, antimicrobial domains from bovine α -lactalbumin.

1.2.1 Mode of actions

1.2.1.1 Transmembrane-pore formation

Most of the natural AMPs are known to achieve antimicrobial activity by permeabilising the cytoplasmic membrane of bacteria. In general, AMPs have preference for negatively charged phospholipids of bacteria (Lehrer and Ganz 1990) (Zasloff 2002). Among several models postulated for transmembrane-pore formation and membrane permeabilisation by AMPs, three models remain persuasive, as exemplified with suitable examples (K. A. Brogden 2005) (Jenssen, Hamill, and Hancock 2006). These models include the barrel-stave model: A mechanism by which the peptides first become inserted in the cytoplasmic membrane, soon orient perpendicular to the plane of the target membrane, and upon oligomerisation form stable, water-filled and channel-like pores (**Fig. 2**), e.g., alamethicin (Boheim, 1974).

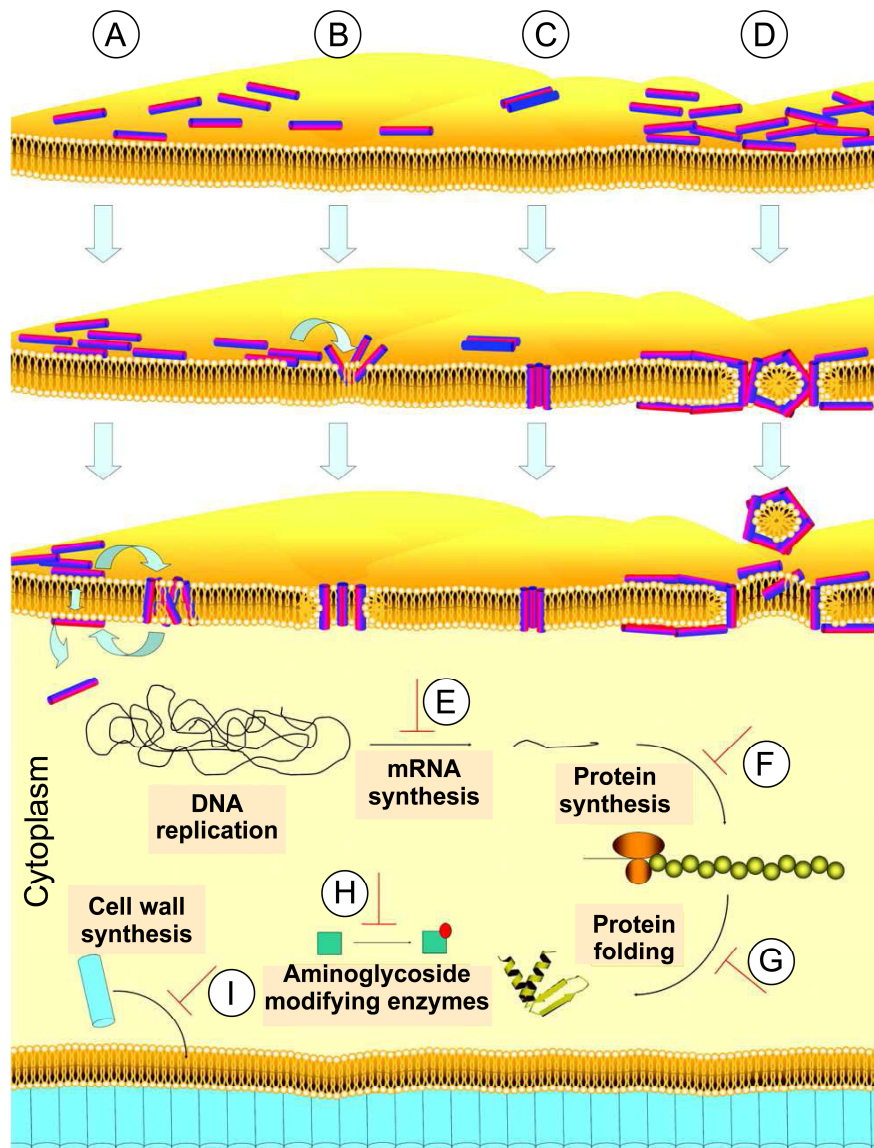


Fig. 2: Mode of actions of AMPs. Bacterial membrane is shown as yellow lipid bilayers on which the AMPs are adhering. Hydrophilic regions of AMPs are coloured red and the hydrophobic regions are coloured blue. Models describing membrane permeabilisation are shown (A to D). In the “aggregate” model (A) the peptides span the membrane by forming a micelle-like complex of peptides and lipids, but without adopting any specific orientation. In the “toroidal pore” model (B) the peptides adopt a perpendicular orientation and insert the bilayer, during which the hydrophilic regions of AMPs interact with the phospholipid head groups, whereas the hydrophobic regions of the AMPs associate with the lipid core. Because of this, the membrane curves inward and the bilayer lines the pores. Also, in the “barrel stave” model (C) the peptides insert the membrane in a perpendicular fashion, but here the hydrophilic regions of the peptides face the lumen of the pore, whereas the hydrophobic regions interact with the lipid bilayer. In “carpet” model (D) the AMPs cover the surface of the target surface in a parallel fashion, after reaching a threshold concentration causes destabilisation of the membrane. Mechanisms other than membrane destabilisation are illustrated in panels E to I. This includes AMPs that inhibit DNA and RNA synthesis (E) (e.g., buforin II), AMPs that hinder protein synthesis (F) (e.g., indolicidin), while several AMPs affect enzymatic activity of the target bacterial cell (G). For instance, pyrrolicidin affect the ATPase activity of DnaK, which is an enzyme implicated in chaperone-assisted protein folding. There are also AMPs that inhibit bacterial cell wall synthesis (I) (e.g., nisin). (modified, Jenssen et al., 2006)

Carpet model: The peptides continuous binding to the target membrane, which resembles a carpet, upon reaching a threshold concentration the peptides start destabilising the target membrane (**Fig. 2**), e.g., cecropin P1 (Gazit et al. 1995)

The toroidal model: This mechanism is comparable to carpet model, the peptides remain attached to the membrane surface in parallel fashion, and soon this results in positive curvature of the membrane. The pores created by this mechanism appear like a torus, with the interior of the pores being lined by the polar peptides residues and the phospholipid head groups (**Fig. 2**), e.g., magainins (Ludtke et al. 1996) (Matsuzaki 1998)

1.2.1.2 Intracellular killing

Apart from the membrane disruption and bacterial killing, the AMPs are known to have many intracellular targets. In brief, the intracellular targets and the consequences include flocculation of cell cytoplasm upon entry of AMPs (K. A. Brogden et al. 1996), reduced cytoplasmic septum formation (Shi et al. 1996), and inhibition of cell wall synthesis (Sahl, Jack, and Bierbaum 1995); (Brötz et al. 1998). AMPs binding to nucleic acids inhibit nucleic acid synthesis (Park, Kim, and Kim 1998), thereby affecting protein synthesis, and enzymatic activity of the target cells (Andreu and Rivas 1998), (Patrzykat et al. 2002). AMPs also induce the induction of autolysins production in the target cells, which causes target cell lysis (Bierbaum and Sahl 1987)

1.2.2 AMPs, the future antibiotics

The natural effector molecules of innate immune system or its synthetic forms could become a plausible therapeutic tool in future, to deal with growing infectious diseases (Zasloff 2002); (Gutsmann et al. 2003); (K. A. Brogden 2005). As the AMPs mainly target the bacterial cell membrane and cause rapid cell disruption, there are very less chances for the target host cells to evolve resistance towards AMPs. On earth, the most dominant life forms are plants and invertebrates, whose successful survival all these years of evolution could exemplify the power of innate immune effector molecules. However, there are less convincing reports available about the AMPs function in vertebrates (Ganz 2003); (Cho et al. 2005) and invertebrate models (Janeway and Medzhitov 2002). As the vertebrate immune system is build by the interplay between innate and acquired immunity, the studies

concerning AMPs remain complicated. Moreover, gene manipulation techniques are less amenable with vertebrate models, such as macrophage. Nevertheless, there are several reports being documented about the mutations in PRRs leading to defect in the downstream partners involved of innate immune system (Thompson and Locarnini 2007). Remarkably, studies on immune effector molecules remain well established in the lower eukaryotes like amoebae.

1.3 *E. histolytica*: a model to study functions of AMPs

The production of AMPs to combat microbial infections is an evolutionarily conserved phenomenon, as exemplified by their presence in all the living organisms (Zasloff 2002). For instance, the lower organisms, such as *E. histolytica* produce AMPs, which are stored in the cytoplasmic granules and employed to kill the phagocytosed intracellular bacterial pathogens. Even though, *E. histolytica* is a causative agent of fatal amoebiasis in human, it has served as a successful model to examine the immune functions of amoebapores, its own immune effector molecules. Strikingly, the antimicrobial mechanism observed with *E. histolytica* remains comparable to the effector molecules of vertebrates, e.g., NK-lysin (porcine Natural Killer cells) and granulysin (human cytotoxic T cells). All these AMPs are stored in the intracellular cytoplasmic granules and may probably function in an oxygen-independent mechanism (M. Leippe 1999) (J. Andrä, Herbst, and Leippe 2003).

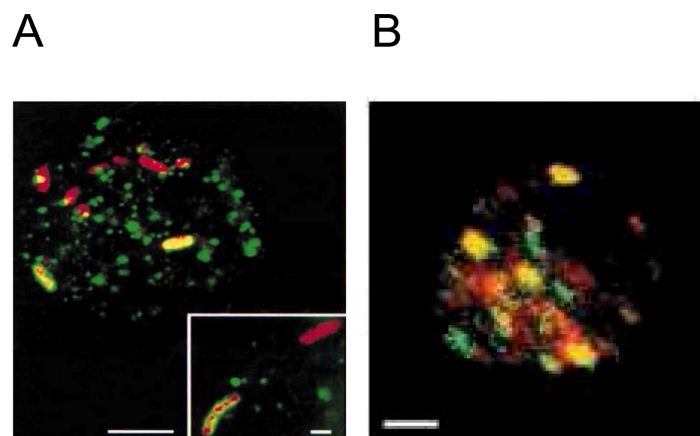


Fig. 3: Effector molecules of innate immune system in *E. histolytica* and cytotoxic T lymphocytes (CTLs). **A)** *E. histolytica* amoeba fed with *E. coli* and subjected to immunocytochemical analyses to detect amoebapore A positive cellular compartments. Cytoplasmic granules containing amoebapore A (green), *E. coli* (red) are shown and the colocalisation (yellow) of amoebapore A and *E. coli* is shown in the blow-up (Andrä *et al.*, 2003). **B)** CTL incubated with *M. tuberculosis* was stained for perforin, a cytolytic protein (red), and for granulysin (green), colocalisation (yellow) (Stenger *et al.*, 1998). Both, **A** and **B** represent overlay images of indicated cells showing effector molecules stored in intracellular cytoplasmic granules.

Confocal microscope images of an *E. histolytica* amoeba showing cytoplasmic granules filled with amoebapore A, which are in contact with *E. coli* (**Fig. 3A**) (Jörg Andrä, Herbst, and Leippe 2003) and the cytoplasmic granules of a cytotoxic T cell containing granulysin and perforin (Stenger 1998) after exposure to *M. tuberculosis* are represented (**Fig. 3B**).

1.3.1 Amoebapores, the antimicrobial armament of *E. histolytica*

E. histolytica, the causative organism of amoebiasis in human is notoriously known for its antimicrobial activity and also for its cytolytic activity against eukaryotic cells. The cytoplasmic granular vesicles of *E. histolytica* constitutes three isoforms of amoebapore (A, B, and C), which are pore-forming peptides. All three isoforms are coded by different genes, which are randomly distributed in the genome, and they share an overall identity of 35 to 57% (J. Andrä and Leippe 1994) (M. Leippe 1999).

1.3.2 Structure of amoebapores

The mature polypeptide of all three isoforms of amoebapore (A, B, and C) consists of 77 amino acid residues. The structural stability of amoebapores is achieved by six cysteine residues, which are involved in three disulfide bonds (M. Leippe 1999). The disulfide bonds are crucial for structure stability and for resistance to heat and protease activity. The primary translation products of all three isoforms possess N-terminal signal peptides (19-24 amino acid residues), which are crucial for targeting the peptides to the destined cellular compartments. Analysis of the 3-dimensional structure of amoebapores (**Fig. 4A**) and its structural and functional counterparts, NK-lysin (**Fig. 4B**) and granulysin (not shown) revealed that all three members are globular proteins with five amphipathic α -helices involved in three disulfide bonds without any random regions or β -sheets (M. Leippe et al. 1992); (H. Bruhn and Leippe 2001a); (M. Leippe et al. 2005).

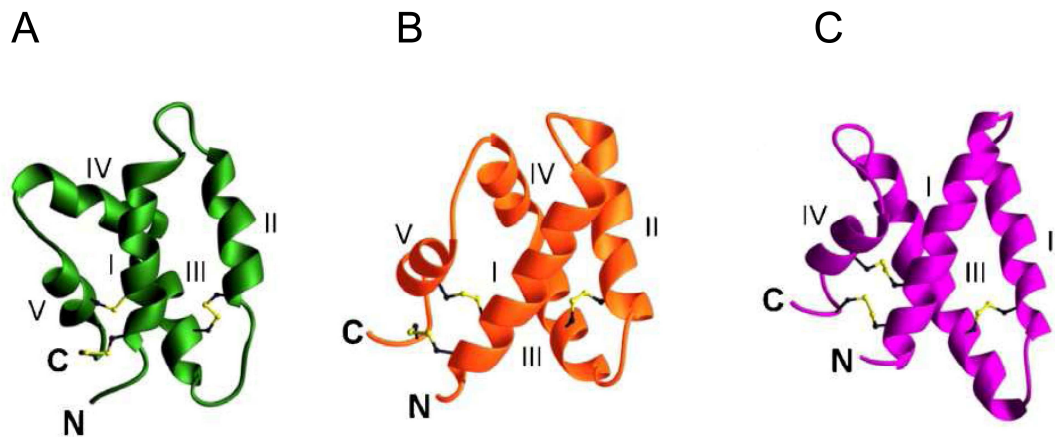


Fig. 4: Ribbon structure representation of SAPLIPs. **A)** amoebapore A, **B)** NK-lysin, and **C)** saposin A. α -helices are represented by numbers I to V, C and N represents C- and N- termini. Disulfide bonds are shown in yellow. (modified, Mysliwy *et al.*, 2010)

Any protein with this characteristic is categorised under saposin-like proteins (SAPLIPs) family and the domain is called as SAPLIP domain. There are several SAPLIP members with less than five amphipathic α -helix, e.g., saposin A (human) has four α -helices and six cysteine residues, implicated in three disulfide bonds (**Fig. 4C**) (Mysliwy *et al.* 2010). However, the SAPLIP fold is highly conserved through evolution (H. Bruhn 2005).

1.3.3 Functions of SAPLIPs

SAPLIPs are known for their antimicrobial and cytolytic function towards microbes and eukaryotic cells. For instance, amoebapores are preferentially antimicrobial against Gram-positive bacteria and are active at acidic pH, and bind to phospholipids with negatively charged head groups. NK-lysin has a broad antimicrobial spectrum and is antimicrobial towards both Gram-positive and Gram-negative bacteria. Unlike amoebapores, the antimicrobial activity of NK-lysin is not pH dependent and is also cytolytic towards eukaryotic cells, but relatively less than amoebapores (Andersson *et al.* 1996); (H. Bruhn *et al.* 2003). When all three amoebapores and NK-lysin were tested on planar lipid bilayers for their pore-forming abilities, the amoebapores were very rapid compared to NK-lysin (Gutsmann *et al.* 2003).

Unlike amoebapores, very high concentration of NK-lysin was required to create pores on various lipid membranes (Gutsmann *et al.* 2003). Granulysin is

known for its broad spectrum of antimicrobial activity, whereas its cytolytic function is achieved in synergy with perforin (Stenger et al 1998). All three effector molecules (Amoebapores, NK-lysin and Granulysin) are known to be stored in the intracellular cytoplasmic granules (J. Andrä, Herbst, and Leippe 2003); (Andersson et al. 1996); (Stenger et al 1998). In addition to antimicrobial and cytolytic activities, SAPLIPs are known for their diverse cellular functions. For instance, human saposins A-D functions as co-factor of lipid metabolism in the lysosomes. Notably, saposins are also involved in antigen presentation functions (Zhou et al. 2004); (Winau et al. 2004); (Kang and Cresswell 2004); (Kolter et al. 2005). Moreover, SAPLIPs function as a part of multi-protein complex. For example, a protein complex in *Dictyostelium discoideum*, named as cell-counting factor constitutes a component called countin, which has a SAPLIP domain. Countin plays a crucial role in determining the aggregate size. Loss of countin results in larger cell aggregates, whereas overproduction of countin causes small aggregates (D. A. Brock et al. 1996); (D. A. Brock and Gomer 1999); (Brown and Firtel 2000). Another protein called acyloxyacyl hydrolase (AOAH) of *D. discoideum* has a SAPLIP domain and a hydrolase domain but its function in *D. discoideum* is unknown at present (Munford, Sheppard, and O'Hara 1995).

1.3.4 Mode of actions of SAPLIPs

Three general mechanisms by which SAPLIPs interact with membrane bilayer include: (i) binding of an autonomous SAPLIP domain to the membrane bilayer (H. Bruhn 2005). Usually the multidomain enzymes are assumed to carry out such functions, e.g., sphingomyelinase (**Fig. 5A**) (Ponting 1994) and acyloxy acylase (Munford and Hunter 1992). (ii) membrane perturbation by autonomous SAPLIP domain, thereby the SAPLIP domain carry out functions such as membrane extraction and lipid presentation for the enzymes in the surrounding milieu (**Fig. 5B**) (H. Bruhn 2005). There are several models predicted and proved concerning the pore formation mechanisms adapted by different antimicrobial peptides.

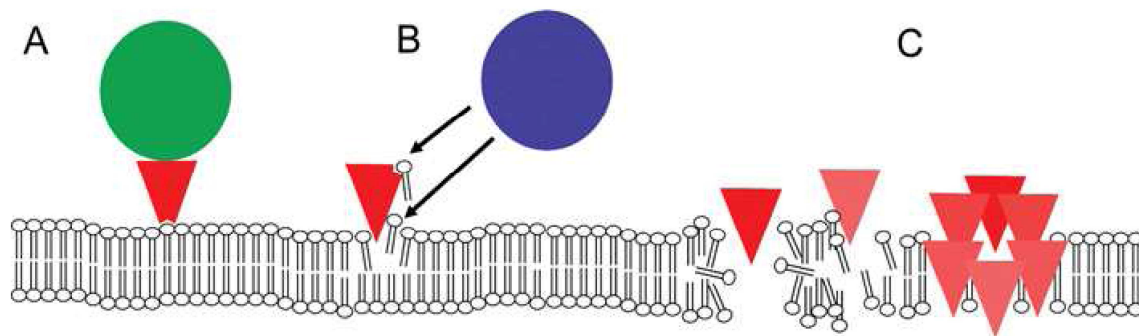


Fig. 5: Mode of actions of SAPLIPs on target membranes. **A)** SAPLIP domain (red triangle) targeting the membrane; green circle represents enzymatic domain. **B)** Individual SAPLIP domain involved in membrane disruption and thereby presenting lipids as substrate for an enzyme (blue circle), and **C)** Autonomous SAPLIP domains involved in membrane permeabilisation and oligomerised SAPLIP domains implicated in pore formation (Bruhn, 2005)

However, the pores created by amoebapores on membrane bilayers were postulated and proved persuasively to be similar to that of barrel-stave model (**Fig. 5C**) (J. Andrä and Leippe 1994); (J. Andrä, Herbst, and Leippe 2003). The planar lipid bilayer experiments also showed similar results (Gutsmann et al. 2003). Moreover, unlike other AMPs, as the amoebapores are amphipathic molecules with neutral net charge, contact with hydrophobic residues allows direct insertion of amoebapores into the membrane bilayer (J. Andrä, Herbst, and Leippe 2003).

1.4 Need for a versatile host model

As already mentioned, the AMPs could become a possible future therapeutic tool to replace the conventional antibiotics. However, there are several reports describing the evolution of microbial resistance against natural peptides. For instance, it is reported that several *Salmonella* species and *Staphylococcus aureus* produce proteases and peptidases that degrade the AMPs (Guina et al. 2000); (Sieprawska-lupa et al. 2004). As a counter measure, the host cells stabilise their AMPs by increasing the intramolecular disulfide bonds, introducing proline residues, and also modify the C-terminal regions that can resist protease and peptidase activity (Tjabringa, Rabe, and Hiemstra 2005). Thus the host-pathogen resistance strategies are continuously evolving. Nevertheless, need for new antibiotics could be possibly achieved by designing synthetic AMPs with some modifications in the natural peptides, such as changing non-essential amino acids without affecting those which are essential for conferring antimicrobial activity.

Therefore, bacterial recognition of conserved AMP motifs could be abolished (Peschel and Sahl 2006). In addition to the already existing antimicrobial peptides, here, in my present study, I have attempted to explore the functions of antimicrobial peptides of *Dictyostelium discoideum*. The professional phagocyte, *D. discoideum* is a soil dwelling solitary amoeba, which feeds on microbes in the soil. Upon onset of starvation the amoebae collect together to lead a social life. For these reasons they are called the social amoebae. Promising advantages with this model system include well established gene manipulation techniques, easy to grow under laboratory conditions (at 22 °C) and its sequenced haploid genome (Eichinger et al. 2005); (Fey et al. 2007).

1.4.1 Life cycle of *D. discoideum*

In *D. discoideum*, starvation is the key event that causes the unicellular amoebae to enter the social life. The starving cells emit cAMP signals and the cells in the surrounding vicinity both, sense and secrete cAMP to relay the signal (**Fig. 6A**) (Clarke and Gomer 1995); (Deery and Gomer 1999); (Schaap 2011). The cAMP gradient in the surrounding vicinity is controlled by phosphodiesterase produced by the amoebae, which degrade the cAMP (Faure et al. 1988); (Bader, Kortholt, and Van Haastert 2007). As a result of continuous cAMP signalling, a mass of 1×10^3 to 1×10^5 cells stream towards a centre, referred to as cell streaming stage of development (**Fig. 6B**). At the end of streaming, the cells form an aggregate, called mound. Soon the mound forms a tip, which acts as a signaling centre for rest of the cells in mound. The mound stage is also where the cells begin to undergo differentiation process (**Fig. 6C**) (Schaap 2011). Continuous cAMP signals induced by the mound tip causes forward movement of rest of the cells in the mound, resulting in the formation of erect structures called first finger, the standing slug (**Fig. 6D**) (Siegert and Weijer 1995). At favourable ambience, the first finger undergoes culmination to form a terminal differentiated structure, called fruiting body. If the conditions are unfavourable, the standing slug falls on the substratum and migrates in search of a suitable ambience.

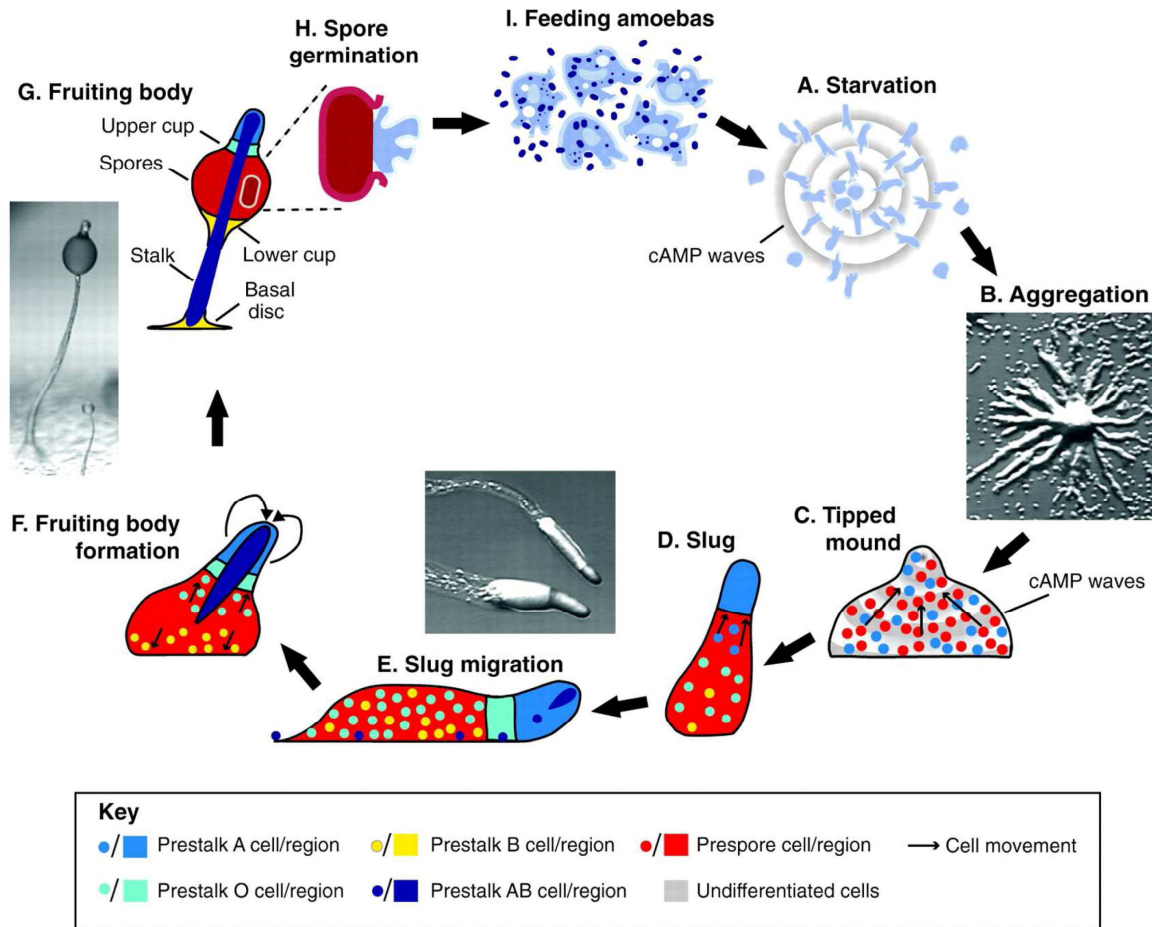


Fig. 6: *D. discoideum* life cycle. **A**) Starving *D. discoideum* amoebae (blue) produce cyclic adenosine monophosphate waves (cAMP, represented as grey circles), **B**) Cells streaming towards a centre in response to cAMP signals, resulting in aggregate formation (mound), **C**) Cells in the mound tip emit cAMP signals to other cells in the mound causing them to migrate in upward direction; pre-stalk and pre-spore differentiation begins in the mound, **D**) Continuous upward cell movement results in first finger formation (erect slugs), **E**) At unfavourable conditions, first finger collapse on substratum and migrate in search of favourable environment. In the slug stage spatial distribution and further cell differentiation occurs. Pre-stalk (A, B, and O region) cells occupy one fifth of slug front and pre-spore (red) cells occupy four fifth of slug rear. **F**) Upon reaching favourable ambience, the slug undergoes culmination or fruiting body formation, **G**) Cells on top (pre-stalk) move inward, towards the ground and form stalk, and basal disc. The differentiated pre-spore cells form the spore mass. The resulting structure is called fruiting body, a globular spore mass held atop a dead stalk. **H**) The dehiscent fruiting body releases spores on soil, at suitable conditions spores germinate **I**) Germinated amoebae feed on bacteria and divide by binary fission (Schaap 2011)

This migrating structure is called slug. In the slug, the spatio-temporal regulation of cells results in two major populations of cells. The pre-stalk (presumptive stalk) cells, which occupy one-fifth of the slug front and the pre-spore (presumptive spore) cells form four-fifth of the slug rear (**Fig. 6E**) (Maeda et al. 2003); (Williams 2010). This morphogenetic cell differentiation in *D. discoideum* is comparable to those of metazoans.

The phototactic and thigmotactic abilities of the slug direct it to find a suitable environment for culmination (Bonner 2003). Upon reaching a favourable environment, the slug undergoes culmination, which includes inward movement of cells in the slug front (pre-stalk) towards the substratum. During this invagination process the pre-stalk cells become vacuolated and synthesise cellulose wall, before reaching the ground. Concurrently, the pre-spore cells move up the stalk during which they synthesise spore coat and differentiate into spores (**Fig. 6F**). This results in the formation of a fruiting body, where the globular spore mass is held atop the dead stalk. The upper and lower cup cells at the top and bottom of the spore mass avoid the spore mass from sliding down the stalk, whereas the basal disc supports the stalk to firmly attach to the substratum (**Fig. 6G**) (Sternfeld 1998); (Yamada et al. 2010); (Schaap 2011). The dehiscent fruiting body liberates the spores in the surrounding environment or the spores may be transferred to a new environment through some bugs. As a result, the dispersed spores germinate and feed on the bacteria available in the new environment, undergo binary fission, and increase their population size (**Fig. 6H and I**) (Schaap 2011). It has been reported recently about a typical characteristic observed in the *D. discoideum* amoebae. In wild, the amoebae stop feeding and conserve some bacteria in their body before the onset of starvation. Presumably, the prestarvation factor (PSF), which is a glycoprotein and cell density sensor, may play an important role here. The amoebae monitor their cell densities and the relative threshold of PSF. If the PSF level exceeds the density of bacteria, they stop feeding (Clarke and Gomer 1995). The conserved bacteria are carried in their body all through the development process and are passed to the spore mass in the terminally differentiated structures. Finally, the release of spores from the fruiting body also liberates the bacteria to the ground, which are seeded in the soil and becomes a new source of food for the germinated amoebae (D. A. Brock et al. 2011). Again, at the onset of starvation, they will undergo the same series of development process.

1.4.2 Evolution of *D. discoideum*

The phylogenetic tree described below was constructed using the proteome data from 17 eukaryotic organisms (**Fig. 7**). The data analysed describe

that similar to other living organisms, *D. discoideum* genome has also undergone horizontal gene transfer (HGT) from the bacterial species, and chromosomal deletions and duplications (Eichinger et al. 2005). Analyses for HGT identified 18 potential protein domains transferred from bacteria to *D. discoideum*. Both, the incidence of HGT genes replaced with new functions and those which have retained the same functions were observed.

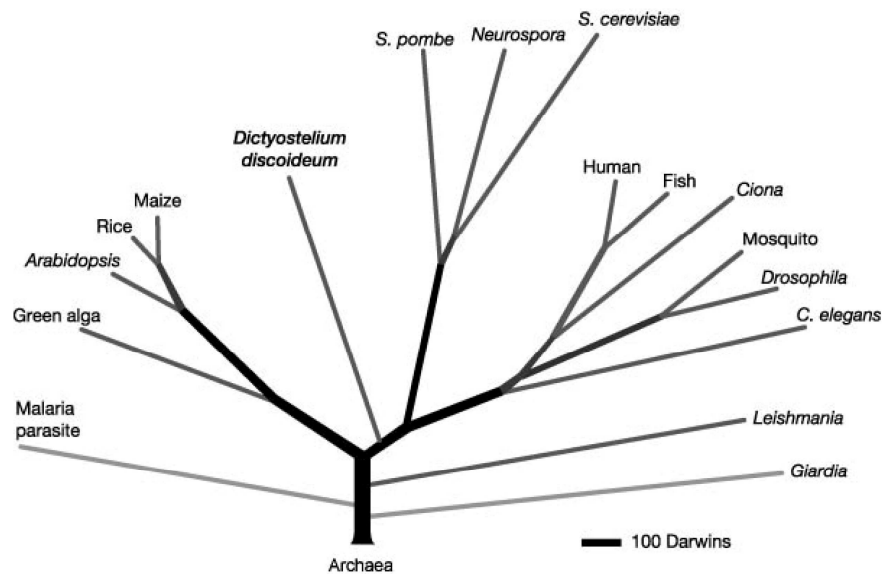


Fig. 7: Evolution of *D. discoideum*. Phylogenetic tree constructed based on a database containing 5,279 orthologous protein clusters, which was derived from 17 eukaryotes shown in the figure. Phylogenetic tree denotes the origin of *D. discoideum* immediately after the divergence of the plant and animal kingdom. Branch length is represented as Darwins (1 Darwin = 1/2,000 of divergence between *S. cerevisiae* and human). Species represented includes *Plasmodium falciparum* (malaria parasite), *Chlamydomonas reinhardtii* (green alga), *Oryza sativa* (rice), *Zea mays* (maize), *Takifugu rubripes* (fish) and *Anopheles gambiae* (mosquito) (Eichinger et al, 2005).

The study performed at the molecular level, which included more than 100 proteins has classified *D. discoideum* under amoebozoa, which had diverged immediately after plant-animal split. The phylogenetic tree also indicates that *D. discoideum* divergence had occurred before the divergence of fungi. Nevertheless, *D. discoideum*, fungi and Metazoans belong to true sister groups, which is supporting the evolutionary notion described above. Despite the early divergence of *D. discoideum*, human and *D. discoideum* share relatively more protein orthologous than shared by *Saccharomyces cerevisiae* with human.

This observation was very interesting because, this data has evoked an idea that *D. discoideum* can be used as a model organism to study these human diseases. Eventhough, human orthologous are present in other species such as *D. melanogaster*, the genetically amenable and experimentally tractable nature of

D. discoideum has made it a relatively more attractive model system. A search for genes related to human disease in *D. discoideum* has identified 64 orthologous and 33 among these are similar in length to human proteins and showed > 70% similarity. However, the number of human disease orthologous in *D. discoideum* is less than those found in *D. melanogaster* and *Caenorhabditis elegans*, but higher than those found in fungi (*Saccharomyces cerevisiae* and *S. pombe*). Among the 33 putative human disease orthologues identified in *D. discoideum*, five are absent in *S. cerevisiae* or *S. pombe*, four are missing in *S. cerevisiae*, and two are not found in *S. pombe* (Eichinger et al. 2005); (Williams 2010).

1.4.3 Immune effector proteins of *D. discoideum*

1.4.3.1 Amoebapore-like peptides (Apls) of *D. discoideum*

As the *D. discoideum* amoebae feed on bacteria their genome may harbour antimicrobial genes and the products of these genes may be implicated in killing and degrading the bacteria. As *D. discoideum* and *E. histolytica* belong to amoebazoa group, presumably *D. discoideum* genome may also possess the SAPLIP members. Supporting this notion, earlier work in our laboratory has identified 17 genes that code for 33 putative SAPLIPs (unpublished data) (**Fig. 8**). As the SAPLIPs in *D. discoideum* were initially identified using protein sequence of amoebapores, the *D. discoideum* SAPLIPs were termed as amoebapore-like peptide coding genes (**apls**). Apls are designated by alphabets starting from A up to R, excluding I (**Fig. 8**). The apl genes are found randomly distributed all over the *D. discoideum* genome without any restricted cluster regions. *D. discoideum* genome also possesses a protein complex (> 450 kDa), which has a SAPLIP domain. For instance, countin, the group size sensor is a component of counting factor complex. In addition, *D. discoideum* genome also constitutes a multidomain protein, including a SAPLIP domain. Acyloxyacyl hydrolase (AOAH) in *D. discoideum* possesses a SAPLIP domains and a hydrolase domain. The functions of both, counting factor and AOAH in *D. discoideum* are unknown at present.

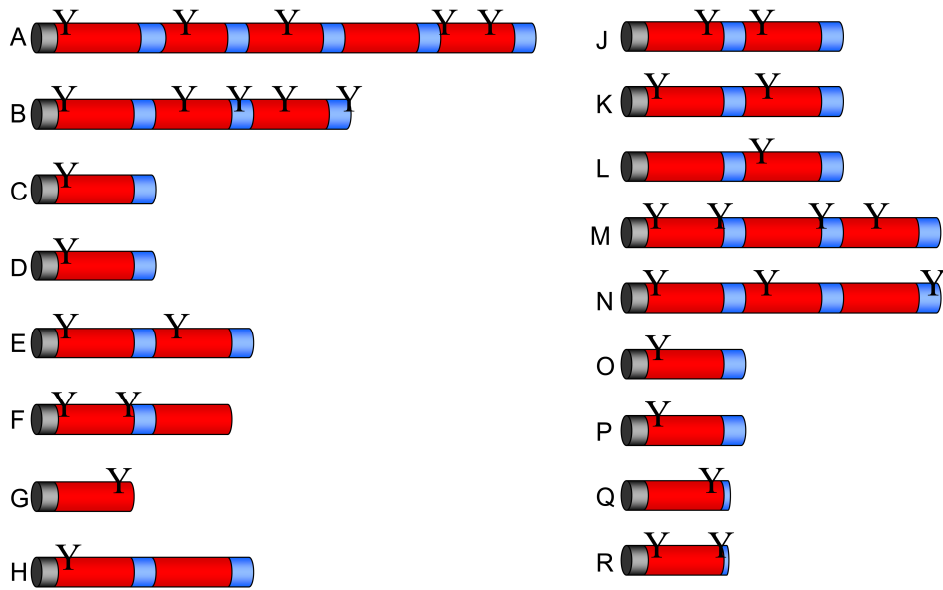


Fig. 8: Apls of *D. discoideum*. Genome of *D. discoideum* analysed for putative SAPLIP members revealed 17 genes, called as amoebapore-like peptide coding genes (*apls*) that potentially code for 33 putative Apls. Each *apl* is designated by alphabets starting from A up to R, excluding I. Signal peptides (grey), SAPLIP domains (red), putative linker and end regions (blue), and potential N-glycosylation sites (Y). (R. Herbst and Leippe, unpublished data)

1.4.3.2 Lysozymes

D. discoideum genome harbours four classes of lysozymes, which include amoeba lysozymes (alys) that is a unique class of lysozymes found in *D. discoideum*. The aly family constitutes aly A, B, C, D, and L. Among all five alys, alyA is characterised both, at gene and protein level (Müller et al. 2005). Intracellular localization studies revealed that AlyA localises to unique cytoplasmic granules, which are dispersed all over the cell (Müller et al. 2005). The chicken type or C-type lysozymes of *D. discoideum* constitute three lysozyme gene members called *lyC1*, *lyC2* and *lyC3*. The T4-phage type lysozymes of *D. discoideum* include two genes, and the *Entamoeba*-type lysozymes (*lyEh*) include six lysozyme genes (*Eh1-Eh6*). In general, many organisms investigated for lysozyme genes usually show a specific type of lysozyme. Presence of different classes of lysozyme in *D. discoideum* brings a notion that apart from bacterial killing, lysozymes are also implicated in digestive functions (**Fig. 9**) (Prager 1996); (M. Leippe 1999).

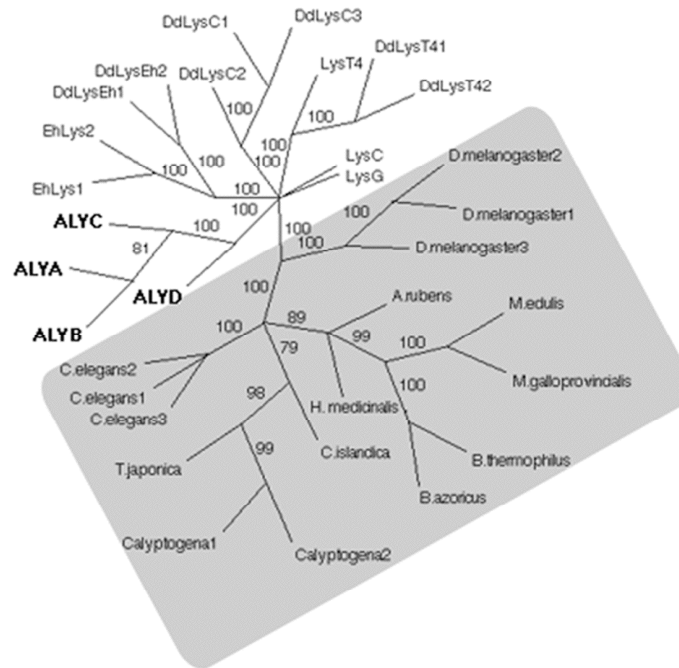


Fig. 9: Phylogenetic tree drawn for lysozymes from different species. Lysozymes of *D. discoideum* are shown in unblocked area and the blocked area represents lysozymes from invertebrates. Different classes of lysozymes in *D. discoideum* include amoeba lysozymes (ALYs, bold), *E. histolytica* type lysozymes (DdLysEh), C-type lysozymes (DdLysC), and T4-phage type lysozymes (DdLysT4). Neighbour joining tree is presented, numbers indicate bootstrap proportions on 1000 replicates and values greater than 70% are shown (Müller et al. 2005). Recent additions, lysozymes (ALYL, DdLysEh3-6) are not shown.

1.4.4 *D. discoideum* as a model organism

Since 1940s, for evolutionary biologists, *D. discoideum* was a tempting model to research on the evolution of multicellular life from unicellular amoebae. This gave rise to theories such as kin preference, trade off (Mehdiabadi et al. 2006) and the cheater phenomenon in *D. discoideum* (Strassmann, Gilbert, and Queller 2011). Also *D. discoideum* is serving as a fascinating model for developmental biologists. cAMP was the first chemoattractant used to discover the chemotactic nature of the amoebae. Following this, several other chemoattractants were successfully tested (Meima and Schaap 1999). The translucent multicellular structures allows studies on cell differentiation, cell movement using vital dyes, fluorescent protein tags, and in situ hybridisation (G. Gerisch et al. 2004); (Maeda et al. 2003).

Thorough studies on developmental and evolutionary grounds have gained the interest of cell biologist to use *D. discoideum* to understand the aspects of growth, pinocytosis and phagocytosis (Cardelli 2001); (Neuhaus, Almers, and Soldati 2002), cell cytoskeleton (Sultana et al. 2009); (Krüger et al. 2012). *D. discoideum* has also been proven as an expression system for the production of eukaryotic genes (Arya, Bhattacharya, and Saini 2008). Easy mass culturing of *D. discoideum*, gene manipulation tools such as gene knock-out (J. Faix et al. 2004), RNAi (Hinas et al. 2007), and the availability of cell-type specific markers, e.g., for pre-stalk cells; *ecmA*, *O*, and *B* and for pre-spore cells; *pspA*, all these were added advantages concerning the experimental perspectives. *D. discoideum* feed on bacteria for food in a mechanism comparable to that of macrophages. Therefore, *D. discoideum* has become a convenient model system to study host-pathogen interactions (Bozzaro and Eichinger 2011).

D. discoideum has been proven as a convenient host model to determine the degree of bacterial virulence and the bacterial genes implicated in virulence mechanisms (Froquet et al. 2009); (Benghezal et al. 2006). The mechanism of cell to cell dissemination of *Mycobacterium tuberculosis*, which causes tuberculosis disease, was studied using *D. discoideum* as a host (Hagedorn et al. 2009). Similarly, *D. discoideum* has served as an elegant model to gain knowledge on *Legionella pneumophila* infections (Hägele et al. 2000); (Solomon et al. 2000); (J. Chen et al. 2004); (Lu and Clarke 2005). Notably, *D. discoideum* has also been used as model for drug screening (Bozzaro and Eichinger 2011). Surprisingly, until now, not much is revealed about the antimicrobial arsenal of *D. discoideum*. A remarkable finding concerning *D. discoideum* immune system was the presence of a special type of cells called sentinel or S cells, isolated from the migrating *D. discoideum* slugs. These S cells are involved in sequestering toxins and removing foreign invaders from the slugs, thereby protecting the developing structures (G. Chen, Zhuchenko, and Kuspa 2007). However, there is a lot more to be uncovered in this area of research, which may possibly shed some new light on ancient immune armaments.

1.5 Objectives

Due to the emergence of antibiotic resistant bacteria, we are in need for new antibiotics. In vertebrates, protection against microbes is accomplished by innate and acquired immune systems, whereas plants and invertebrates rely on innate immunity to fulfill their immune functions. Even before the evolution of these immune systems, the antimicrobial peptides (AMPs) were implicated in microbial killing. For instance, in the unicellular and pathogenic amoeba *E. histolytica*, which feeds on bacteria, the antimicrobial functions are carried out by amoebapores and lysozymes. The amoebapores are peptides made of 77 amino acid residues that are involved in bacterial killing. Also, it had been reported that shorter, synthetic forms of amoebapores showed antimicrobial activity, which could be a promising antibiotic in future. Likewise, in *D. discoideum*, a non-pathogenic, professional phagocyte, the genome constitutes 17 amoebapore-like peptide coding genes (***apls***), that may produce 33 putative Apls. Additionally, *D. discoideum* genome also comprises different classes of lysozymes, in total at least 15 lysozyme genes. So far, not much is reported about the Apls and lysozymes of *D. discoideum*. The only lysozyme characterised at gene and protein level is AlyA (*alyA*). Aim of my doctoral thesis was to explore the functions of *apls* and lysozyme genes in *D. discoideum*. My interest was to understand whether any of these putative antimicrobial gene products are specifically required for killing a particular bacterial strain or whether they play a synergistic role to achieve antimicrobial functions.

2 MATERIALS

2.1 Chemicals

Acrylamide solution	AppliChem
Agar-Agar	ROTH
Agarose Ultrapure	Invitrogen
Ammonium persulphate (APS)	AppliChem
Ampicillin sodium salt	ROTH
Bacto yeast Extract	Becton Dickinson and Company
Bacteriological peptone (LP0037)	Oxoid
Blasticidin S	Sigma
β -Mercaptoethanol	AppliChem
Bovine serum albumin	Sigma
Calcium chloride	Merck
CHAPS	Calbiochem
Chloroform	Merck
DMSO	ROTH
Di-potassium hydrogen phosphate (K_2HPO_4)	ROTH
Di-sodium hydrogen phosphate (Na_2HPO_4)	ROTH
dNTPs	Fermentas
EDTA, di-sodium salt	ROTH
Ethanol ($\geq 99.8\%$ p.a.)	ROTH
Ethidium bromide	ROTH
Gelatin (from Porcine skin)	Sigma
Geneticin (G418 disulfate salt)	Sigma
Glucose	ROTH
Glycerine ($\geq 86\%$ p.a.)	ROTH
Glycerol	SERVA
Glycin	Merck
HEPES	ROTH
Hydrogen peroxide (H_2O_2)	ROTH
Hydrochloric acid (HCl) 37% (w/v)	ROTH

Isopropanol	ROTH
IPTG	AppliChem
LB Broth Base	ROTH
Methanol	ROTH
Magnesium chloride (MgCl ₂)	Sigma
Magnesium sulfate (MgSO ₄)	Merck
Manganese (II) chloride tetrahydrate (Cl ₂ Mn.4H ₂ O)	AppliChem
Mops	AppliChem
Nonidet P-40	Sigma
Penicillin	Sigma
Paraformaldehyde	AppliChem
Potassium acetate (C ₂ H ₃ KO ₂)	AppliChem
Potassium dihydrogen phosphate (KH ₂ PO ₄)	AppliChem
Potassium chloride (KCl)	AppliChem
Protease Inhibitor Cocktail Tablets Complete EDTA-free	Roche
Proteinase K	Fermentas
Proteose-Peptone	Oxoid
RNase Inhibitor	Invitrogen
Saponin	Sigma
Sodium acetate (CH ₃ COONa)	AppliChem
Sodium bicarbonate (NaHCO ₃)	ROTH
Sodium chloride (NaCl)	ROTH
Sodium dihydrogen phosphate (NaH ₂ PO ₄)	ROTH
Sodium dodecyl sulfate	MP Biomedicals, LLC
Sodium hydroxide (NaOH)	ROTH
Streptomycin	Sigma
Sucrose	ROTH
TEMED	AppliChem
Tris	ROTH
Triton X-100	AppliChem

Tricine	ROTH
Tween 20	AppliChem
Urea	ROTH

2.2 Protein marker

SeeBlue plus2, Pre-stained Standard	Invitrogen
-------------------------------------	------------

2.3 DNA ladder

GeneRuler™ DNA Ladder Mix 100-1000 bp	Fermentas
GeneRuler™ 100 bp DNA Ladder plus	Fermentas

2.4 Dyes and substrates

BCIP	Promega, Mannheim
Bromophenolblue (BPB)	Merck
Hoechst 33258	Sigma
NBT	Sigma
Neutral red	Merck
X-Gal	AppliChem
Xylencyanol	AppliChem

2.5 Antibodies

2.5.1 Primary antibodies:

Mouse Anti-comitin, marker for Golgi and Mouse Anti-Vat A, marker for contractile vacuole and endosomes	90-340-8 (++++ 0208 III) 21-35-2, (Prof. Dr. A. A. Noegel's laboratory, University of Colonge)
Mouse Anti-FLAG® M2 Monoclonal, (F3165/ 080M6034)	Sigma Life science
Mouse Anti-PDI (protein disulfide isomerase) marker for ER (endoplasmic reticulum), Monoclonal [RL90]	Abcam (ab2792)
Mouse Anti-vacuolin, a postlysosomes marker	263-79-2 (Prof. Dr. M. Maniak's laboratory, University of Kassel)
Rabbit Anti-PDI, Polyclonal, ER marker	Abcam (ab31811)

2.5.2 Secondary antibodies:

Goat Anti-mouse-IgM (heavy chain) AP (Alkaline Phosphatase) conjugated	Molecular Probes
Goat Anti-mouse-IgG (H+L) AP conjugated	Jackson ImmunoResearch laboratories
Horse Anti-mouse-IgG, Dylight 488 (green) conjugated	Vector laboratories
Horse Anti-mouse-IgG, Dylight 549 (red) conjugated	Vector laboratories
Rabbit Anti-mouse- IgG (H+L) Horseradish peroxidase (HRP) conjugated	P 0161, DAKO A/S, Denmark

2.6 Enzymes

Pfu DNA Polymerase	Fermentas
Proteinase K	Fermentas
Restriction enzymes	FastDigest, Thermo scientific
SuperScript [®] III Reverse Transcriptase	Invitrogen
Taq DNA Polymerase	Fermentas
T4 DNA ligase	Fermentas

2.7 Media

Maltose-HL5	14.3 g Bacteriological Peptone, 7.15 g Bacto (dictybase) Yeast Extract, 18 g Maltose monohydrate, 0.64 g Na ₂ HPO ₄ ·2H ₂ O, and 0.49 g KH ₂ PO ₄ . pH 6.6, volume raised to 1L with dH ₂ O and autoclaved (Cornillon et al. 1994)
LB-Medium	1% (w/v) NaCl, 1% (w/v) Tryptone, and 0.5% (w/v) Yeast Extract dissolved in dH ₂ O.
LB-Amp-Medium	LB-Medium, 50 µg/ml Ampicillin (added after autoclave)
LB-Agar	LB-Medium, 1.5% (w/v) Agar-Agar

2% SM-Agar (G+)	10 g Agar-Agar, 5 g Bacteriological peptone, 0.5 g Bacto yeast extract, 1.1 g KH_2PO_4 , 0.5 g K_2HPO_4 , 0.5 g $\text{MgSO}_4 \cdot 7\text{H}_2\text{O}$, and 1% (w/v) Glucose (25 ml from 20% glucose [filter sterilised] was added after autoclave in 475 ml of G+ medium) was dissolved in dH_2O (Sussmann et al., 1966)
2% SM-Agar (G-)	10 g Agar-Agar, 5 g, Bacteriological peptone, 0.5 g Bacto yeast extract, 1.1 g KH_2PO_4 , 0.5 g K_2HPO_4 , 0.5 g $\text{MgSO}_4 \cdot 7\text{H}_2\text{O}$, volume was raised to 500 ml with dH_2O and autoclaved. (Pierre Cosson's lab)
2% SM-Agar plates (G+/ G-)	35 ml SM -Agar (G+/ G-) poured per Petri dish (8 cm diameter)
SOC-Medium	2% (w/v) Tryptone, 0.5% (w/v) Yeast Extract, 10 mM NaCl, 25 mM KCl, 10 mM MgCl_2 , 10 mM MgSO_4 , and 20 mM Glucose (100 μl from 2 M Glucose [filter sterilised] was added after autoclave) dissolved in dH_2O

2.8 Microscope

Inverted, Phase contrast ULWCD 0.30 microscope	Olympus
Fluorescence microscope: Imager. Z1, with ApoTome; Axio Cam MRc and MRm camera	Zeiss
Stereo light optical microscope	Leica WILD MZ8
Stereo microscope	Leica M80
SZX12 Fluorescence stereozoom microscope with DP71, U-TV1X-2, U-CMAD3 camera	Olympus
Software for the Imager. Z1: AxioVision Rel 4.7.1 (08-2008)	Zeiss
Software for the SZX12 fluorescence microscope: cellA, Olympus soft imaging solutions	Olympus

2.9 Oligonucleotides

2.9.1 PCR primers for the gene targeting vector

<i>sapA</i> 1-5' FP	5'-CGCGGATCCGGGAGTACTTTGAAACCACC-3'
<i>sapA</i> 1-5' RP	5'-CGCCTGCAGGAAGCTAATATTATTGTG-3'
<i>sapA</i> 1-3' FP	5'-GCAAGCTTGCAAACAATTTGTTGATTCAAATT TCC-3'
<i>sapA</i> 1-3' RP	5'-CGCGTTCGACCATTAAACAGATTTAGA TATCC-3'
* <i>Dall</i> -5' FP	5'-CTCGGATCCAAATCCATTTTCAGGGGAT-3'
* <i>Dall</i> -5' RP	5'-CTCCTGCAGTTTCACAAATTTTCGCAACC CAC-3'
* <i>Dall</i> -3' FP	5'-CTCGTTCGACCATCAGATCTCCCATCAGT AGG-3'
* <i>Dall</i> -3' RP	5'-CTCGGTACCCAATGGTGATGGACAGACA CAC-3'
* <i>DalP</i> -5' FP	5'-CGCGGATCCATCCTAAAACATAACCG AATC-3'
* <i>DalP</i> -5' RP	TCCTGCAGCAGCAAATTCACATAAATCACA GCC-3'
* <i>DalP</i> -3' FP	CGCAAGCTTATGATATTAGCAGCTCCAATT GC-3'
* <i>DalP</i> -3' RP	CTCGTTCGACGATATGAAATCTTTGCCAC CTC-3'
C2-5' FP	5'-CTCGGATCCGAATCAAATCTTCTTCC-3'
C2-5' RP	5'-CGCCTGCAGTAGTGGTTAGAGTTGGACC-3'
C2-3' FP	CGCAAGCTTTTCTCCAGAACATTGTGG TG-3'
C2-3' RP	5'-CGCGTTCGACGTAGTAAATTAATTTGTTTAC-3'
C3-5' FP	CGCGGATCCCAAACACTGCTATAAATATC TGC-3'
C3-5' RP	CTGCAGGAGCAATACAAATCATATCAGTTT GG-3'
C3-3' FP	5'-CTCAAGCTTAAGGATGGAACACATGTATGG-3'

C3-3'RP 5'-GCGTCGACCCAAGTTTGTTTAATACTACT
CG-3'

2.9.2 PCR primers for screening the knock-out clones

*DalD (sapA1)

U1-FP 5'-AGTGAAGAAATTGTGGGTGTGTG-3'
U1-RP 5'-CATTTCGGCAGTACATATTGAAGCG-3'
D1-FP 5'-GTGGAGTATGTGGCTCTTCTGATG-3'
D1-RP 5'-CGAGTTTTAAACAATTCATTAC-3'

*Dal I

SET-1-FP 5'-CGCGGATCCGA ACTATCATAACTACCATG
TGG-3'
SET-1-FP 5'-CTTGATAGTATTGATGGTACACC-3'
SET-1-RP 5'-CTGCAGGGTAAAGTGTTTAAAGCGTTGGG
TG-3'
SET-2-FP 5'-CTCGGATCCAAATCCATTT CAGGGGAT-3'
SET-2-RP 5'-CGCTTCAATATG TACTGCCGAAATG-3'
SET-2-Dup.RP 5'-GAAGATTGTGAACATAATCCAAGTTGATC
GC-3'
SET-3-FP 5'-CTCATGCACACTAATTATTTGAAATCTCG-3'
SET-3-RP 5'-CTGGTGATCCTGTTGGTGTATTATTGC-3'

*Dal P

SET-1-FP 5'-GCATAACTAAGAAATTTAACAAG
ATTCGAACCC-3'
SET-1-RP 5'-CTCCTGCAGCAGCAAATTCACA
TAAATCACAGCC-3'
SET-2-FP 5'-CGCGGATCCATCCTAAAACATAACCGA
ATC-3'
SET-2-RP 5'-CGCTTCAATATG TACTGCCGAAATG-3'
SET-2-Dup.RP 5'-ATACCTCCATTGTAATATTTGATGG-3'
SET-3-FP 5'-CGCAAGCTTATGATATTAGCAG
CTCCAATTATTGC-3'
SET-3-RP 5'-GAAAATGCATGTTGTTAATGGGTC-3'

lyC2

SET-1-FP	5'-CAGAATGTTTCGTTAACTGGTAAGTA-3'
SET-1-RP	5'-CGTAAACTGATGTACACATTCATAGT GG-3'
SET-2-FP	5'-AAGGTGATACTTACACATGTAGTCAAAT GC-3'
SET-2-RP	5'-CGCTTCAATATGTAAGTCCGAAATG-3'
SET-2-Dup.RP	5'-GATGTTGGGTTAATGGCTTGAGT-3'
SET-3-FP	5'-ATCAACTCATGGCTCAACAACTC-3'
SET-3-RP	5'-AGAACAAACATTCATATTACTTCAGGG-3'
SET-1-FP (A)	5'-TTTTTGTGTGGCGTAGCAAAT-3'
SET-1-FP (B)	5'-GGGTGTTATTGTTGATAAACATGTG-3'
SET-1-FP (C)	5'-AAAAACACACCGCATCGTTTAG-3'

lyC3

SET-1-FP	5'-CTCGGATCCATTGCAGGTCACAATGAA CC-3'
SET-1-RP	5'-CGCCTGCAGGAGCAATACAAAT CATATCAGTTTGG-3'
SET-2-FP	5'-CGCGGATCCCCAAACTGCTATAAATATC TG-3'
SET-2-RP	5'-CGCTTCAATATGTAAGTCCGAAATG-3'
SET-2-Dup.RP	5'-GATTTGTAGCTGTTGGATTCC-3'
SET-3-FP	5'-CTCAAGCTTAAGGATGGAACACATGTATGG-3'
SET-3-RP	5'-GTGAATAAGATCTTGTCAATAACTAGTTG-3'

2.9.3 Quantitative real-time PCR (qRT-PCR) primers

<i>aplD</i> 5' FP	5'-TCACAATAATATTAGCTTCATTATTTGC-3'
<i>aplD</i> 5' RP	5'-AATCCATGTTCAATACTTCAACTG-3'
<i>GAPDH</i> FP	5'-TGTCCCAATTGGTATTAATGG-3'
<i>GAPDH</i> RP	5'-GTGGGTTGAATCATATTTGAAC-3'
<i>rnlA</i> FP	5'-AGTCGATCAGAGACGCAAG-3'
<i>rnlA</i> RP	5'-GGTGCCGAACCACATAAC-3'

2.9.4 PCR primers for the *ApID*-FLAG intracellular localisation

pDNeoDP 5'-CCGCTGCAGAAAATGTATAAAATTA
ATATTTATTTATTAATATTCAC-3'

pDNeoDP 5'-CCAGGATCCATTTTTAATACTATTTT
GTTTTTCAAATGTC-3'

2.9.5 PCR primers for the *apID* expression under *apID* promoter

FP2 5'-CAGCTCGAGCAAAAAGTATCTTAAGT-3'

RP1 AGACTAGTATTTTTAATACTATTTTGTTT
TTCAAATGTC-3'

2.9.6 PCR primers for the *apID* expression under *act15* promoter

FP3 5'-CCGACTAGTATGTATAAAATTAATATTT
ATTTATTAATATTCAC-3'

RP1 5'-CAGACTAGTATTTTTAATACTATTTTGT
TTTTTCAAATGTC-3'

RH1 5'-TATATGCATTAGATGTAAAACAGCCA-3'

pDM1 5'-TCCATGTTCAATTAATTCAACTG-3'

pDM2 5'-GTCAACTTCATTAACTTGTACCT-3'

pDM3 5'-TCACTTCTTTAACACCCACACAC-3'

2.9.7 pDrive and TOPO vector primers for PCR and DNA sequencing

M13rev -29 5'-AACAGCTATGACCATG-3'

T7 Promoter 5'-TAATACGACTCACTATAGGG-3'

Oligo-dT₁₇ 5'-GACTCGAGTCGACATCGAT₁₇-3'

Note: *Dal* renamed as *apl*, *Dall* renamed as *aplJ*

2.10 Instruments

Biometra TI3	Biometra biomedizinische analytic GmbH
Digital Graphic Printer UP-D897	Sony
Water filtration unit	TKA-GenPure
DNA electroporation unit	BTX ECM 830 electroporator holder, BTX ECM 630 electroporator
DNA electroporation unit	Gene Pulser [®] II, Bio-Rad Laboratories GmbH
Electronic Delta Range balance	Mettlar PM4600
Electroporation cuvettes (1 mm)	Cell projects
Electroporation cuvettes (2 mm)	BTX Harvard Apparatus
Electrophoresis unit	Peqlab biotechnology GmbH
IKA-COMBIMAG RET	Janke & Kunkel GmbH
Ionmeter	WTW
KERN ABJ electronic balance	KERN & Sohn GmbH
Mastercycler ep gradient	Eppendorf
Nucleic acid/ Protein quantification	NanoDrop [®] , ND-1000 Spectrophotometer, ND-1000 V3.7.1
Photometer Ultraspec 1100 pro qRT-PCR	Amersham Bioscience LightCycler Run 5.10-LC DO.Exp, Roche; equipped with lightcycler software version 3.5, Roche molecular biochemicals
Thermomixer comfort	Eppendorf
UV- Transilluminator	PHASE (http://www.phase-hl.com)
UV transilluminator	Bio-Rad Laboratories GmbH
Vortex	Heidolph
Western blotting unit	PHASE

2.10.1 Incubators/ Shakers

Incubator	Heraeus
-----------	---------

Innova [®] 40 incubator shaker series	New Brunswick Scientific
Shaker/ Incubator	Infors HT Multitron
Shaker/ Incubator	Innova [®] 4230, refrigerated incubator shaker, Edison, NJ-USA, New Brunswick Scientific.

2.10.2 Centrifuges

Centrikon H-401 refrigerated centrifuge	Kontron, München
Mini Tabletop centrifuge	ROTH
Mini Spin	Eppendorf
Refrigerated centrifuge Rotanta 460R	Hettich
Refrigerated centrifuge 5402	Eppendorf

2.10.3 Sterile air flow units

LaminAir HB 2448 K	Heraeus Instruments
KOJAIR [®]	Kojair Tech, Finland

2.11 Accessories

Blotting paper (Whatman 3MM Chr; GB33, western blotting)	A. Hartenstein
Cover slips (Ø 18 mm, #1)	Thermo scientific
Cryo container	Nalgene, Nalge Nunc International
Cryo tubes	Sarstedt
Membrane filters (0.2 µm)	STERILE R, Sarstedt
Needle (slug infection)	(Ø 0.60 x 30 mm, 23G x 1 ^{1/4}), Sterican
Needle (slug cutting)	(Ø 0.30 x 12 mm, 30G x 1 ^{1/2}) Sterican

PVDF membrane Immuno-Blot™	ROTH
Syringe (slug infection and slug cutting)	(0.01 – 1 ml/ Luer Solo), STERILE EO, B BRAUN Injekt F
Petri dishes (8 cm dia, tissue culture)	Sarstedt
Petri dishes (3.2 cm, 5 cm, 8.5 cm and 14 cm)	STERILE R, Sarstedt
24-well tissue culture plates	Sarstedt

3 METHODS

3.1 *D. discoideum* cultures

All experiments were performed using *D. discoideum* Ax2-214, referred to as Ax2 wild type strain and all five single gene knock-out (KO) mutants were generated in the Ax2 background. Frozen amoebae stocks (stored in liquid nitrogen) or spore stocks (-80 °C) were used to start the pre-cultures. *D. discoideum* cells were grown in Petri dishes (8.5 cm diameter) with 10 ml Maltose-HL5 medium per Petri dish. To avoid bacterial and fungal contaminations, 10 µg/ml Penicillin-Streptomycin mix (Sigma) was added to pre-cultures. All experiments were performed with cells grown in Petri dishes, with Maltose-HL5 medium for no longer than four weeks.

3.2 *D. discoideum* cell stock and culture preparation

The Petri dishes with monolayer of adhering cells were used to prepare the amoebae stocks. The existing Maltose-HL5 medium was removed to get rid of the floating cells and the plates were gently tapped at the rim to detach the adhering cells. The cells were harvested in Maltose HL5 medium and centrifuged at 510 x g for 7 min at 18 °C. The cell pellet was resuspended in 2 ml cold Maltose-HL5 medium containing 10% DMSO. This cell suspension was transferred into the pre-chilled cryo tubes and placed in the pre-chilled cryo box (Nalgene, Nalge Nunc International) overnight at -80 °C, before transferring to liquid nitrogen. To start a pre-culture, the frozen amoebae stock was removed from liquid nitrogen and quickly thawed in the running tap water. The cryo tube was opened under the laminar air flow chamber and the cell suspension was emptied into a Petri dish with 10 ml Maltose-HL5 medium. When reviving transgenic strains, the appropriate antibiotic selection was added after 24 h. Exponential cell growth was observed after a week.

3.3 *D. discoideum* spore stock preparation and reviving spore stocks

Axenically grown *D. discoideum* amoebae were harvested from the Petri dishes and centrifuged at 510 x *g* for 7 min at 18 °C. The cell pellet was resuspended in SB, washed once and finally resuspended in 100 µl-SB, before plating on 1%-SB agar plate. The plate was incubated in a dark, moist chamber at 22 °C and the mature fruiting bodies were collected after 48 h. The spore heads were touched with a micropipette tip and resuspended in 25% glycerol prepared in SB. The spore suspension was incubated on ice for 10 min before transferring to -80 °C. To start a pre-culture, the frozen spore stock was opened under the laminar air flow chamber and a pinch of frozen stock was transferred to a Petri dish with Maltose-HL5medium. To avoid fungal contamination 10 µg/ml Penicillin-Streptomycin mix was added to the culture plate. A confluent monolayer of amoebae was observed within a week.

3.4 Bacterial stocks preparation and reviving frozen stocks

A volume of 750 µl of overnight bacterial culture was mixed with 250 µl of glycerol and transferred to a cryo tube. The cryo tube was incubated on ice for 10 min and then stored at -80 °C. To prepare overnight bacterial cultures, the frozen stock was streaked on the LB agar plates and incubated overnight at 37 °C. At required conditions the appropriate antibiotic selections were added. The next day, a single colony was used to start the overnight culture.

3.5 *D. discoideum* genomic DNA isolation

Nuclear lysis buffer	50 mM HEPES (pH 7.5, 1 M stock), 40 mM MgCl ₂ (1 M stock), 20 mM KCl (1 M stock), 5% (v/v) Sucrose (10% (w/v) stock, filter sterilised), and 1% (v/v) Nonidet P-40 dissolved in dH ₂ O
----------------------	--

The nuclear lysis buffer was freshly prepared from the stock solutions before starting the genomic DNA isolation.

SDS lysis buffer	0.7% (w/v) SDS dissolved in TE buffer
TE buffer	10 mM Tris-Cl (pH 7.5, 1 M stock), 500 mM EDTA (pH 8.0, 1 M stock)
Proteinase K	140 μ l (2.6 mg/ml, Fermentas)
CH ₃ COONa	3 M

This protocol was adopted from dictybase.org (Hughes, Ashtorab, and Welker 1988) with some minor modifications. The axenically grown Ax2 cells were harvested from the Petri dishes and a total number of 1×10^8 cells were centrifuged at $300 \times g$ at 20°C for 6 min. The cell pellet was washed with ice-cold KK2 buffer and resuspended in 45 ml of the nuclear lysis buffer, before adding the non-ionic detergent, Nonidet P-40 (NP40) until the solution becomes clear, maximum 5 ml. This resulted in cell lysis, but the nucleus remained intact. The cell lysate was sedimented at $3,500 \times g$ at RT for 15 min to pellet the nucleus, which was resuspended in 5 ml of SDS lysis buffer containing 200 $\mu\text{g/ml}$ Proteinase K. The cell suspension was mixed gently by inverting the tube and was incubated at 60°C for 2 h. Subsequently, the nuclear suspension was divided into 1 ml aliquots in microcentrifuge tubes, followed by addition of an equal volume of phenol:chloroform. The samples were mixed by inverting the tubes for 10 times before centrifugation at $18,000 \times g$ at RT for 12 min. The resulting aqueous phase was extracted with an equal volume of chloroform. Chloroform extraction step was repeated until the aqueous phase becomes clear. The genomic DNA was precipitated by adding 1/10 volume of 3 M sodium acetate and twice the volume of absolute Ethanol (EtOH) to the aqueous phase and centrifuged at $15,294 \times g$ for 12 min. After washing the DNA pellets with 70% EtOH ($15,294 \times g$, 10 min at RT), the DNA pellets were air dried at 37°C for 20 min, resuspended in 100 μl of ice-cold dH₂O, and stored at 4°C .

3.6 DNA manipulation reactions

3.6.1 Amplification of DNA fragments by Polymerase chain reaction (PCR)

To amplify the DNA fragments of interest by PCR, the standard PCR mix was prepared as described below (**Tab. 2**). All the PCR analyses were carried out using the Thermal Cycler (Eppendorf). The DNA fragments of interest were amplified by subjecting the PCR mix in the PCR programme detailed below (**Fig. 10**). Although the optimal temperature for the Taq DNA polymerase to carry out DNA amplification is at 72 °C, the AT rich genome of *D. discoideum* allows DNA amplification best at 62 °C (Su et al. 1996). For this reason both, the primer extension (**Fig. 10D**) and the final extension (**Fig. 10E**) steps were carried out at 62 °C. The resulting DNA samples were used for downstream processes such as agarose gel electrophoresis, restriction digestion and DNA ligation.

Tab. 2: Standard PCR mix

*At required conditions 1:20 ratio of the *Pfu* DNA polymerase (2.5 U/μl, recombinant) and the *Taq* DNA polymerase were used in the standard PCR mix.

Constituents	Test	Water control
10X Advantage 2 PCR buffer	2 μl	2 μl
dNTPs mix (10 mM each)	1 μl	1 μl
Forward primer (10 μM)	1 μl	1 μl
Reverse primer (10 μM)	1 μl	1 μl
DNA sample	1 μl (< 10 ng)	-----
* <i>Taq</i> DNA polymerase (5 U/μl)	0.4 μl	0.4 μl
dH ₂ O	13.6 μl	14.6 μl
Total	20 μl	20 μl

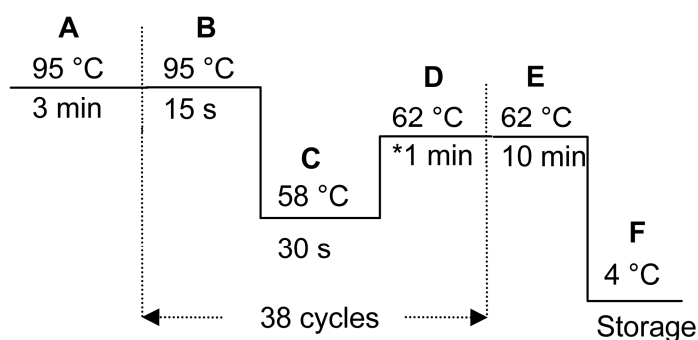


Fig 10: Standard PCR programme. PCR samples were incubated in thermal cycler at **A**= 95 °C 3min; initial denaturation, **B**= 95 °C 15 s; denaturation, **C**= 58 °C 30 s; primer annealing, **D**= 62 °C 1 min; primer extension, (*) duration varies with amplicon size, **E**= 62 °C 10 min; final extension and **F**= 4 °C; product storage.

3.6.2 PCR product purification

The PCR product was purified according to the manufacturer's instructions (PCR clean-up, MACHEREY NAGEL). DNA samples were mixed with twice the volume of binding buffer (NT), before loading onto a NucleoSpin Extract II column and centrifugation at 11,000 x *g* at RT for 2 min. Columns were washed with 700 µl of wash buffer (NT3) and empty columns were spun at 11,000 x *g* at RT for 3 min or incubated at 70 °C for 2 min to remove residual wash buffer. DNA was eluted from the columns by adding 20 µl of elution buffer (NE) and centrifugation at 11,000 x *g* at RT for 2 min. The DNA samples were stored at 4 °C for short term or -20 °C for long term.

3.6.3 Small scale plasmid DNA isolation

Plasmid DNA isolations were carried out with the NucleoSpin plasmid quickpure kit (MACHEREY NAGEL), with some minor modifications to increase the plasmid yield. The bacterial cultures were grown with appropriate antibiotic, overnight at 37 °C. The cultures were harvested at 9,700 x *g* at RT for 2 min and the bacterial pellets were resuspended in 100 µl of ice-cold resuspension buffer (A1). The bacterial suspensions were sedimented again and the pellets were resuspended in 250 µl of ice-cold A1 buffer. Lysis of bacteria was achieved by adding 250 µl of lysis buffer (A2) and incubation at RT for 5 min. Following this, 300 µl of neutralisation buffer (A3) was added and mixed by inverting the tubes. Cell lysates were centrifuged at 9,700 x *g* at RT for 7 min and the supernatants were loaded onto the columns. Columns were centrifuged at 9,700 x *g* at RT for 2 min and the flow through was discarded. After washing with 450 µl of wash buffer (AQ), the columns were placed in fresh microcentrifuge tubes and incubated with 15 µl-elution buffer (AE) at RT for 5 min. Finally, the columns were centrifuged at 9,700 x *g* at RT for 3 min to elute the DNA and stored at 4 °C or -20 °C.

3.6.4 Large scale plasmid DNA isolation

Frozen bacterial stock was revived as described in **section 3.4** and 1 ml overnight bacterial culture was removed to inoculate a 100 ml LB broth containing antibiotic selection. The culture flask was incubated overnight at 37 °C, 220 rpm. Before starting the plasmid isolation, the culture was stored at 4 °C for 30 min to stop cell doubling. The overnight culture was centrifuged at 4,430 x g at 4 °C for 12 min and the plasmid DNA was isolated following the manufacturer's guidelines (Qiagen Maxi prep kit). The DNA pellet was dissolved in ice-cold dH₂O, incubated on ice for 10 min and stored at -20 °C.

3.6.5 Restriction endonuclease digestions

Restriction digestion reactions were performed following the manufacturer's directions (Fast digest, Thermo scientific). Restriction endonuclease digestion DNA samples were prepared as described in the standard reaction mix (**Tab. 3**) and the desired DNA nicks were achieved by incubating the samples in the standard reaction programme described below (**Fig. 11**). The restriction digested DNA samples were analysed on an agarose gel. Successful DNA samples were column purified (NucleoSpin Extract II columns, MACHERY NAGEL) and the DNA concentration was measured with NanoDrop.

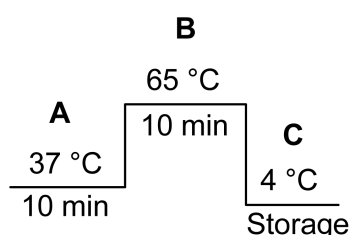


Fig. 11: Standard reaction set-up. Restriction digestion reactions were carried out by incubating samples at **A**= 37 °C for 10 min; restriction digestion, **B**= 65 °C for 10 min; enzyme inactivation, and **C**= 4 °C; product storage.

Tab. 3: Standard reaction mix

The volume of the DNA sample was scaled up to 10 µl or down to 0.5 µl depending on the DNA concentration and the volume of water was corrected to keep the indicated total reaction volume. The same reaction standards were followed for double digestions.

Constituents	Plasmid DNA	PCR product
Water (nuclease free)	15.5 µl	17.5 µl
10X buffer	2 µl	2 µl
DNA samples	2 µl (up to 1 µg)*	10 µl (0.2 µg)*
Enzyme	0.5 µl	0.5 µl
Total	20 µl	30 µl

3.6.6 Agarose gel electrophoresis

DNA loading dye	50% (v/v) Glycerin (87%), 10 mM EDTA, 0.1% (w/v) SDS, 0.025% (w/v) Bromophenol blue (BPB), and 0.025% (w/v) Xylene cyanol, pH 8.0
50X TAE buffer	242 g Tris-base, 57.1 ml Glacial acetic acid, and 18.6 g EDTA dissolved in 1L dH ₂ O
UltraPure Agarose	1.5% (w/v)

1.5% agarose gel in 1X TAE buffer was prepared according to routine lab practise. In general, 1.5 µl ethidium bromide (EtBr) was added to a 20 ml-agarose preparation. Finally, DNA samples were mixed with the DNA loading dye before separation on the agarose gel. For the mini-gels (5 cm x 5 cm), initial voltage was set as 30 V for 20 min, then increased to 80 V. For large gels (10 cm x 10 cm), the initial voltage was set as 60 V for 20 min and later increased to 100 V. DNA was visualised using a UV transilluminator.

3.6.7 DNA extraction from agarose gel

DNA samples were excised from gels under UV-light. Gel pieces were placed on the columns (Ambion) and centrifuged at 14,000 x *g* at RT for 5 min. During centrifugation the DNA was forced through the columns and was collected in the collection tubes. The concentration of DNA samples were measured with the NanoDrop.

3.7 DNA ligation

Linearised plasmid DNA and the desired insert (PCR product) were ligated as described in the standard reaction mix (**Tab. 4**). As a control, linearised vector alone was used to determine self-ligation rate. In general, the vector and the insert were mixed at a molar ratio of 1:5. The quantity of insert required was calculated

using the formula described below. Ligation reactions were incubated at 4 °C overnight, followed by bacterial transformation.

$$\text{Insert quantity (ng)} = \frac{\text{Vector quantity (ng)} \times \text{insert length (bps)} \times (\text{V:I}) \text{ molar ratio}}{\text{Vector length (bps)}} \times 100$$

ng= nano grams

bps= base pairs

V= Vector, I= Insert

Tab. 4: Standard reaction mix

Constituents	Test	Vector control
10X T4 DNA Ligase buffer	1 µl	1 µl
Vector (plasmid DNA)	2 µl (up to 25 ng)	2 µl (up to 25 ng)
Insert (PCR product)	2 µl	-----
Polyethylene glycol (PEG)	1 µl	1 µl
T4 DNA Ligase (5 U/µl)	0.5 µl	0.5 µl
dH ₂ O	3.5 µl	5.5 µl
Total	10 µl	10 µl

3.8 Bacterial transformation

3.8.1 Chemical competent cells preparation with *E. coli* DH5α

TfB-I 30 mM C₂H₃KO₂, 50 mM Cl₂Mn.4H₂O, 100 mM KCl, 10 mM CaCl₂, and 15% (v/v) Glycerin.

TfB-II 10 mM Mops, 75 mM CaCl₂, 10 mM KCl, and 15% (v/v) Glycerin dissolved in dH₂O, pH 7.0 (adjusted with NaOH)

TfB-I and TfB-II buffers were filter sterilised (0.2 µm filter) and stored at 4 °C no longer than a month.

The frozen bacterial stock was revived as described before (see **section 3.4**). LB broth was inoculated with 1%-overnight culture and incubated at 37 °C, 220 rpm until OD₆₀₀ reached 0.48 to 0.50. Cells were incubated on ice for

15 min before centrifugation at 1,970 x *g* at 4 °C for 5 min. Bacterial pellet was resuspended in 15 ml of ice-cold TfB-I buffer and incubated on ice for 15 min. Cells were harvested at 1,970 x *g* at 4 °C for 5 min, resuspended in 4 ml ice-cold TfB-II buffer and incubated on ice for 15 min. Aliquots of 200 µl were prepared in the ice-cold microcentrifuge tubes and stored at -80 °C.

3.8.2 Transformation

Frozen chemical competent cells were thawed on ice. After addition of DNA ligation mix, the cell suspensions were incubated on ice for 30 min, then heat shocked at 42 °C for 90 s and incubated on ice for 90 s. To proceed with recovery phase, 1 ml LB broth was added to the cell suspensions and incubated at 37 °C for 45 min, before selection on LB agar plates with appropriate antibiotics.

3.9 Colony PCR

Bacterial clones obtained after transformations were analysed by PCR to identify the positive clones. Colony PCR was performed as described earlier (see **Tab. 2**). Instead of using DNA templates, individual bacterial clones were mixed in the standard reaction mix, then subjected to regular PCR programme (**Fig. 10**). Standard primers used for colony PCR include M13 forward and reverse primers or gene specific primers.

3.10 DNA sequencing

DNA fragments or plasmids were sequenced by Eurofins MWG Operon (<http://www.eurofindna.com>). The standard primers used for DNA sequencing includes, M13 forward (-20), M13 reverse (-29), and T7 promoter or gene specific primers.

3.11 Bioinformatics

In general, all DNA and protein information concerning *D. discoideum* was retrieved from dictyBase (<http://dictybase.org>). *D. discoideum* genes were subjected to BLAST analysis using the tool available at dictyBase (<http://dictybase.org/tools/blast>). Additionally, *D. discoideum* gene homologues and paralogues were examined using the BLAST analysis tool available at the pubmed/NCBI (<http://blast.ncbi.nlm.nih.gov/>). *D. discoideum* cDNA information was obtained from *D. discoideum* cDNA Distribution Centre Japan and National Bio Resource Project Japan (<http://nenkin.lab.nig.ac.jp>, NBRP). DNA sequencing results were analysed using ClustalW2 available at EMBL-EBI Institute (<http://www.ebi.ac.uk/Tools/msa/clustalw2/>).

3.12 Analytical tools

Various analytical tools were used to investigate the experimental data. Phagocytosis and killing assay graphs were created using SigmaPlot 10 (www.systat.com) and also tested using R, the computer programming tool for statistical analyses (version 2.15.0) to derive the statistical significances. The *ap1D* fold expression (during Ax2 development) graph was generated using Microsoft Office Excel 2003. The charts for spore viability spore formation efficiency and the graph for *ap1D* fold expression in xenic Ax2 cultures were created with using the software analytical tool GraphPad Prism, version 3.02 (www.graphpad.com).

3.13 *D. discoideum* transfection

H50 electroporation buffer	20 mM HEPES, 50 mM KCl, 10 mM NaCl, 1 mM MgSO ₄ , 5 mM NaHCO ₃ , and 1 mM NaH ₂ PO ₄ dissolved in dH ₂ O and autoclaved, stored at -20 °C
----------------------------	--

D. discoideum transfections were achieved using electroporation technique (Schlatterer, Knoll, and Malchow 1992); (Pang, Lynes, and Knecht 1999). Axenic

After electroporation, cuvettes were incubated on ice for 10 min and cell suspensions were transferred to Petri dishes with 10 ml Maltose-HL5 medium. The culture was incubated at 22 °C and 24 h later 8 µg/ml Blasticidin selection was added. Clones appeared after a week. Blasticidin resistant clones were aspirated from the Petri dishes and seeded in multi-well plates for later PCR analyses.

3.16 *D. discoideum* genomic DNA isolation

The exponentially growing individual clones were harvested from multi-well plates and sedimented at 1,700 x g at RT for 2 min. The genomic DNA was isolated as described in the following sections.

3.16.1 Method-I

Ax2 genomic DNA was isolated using the High pure PCR template purification kit (Roche). A total number of 1×10^7 cells were used for each preparation and the isolated genomic DNA was stored at 4 °C.

3.16.2 Method-II

Lysis buffer 50 mM KCl, 10 mM Tris (pH 8.3), 2.5 mM MgCl₂, 0.45% (v/v) Nonidet P-40, and 0.45% (v/v) Tween 20 dissolved in dH₂O.

Genomic DNA was isolated from the *D. discoideum* KO clones to carry out PCR analyses (Charette and Cosson 2004). KO clones were harvested at 500 x g at RT for 7 min. Cell pellets were resuspended in 5 µl of Maltose-HL5 medium and 20 µl of lysis buffer, including 1 µl of 2.6 mg/ml Proteinase K (Fermentas) and mixed thoroughly by pipetting. For a 20 µl-PCR reaction, 1 µl cell lysate was added and remaining cell lysate was stored at -20 °C

3.17 RNA isolation

Axenically grown *D. discoideum* cells were harvested and cell density was determined. A total number of 5×10^6 cells were collected at $500 \times g$ at $18 \text{ }^\circ\text{C}$ for 7 min and RNA was isolated using the RNA magic kit (Bio-Budget Technologies GmbH). RNA pellet was resuspended in $15 \text{ }\mu\text{l-dH}_2\text{O}$, incubated on ice for 15 min and stored at $-80 \text{ }^\circ\text{C}$.

3.18 First strand cDNA synthesis

cDNA synthesis was carried out according to manufacturer's instructions (Fermentas). cDNA reaction mix was prepared as described below (**Tab. 5**) and cDNA synthesis was carried out by incubating the samples in the standard cDNA synthesis programme (**Fig. 12**). cDNA samples were purified (NucleoSpin Extract II, MACHEREY NAGEL) and stored at $-20 \text{ }^\circ\text{C}$ no longer than 3 days, before proceeding to quantitative RT-PCR experiments (qRT-PCR).

Tab. 5: Standard cDNA reaction mix

Mix-I	2 μg RNA, 5 μM Oligo dTT or 3'- RACE primers from 50 μM stock, 1 mM dNTPs from 10 mM stock, volume increased to 10 μl with dH_2O
Mix-II	4 μl 5X First strand buffer, 1 μl RNase inhibitor (RNaseOUT, Invitrogen) and 4 μl dH_2O
Reverse transcriptase	1 μl SuperScript III (Invitrogen)

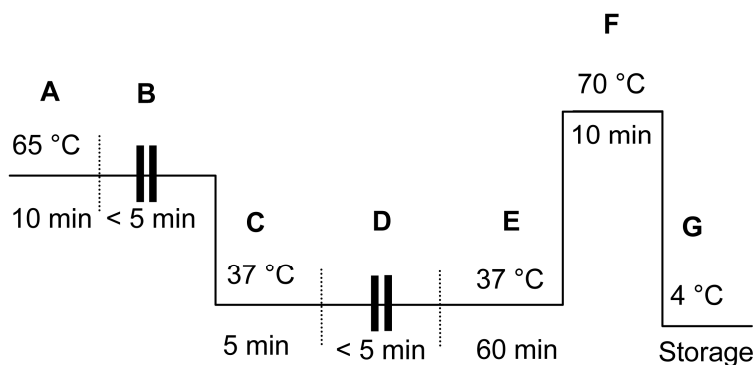


Fig. 12: Standard cDNA synthesis programme. cDNA was synthesised by incubating the standard cDNA reaction mix in the following programme. **A**= 65 °C for 10 min; denaturation, **B**= 5 min pause to add Mix-I, **C**= 37 °C for 5 min; primer annealing, **D**= 5 min pause to add Mix-II, **E**= 37 °C for 60 min; cDNA synthesis, **F**= 70 °C for 10 min; enzyme inactivation, and **G**= 4 °C; product storage

3.19 Cell lysate preparation for western blotting

Extraction buffer	3 M Urea, 2% (w/v) SDS, 1% (w/v) Chaps, and 10% (v/v) Glycerol dissolved in dH ₂ O, pH 6.8
Protease Inhibitor Complete (PIC)	1 tablet dissolved in 1 ml dH ₂ O (50X) Before use, the PIC (Roche) solution and the extraction buffer were mixed at a ratio of 1:20

Cell lysates were prepared from *aplD*⁻ cells transfected with the pDneo2a-3xFLAG[*act6/aplD*] plasmid to confirm the AplD-FLAG fusion protein expression. Non-transfected *aplD*⁻ cells were used as negative control for western blot analysis. To prepare the cell lysate, 1 x 10⁶ cells were mixed with 100 µl of extraction buffer. Cell suspensions were mixed vigorously to dissolve the cell pellets. This was followed by centrifugation at 20,000 x *g* at 4 °C for 20 min. The supernatants were collected and stored at -20 °C.

3.20 SDS-polyacrylamide gel electrophoresis (SDS-PAGE)

30% Acrylamide (32:1 ratio)	
30% Acrylamide (49:1 ratio)	
Ammonium persulfate (APS) 40% (w/v)	400 mg in 1 ml dH ₂ O
Gel buffer (3X)	36.3 g Tris and 0.3 g SDS was dissolved in 80 ml dH ₂ O, pH 6.8 (adjusted with 12.5 N HCl) and the final volume was increased to 100 ml with dH ₂ O.
DTT sample buffer (6X)	0.35 M Tris-HCl (pH 6.8), 10.28% (w/v) SDS, 36% (v/v) Glycerol, and BPB dissolved in dH ₂ O.
N,N,N',N'- Tetramethylethylenediamine (TEMED)	
Separating gel (13%)	6.5 ml of 30% (v/v) Acrylamide (49:1), 3 ml of 86% (v/v) Glycerine, 4.5 ml Gel

	buffer (3X), 1 ml dH ₂ O, 7.5 µl TEMED, and 16 µl of 40% (w/v) APS
Stacking gel (4%)	1.3 ml of 30% (v/v) Acrylamide (32:1), 2.25 ml Gel buffer (3X), 6.45 ml dH ₂ O, 10 µl TEMED, and 18 µl of 40% (w/v) APS.
Anode buffer	200 mM Tris, pH 8.9 (adjusted with HCl)
Cathode buffer	100 mM Tris, 100 mM Tricine, and 0.1% (w/v) SDS, pH 8.4
10X Lämmli buffer	144 g Glycin, 30 g Tris, and 10 g SDS dissolved in 1L dH ₂ O

Protein separation was carried out by SDS-PAGE. Tricine buffer system was used to facilitate separation of low molecular weight proteins, ranging between 1 to 100 kDa (Schägger and von Jagow 1987). SDS-PAGE gel used for the protein separation constitutes 13% separating gel and 4% stacking gel (**section 3.20**). Concentration of the protein samples were determined using NanoDrop and 20 µg protein was mixed with the 6X DTT sample buffer to achieve 3X final concentration. Before SDS-PAGE analysis, protein samples were boiled at 70 °C for 15 min and centrifuged at 20,000 x *g* at RT for 2 min. Protein separation was initially carried out at 25 mA for 30 min and then increased to 30 mA until the BPB migrated to the bottom of the gel (~3 h). Finally, the gel was removed from the electrophoresis unit and transferred to the Lämmli buffer until being used for western blotting.

3.21 Western blotting

Transfer buffer	20% (v/v) Methanol (MeOH) in 1X SDS-electrophoresis buffer
10X SDS-electrophoresis buffer	30.3 g Tris-HCl, 144.1 g Glycin, and 10 g SDS dissolved in 1L dH ₂ O, pH 8.3
10X TBS	200 mM Tris, 1.5 M NaCl, pH 7.5 (adjusted with HCl)

TBST buffer	0.1% (v/v) Tween 20 in 1X TBS buffer
Blocking solution	3% (w/v) BSA in 1X TBS buffer
AP buffer	100 mM Tris, 100 mM NaCl, and 5 mM MgCl ₂ dissolved in dH ₂ O, pH 9.5 (adjusted with 1 N HCl)
Primary antibody	Mouse anti-FLAG M2, diluted 1:1000 in 10 ml TBST buffer
Secondary antibody	Goat anti-mouse IgG (H+L), Alkaline Phosphatase (AP) conjugated, diluted 1:10,000 in 10 ml TBST buffer
Substrate	150 mM Nitro blue tetrazolium chloride (NBT) and 150 mM 5-Bromo-4-chloro-3-indolyl-phosphate (BCIP) in AP buffer

PVDF membrane was activated in 100% MeOH for 3 min and Whatman papers were soaked in the transfer buffer for 2 min. Protein transfer process was carried out using the protein blotting unit (PHASE). The gel and the PVDF membrane were sandwiched in between stacks of Whatman papers. Protein transfer was carried out at 63 volts at RT for 30 min. After protein transfer, membrane was incubated in blocking solution for 1 h, rocking at RT, and washed with excess of 1X TBST buffer by rocking at RT for 10 min. After washing, the membrane was incubated in the primary antibody (Mouse anti-FLAG) for 2 days at 8 °C, rocking and washed 5 times with 1X TBST buffer. This was followed by incubation with the secondary antibody (Goat anti-mouse, AP conjugated) for 1 h, rocking at RT, and the membrane was washed 5 times with 1X TBST buffer. Subsequently, the membrane was incubated in the AP buffer for 5 min, rocking at RT. Finally, the substrate for alkaline phosphatase (BCIP and NBT) was added on the membrane. Upon colour development, the reaction was stopped by replacing substrate with dH₂O.

3.22 Growth assays using 24-well plates

2% SM-Agar (G+)	10 g Agar-Agar, 5 g Bacteriological peptone, 0.5 g Bacto yeast extract, 1.1 g KH ₂ PO ₄ , 0.5 g K ₂ HPO ₄ ,
-----------------	---

and 0.5 g $\text{MgSO}_4 \cdot 7\text{H}_2\text{O}$ was dissolved in 475 ml dH_2O and autoclaved. 1% (w/v) glucose (25 ml from 20% (w/v) glucose [filter sterilised]) was added after autoclaving.

2% SM-Agar (G-)

10 g Agar-Agar, 5 g Bacteriological peptone, 0.5 g Bacto yeast extract, 1.1 g KH_2PO_4 , 0.5 g K_2HPO_4 , and 0.5 g $\text{MgSO}_4 \cdot 7\text{H}_2\text{O}$ was dissolved in dH_2O . The final volume was increased to 500 ml with dH_2O and autoclaved.

Both G+ and G- growth assay plates were poured the same way. In a sterile 24-well plate, a volume of 2 ml agar was poured per well and kept undisturbed overnight at RT and stored at 8 °C not more than two weeks.

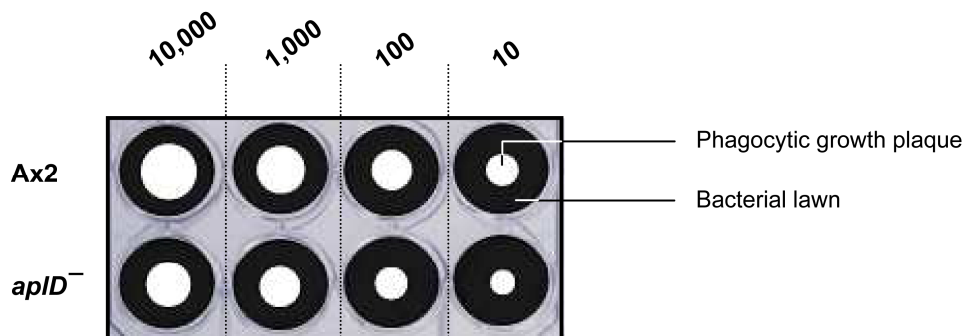


Fig. 13: Diagrammatic representation of a section of the 24-well growth assay plate. The (G+/G-) agar surface was layered with overnight bacterial culture (filled circles) and the *D. discoideum* amoebae were spotted at the centre of the bacterial lawn. Continuous feeding of *D. discoideum* cells result in the phagocytic growth plaques (open circles). In the first row varying numbers of Ax2 cells were deposited and in the second row varying numbers of *apID*⁻ cells were deposited as indicated above the figure.

The ability of the *D. discoideum* cells, Ax2 and *apID*⁻ to grow on different bacterial strains was investigated. Bacterial strains tested in this study are listed below (**Tab. 6**). Fifty microlitre of overnight bacterial culture was seeded in each well of the 24-well assay (G+ and G-) plates. Axenically grown *D. discoideum* cells were harvested from the Petri dishes and their densities were determined. The *D. discoideum* cultures were serially diluted to obtain 2×10^6 cells/ml, 2×10^5 cells/ml, 2×10^4 cells/ml, and 2×10^3 cells/ml. A volume of 5 μl from each dilution was dispensed in individual wells of the 24-well plate, resulting in 10,000, 1,000, 100 and 10 cells per well (**Fig. 13**). The plates were incubated in the dark at 22 °C for a week.

The bacterial virulence grades were determined based on the number of *D. discoideum* cells required to create plaques (Fig. 14).

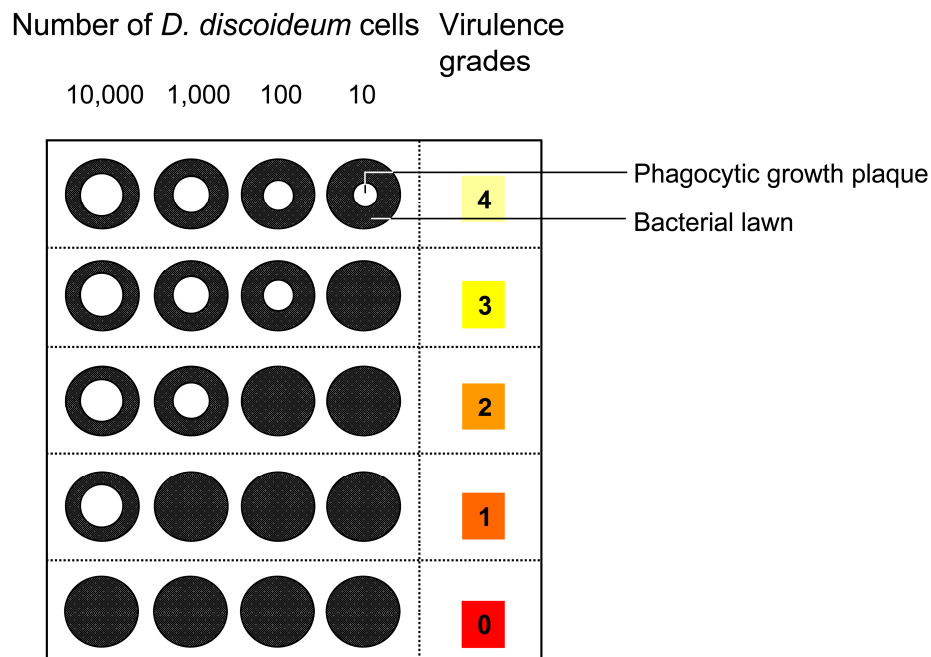


Fig. 14: Bacterial growth assay and virulence grades. Based on the permissiveness for growth plaque formation by *D. discoideum* amoebae, the degree of bacterial virulence was graded (Froquet et al. 2009). The virulence grades start with 4, where even 10 *D. discoideum* cells were sufficient to create growth plaques on the bacterial lawn and the virulence grade ends at 0, where even 10,000 *D. discoideum* cells remain non-permissive for phagocytic plaque formation on the bacterial lawn. The closed circles represent bacterial lawn and open circles in the centre symbolises *D. discoideum* growth plaques.

Tab. 6: List of bacterial strains used for the growth assays

Bacterial strains	Phenotypes
<i>B. subtilis</i>	A non-pathogenic laboratory strain, ATCC# 6051
<i>E. coli</i> B/r	A non-pathogenic food bacteria for <i>D. discoideum</i> (Dicty stock centre)
<i>K. pneumoniae</i>	A non-pathogenic laboratory strain, ATCC# 13883
<i>K. pneumoniae</i> Kp52145	A virulent, encapsulated bacteria with plasmid mediated virulence (Nassif et al. 1989) and (Benghezal et al. 2006).
<i>K. pneumoniae</i> (K^-)	A mutant derivative of Kp52145, defective for capsule synthesis (Nassif et al. 1989).
<i>K. pneumoniae</i> KpLM21	A clinical isolate which produces huge polysaccharide capsule, belongs to serotype K35, typed at the World Health Organisation International <i>Escherichia</i> and <i>Klebsiella</i> Centre, Copenhagen, Denmark ((Favre-Bonté et al. 1999) and (Balestrino et al. 2005)).
<i>K. pneumoniae</i> (<i>waaC</i> ⁻)	A mutant defective for the synthesis of core lipo-polysaccharide of the bacterial outer membrane (Regué et al. 2001).
<i>P. aeruginosa</i> (DP5)	A <i>trpD</i> (in <i>trpGDC</i> operon) mutant defective for tryptophan synthesis (Alibaud et al. 2008)
<i>P. aeruginosa</i> (DP28)	A <i>pchH</i> gene mutant. pyochelin is a siderophore involved in iron uptake in <i>P. aeruginosa</i> (Alibaud et al. 2008)
<i>P. aeruginosa</i> (PT531)	A quorum sensing mutant defective for <i>rhIR</i> and <i>lasR</i> genes (Cosson et al. 2002)

3.23 Phagocytosis and killing of *B. subtilis* (ATCC# 6051) and *KpLM21*

Sucrose	40% (w/v) prepared in filter sterilised SB
Saponin	5% (w/v) prepared in filter sterilised SB
Triton X 100	0.1% (v/v) prepared in filter sterilised SB
SB	8.0 g KH_2PO_4 and 1.16 g Na_2HPO_4 (or 2.2 g $\text{Na}_2\text{HPO}_4 \cdot 7\text{H}_2\text{O}$) pH 6.0 ± 0.1 , volume was raised to 4L with dH_2O and autoclaved. (G Gerisch, Lüderitz, and Ruschmann 1967)

Frozen *B. subtilis* was revived as described before (**section 3.4**). Overnight culture of OD_{600} 2.0 was sedimented at $3,824 \times g$ at RT for 5 min and diluted to OD_{600} of 0.2 in SB. The bacterial suspension was subsequently diluted 1:10 and 1:100 and incubated at RT for 1 h until the *D. discoideum* cultures were prepared. *D. discoideum* cultures at densities 0.5 to 1×10^6 cells/ml were harvested from the petri dishes. A total number of 2×10^6 cells from Ax2 and *aplD*⁻ were harvested at $1,700 \times g$ at RT for 2 min. The cell pellets were resuspended in SB and washed once. The pellets were resuspended in 250 μl SB, before incubating the *D. discoideum* cultures at 22 °C and 200 rpm, 250 μl bacterial culture was added. An aliquot of 10 μl cell mixture was removed at each time point, samples were collected after 0, 15, 30, 45, 60, 90, and 120 min. Samples were mixed with 40 μl of ice-cold sucrose and incubated on ice for 5 min. Before plating the samples on LB agar plates, 150 μl of ice-cold saponin solution was added to lyse the *D. discoideum* cells. The LB agar plates were incubated at 37 °C overnight. The rate of *B. subtilis* killing by the *D. discoideum* amoebae was quantified by counting the number of colony forming units (CFU) obtained at respective time points. For killing assays with *KpLM21*, 5 h-old bacterial culture was prepared and 1 μl inoculum was used to obtain an (12 h) overnight culture. *KpLM21* culture at OD_{600} 0.3 was serially diluted 1:100 and 1:100. Bacterial suspensions were incubated at RT for 1 h, during which the *D. discoideum* cultures were prepared. *D. discoideum* cells (Ax2 and *aplD*⁻) were mixed with *KpLM21* at a ratio of 10:1 and incubated at 22 °C and 200 rpm. Ten microlitre aliquots were removed at 0, 0.5, 1, 2, 4, and 6 h, and amoebae were lysed using Triton solution.

The rate of KpLM21 killing by the *D. discoideum* amoebae was quantified by counting the number of CFU obtained at each time point. To measure intracellular killing of KpLM21 by *D. discoideum* cells, 100 µl of the cell mixture was removed at each time point and washed three times with ice-cold Maltose-HL5 medium to remove extracellular bacteria. Amoebae pellets were resuspended in 40 µl sucrose solution and lysed with 150 µl saponin solution before plating on LB agar plates. The rate of KpLM21 killing by *D. discoideum* was quantified by counting the number of CFU obtained at different time points (Benghezal et al. 2006).

3.24 Analyses of *apID*⁻ development

10X KK2 22 g KH₂PO₄ and 7.0 g K₂HPO₄ dissolved in dH₂O, volume was raised to 1L with dH₂O and autoclaved. (dicty stock centre recipe)

Axenic *D. discoideum* cultures, Ax2 and *apID*⁻ were harvested and cell densities were determined. The cultures were sedimented at 510 x *g* at 18 °C for 7 min and washed with SB. The cell pellets were resuspended in 100 µl-SB and applied on 1%-SB agar plates at a density of 5 x 10⁵ cells/cm² and transferred to a dark, moist chamber at 22 °C. The developmental structures were imaged under the microscope at different time points, which includes 8 h late cell streaming, 12 h mounds, 20 h slugs, 24 h fruiting bodies and mature spores at 48 h. Development structures between 8 to 24h were imaged under SZX12 Olympus microscope and the spores (> 48 h) were imaged under Imager. Z1, Zeiss.

3.25 Spore formation efficiency (sfe)

Axenically grown *D. discoideum* cells, Ax2 and *apID*⁻ were harvested from the Petri dishes and washed with SB. The cell pellets were resuspended in SB and incubated at 22 °C, 150 rpm for 3 h. During this incubation cell division may occur therefore cell densities were determined after 3 h and the required number of cells was collected at 510 x *g* at 18 °C for 7 min.

The cell pellets were resuspended in SB and applied on 1% SB agar plates at a density of 5×10^5 cells/cm². The plates were incubated in a dark, moist chamber at 22 °C. After 2 days, the mature fruiting bodies were harvested and resuspended in SB. The spore densities were determined by counting the spores using a haemocytometer (Neubauer, Assistant) and the sfe was calculated using the formula described below (Y. Hashimoto, Cohen, and Biology 1975).

$$\text{Sfe} = \frac{\text{Total number of spores counted}}{\text{Total number of cells plated}} \times 100$$

3.26 Spore viability assay

The entire assay, except the heat shock at 45 °C for 30 min was carried out at RT. Ax2 and *apID*⁻ spores used for the spore viability assays were obtained from axenically grown amoebae. The cells were harvested from Petri dishes, washed with SB and applied on 1%-SB agar plates at a density of 5×10^5 cells/cm². The plates were incubated in a dark, moist chamber at 22 °C and the mature spores were collected after 48 h. The spores were resuspended in SB and washed at 9,700 x *g* at RT for 2 min. The washing step was repeated once to remove the spore germination inhibitors. The spore densities were determined and spore suspensions of same densities were prepared for Ax2 and *apID*⁻ spores. The spore suspensions were added with 0.1% of the Nonidet P-40, incubated at 45 °C (Thermomixer Compact, eppendorf) for 30 min and then diluted in SB (B. Y. D. A. Cotter and Raper 1966) (Germination, Cotter, and Raper 1968). The volume of spore suspensions containing 100 spores were mixed with 500 µl of *E. coli* /*r* suspension and applied on 1%-SB agar plates. The plates were incubated at 22 °C and the spore viability was scored by counting the number of phagocytic plaques observed after a week.

3.27 Pre-stalk and pre-spore patterns in *apID*⁻ slugs

The reporter (GFP/ RFP) fusions of *ecm* and *pspA* genes are routinely used to study the pre-stalk and pre-spore patterns in the morphogenetic mutants of

D. discoideum (Williams 2006). The misexpression of pre-stalk and pre-spore cells can be observed when the cells transfected with the reporter constructs were mixed with the untransfected cells and analysed for their developmental patterns (**Fig. 15**) (Parkinson et al. 2009). Similar mixing experiments were performed to analyse the pre-stalk and pre-spore patterning in the *ap1D*⁻ slugs. The axenic cultures of *ap1D*⁻ cells transfected with *ecmA*O-RFP plasmids and the untransfected *ap1D*⁻ cells were harvested and their cell densities were determined. The transfected and untransfected cells were mixed at a ratio of 20%:80% and applied on the 1%-SB agar plates for development. The cells were plated at a density of 5×10^5 cells/cm². In parallel, the control experiment was performed with Ax2 cells. The plates were incubated in a dark, moist chamber at 22 °C. After 20 h, the slugs were imaged under the fluorescence microscope (SZX12 Olympus). To analyse the *pspA* expression patterns (pre-spore), 80% of *D. discoideum* cells transfected with *pspA*-RFP plasmid were mixed with 20% of untransfected *D. discoideum* cells and subjected to development. After 20 h, the slugs were imaged under the fluorescence microscope (SZX12 Olympus).

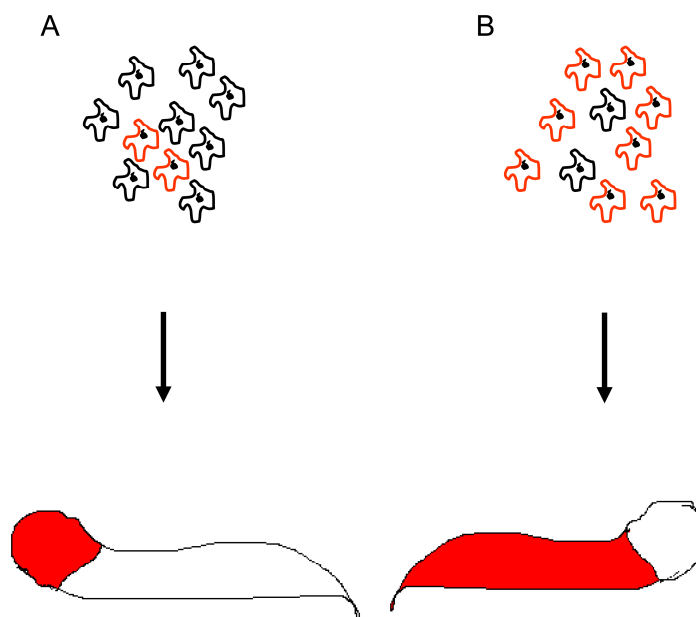


Fig. 15: Pre-stalk and pre-spore patterning in *D. discoideum* slugs. **A)** *D. discoideum* amoebae transfected with *ecmA*O-RFP plasmid (20%, red) were mixed with untransfected amoebae (80%, black) and subjected to development. *ecmA*O-RFP expression can be detected in the slug front (red). **B)** *D. discoideum* amoebae transfected with *pspA*-RFP plasmid (80%, red) were mixed with untransfected amoebae (20%, black) and subjected to development. *pspA*-RFP expression can be detected in the slug rear (red).

3.28 *ApID* expression analysis by qRT-PCR

apID transcript levels in the axenic Ax2 culture, during Ax2 development on non-nutrient agar plates, in the Ax2 cells challenged with bacteria (xenic) and the relative expression of *apID* in the pre-stalk and pre-spore regions of the Ax2 slugs were analysed by qRT-PCR as described in the following sections.

3.28.1 *ApID* expression analysis in axenic *D. discoideum* cells

RNA was isolated (Bio-Budget technologies GmbH) from 5×10^6 axenic Ax2 and *apID*⁻ cells. The cDNA was synthesised with 2 µg RNA template. After column purification (NucleoSpin Extract II, MACHERY NAGEL), 1.5 µl cDNA samples were used for the qRT-PCR analyses. The standard qRT-PCR experiment set-up is described below (Tab. 7 and Fig. 16).

Tab. 7: Standard reaction mix

Constituents	Reaction volume
SYBR mix (TAKARA)	5 µl
Forward primer (10 µM)	1 µl
Reverse primer (10 µM)	1 µl
dH ₂ O	1.5 µl
cDNA	1.5 µl
Total	10 µl

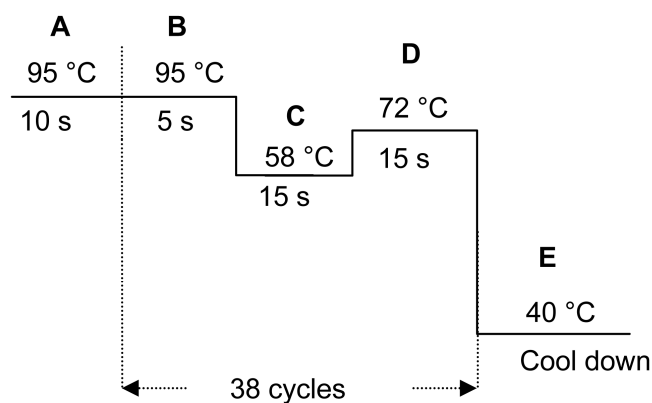


Fig. 16: Standard qRT-PCR programme (Light cycler, Roche). The cDNA samples were quantified by incubating the samples at **A**= 95 °C for 10 s; pre-denaturation, **B**= 95 °C for 5 s; denaturation, **C**= 58 °C for 15 s; primer annealing, **D**= 72 °C for 15 s; primer extension and **E**= 40 °C; reaction end.

3.28.2 *ApID* expression during Ax2 development

The axenically grown Ax2 cells were harvested from the Petri dishes and the cell density was determined. The cells were sedimented at 510 x *g* at 18 °C for 7 min. The cell pellet was resuspended in 1X KK2 buffer and washed once. The Ax2 cells were applied on the 1%-KK2 agar plates at a density of 5 x 10⁵ cells/cm². The plates were dried under the laminar air flow chamber for 10 min and transferred to a dark, moist chamber at 22°C. RNA was isolated using RNAmagic (Bio-Budget technologies GmbH) at different stages of development, which includes 0 h amoebae, 8 h late cell streaming, 12 h mounds, 16 h slugs, and 24 h fruiting bodies. RNA samples were quantified using NanoDrop and 2 µg RNA was used for cDNA synthesis. cDNA samples were purified (NucleoSpin Extract II, MACHEREY NAGEL) and 1.5 µl of cDNA template was used for qRT-PCR analysis as described earlier (see **Tab. 7** and **Fig. 16**). For both, the house keeping genes and *apID* gene the expected amplicon sizes were about 300 bps.

3.28.3 *ApID* expression in xenic Ax2 cells

The axenic Ax2 cells were harvested from the Petri dishes and the culture density was determined. The culture volume containing 5.4 x 10⁶ cells was filled in two centrifuge tubes and spun down at 510 x *g* at 18 °C for 7 min. The cell pellet in each tube was resuspended in 5 ml fresh Maltose-HL5 medium and transferred to the culture flasks (25 ml, Scott Duran). Before incubating at 22 °C; 140 rpm, the flasks were labelled axenic and xenic. Frozen bacterial stock was streaked out and overnight bacterial cultures were prepared as described below (**Tab. 8**). Ten fold excess bacteria (5.4 x 10⁷) were introduced into the xenic flask and 8 h later both, axenic and xenic Ax2 cells were harvested for the downstream processes. RNA isolation, cDNA synthesis and qRT-PCR analysis were performed as described before (**section 3.17, 3.18** and **Tab. 7, Fig. 16**)

Tab 8: Bacterial cultures used for xenic qRT-PCR

Bacterial culture preparations	OD ₆₀₀ = 0.1
<i>B. subtilis</i> (ATCC# 6051) was incubated overnight at 37 °C up to an OD ₆₀₀ of 2.0.	2.3 x 10 ⁶ CFU/ml
<i>K. pneumoniae</i> (KpLM21) was incubated at 37 °C shaker for 5 h. A volume of 1 µl inoculum from this 5 h culture was used to inoculate a fresh 3 ml LB broth. This fresh culture was incubated for 12 h at 37 °C.	3.3 x 10 ⁷ CFU/ml
<i>P. aeruginosa</i> (PT531) was incubated for 12 h at 37 °C	6.3 x 10 ⁷ CFU/ml

3.28.4 *ApID* expression in pre-stalk and pre-spore regions of Ax2 slugs

The axenic Ax2 cells were washed with 1X KK2 buffer and applied on the 1%-KK2 agar plates at a density of 5 x 10⁵ cells/cm². The plates were incubated in dark at 22 °C for 20 h. After 20 h, under stereo microscope, the pre-stalk and pre-spore regions of the Ax2 slugs were dissected and isolated using the sterile needles (30G x ^{1/2}). RNA isolation, cDNA synthesis and qRT-PCR analysis were performed as described earlier (**section 3.17, 3.18, and Tab. 7, Fig. 16**). *ApID* fold expression in the pre-spore region was determined by assuming *apID* fold expression in the pre-stalk region as reference (G. Chen, Zhuchenko, and Kuspa 2007)

3.29 Examination of sentinel (S) cells in *apID*⁻ slugs

D. discoideum cells, Ax2 and *apID*⁻ were harvested from the axenic culture plates and their densities were determined. A total number of 2.5 x 10⁷ cells from each culture was centrifuged at 500 x *g* at RT for 9 min and washed once with SB. The cell pellets were resuspended in 50 µl of the SB. 1%-SB agar plates were freshly prepared and a volume of 12 ml agar was poured per Petri dish (6 cm diameter). 3 µg/ml EtBr was added to the agar just before pouring the plates (G. Chen, Zhuchenko, and Kuspa 2007). A straight line of 4 cm was drawn at the bottom of the agar plates. 50 µl-cell suspension containing 2.5 x 10⁷ *D. discoideum* cells (Ax2 or *apID*⁻) was placed on the EtBr agar plate by following the line drawn at the bottom of the agar plate. The plates were dried under the fume hood for 3 min and incubated in a dark, moist chamber with a unidirectional light source for 20 h. During this time, the *D. discoideum* cells form the slug structures and migrate on the EtBr agar. After 20 h, the plates were observed under the fluorescence microscope (SZX12 Olympus) to investigate the S cells.

3.30 *D. discoideum* slugs infection with bacteria

The axenically grown *D. discoideum* cells, Ax2 and *apID*⁻ were harvested from the Petri dishes and 5×10^8 cells/ml was centrifuged at $500 \times g$ at RT for 9 min. Pellets were washed once with SB and resuspended in 1ml-SB. 50 μ l of the cell suspension was placed on 1%-SB agar plate and slugs were obtained as described before (**section 3.29**). Frozen bacterial stocks were revived as described earlier (**section 3.4**) and 16 ml-overnight cultures were prepared with appropriate antibiotics. The GFP-expressing strain of *K. pneumoniae* (*KpGFP*) (Benghezal et al. 2006) was grown with 1 mg/ml ampicillin for 12 h at 37 °C and 220 rpm. The *E. coli* DsRed (laboratory strain) cultures were grown with 100 mM IPTG and 150 μ g/ml Kanamycin, incubated at 37 °C and 220 rpm for 48 h. From 16 ml-overnight cultures, 1 ml was removed to measure the OD₆₀₀ of cultures and remaining 15 ml-cultures were sedimented at $2,151 \times g$ at RT for 12 min and washed once with 20 ml-SB. Finally, bacterial pellets were resuspended in 200 μ l-SB, and 50 μ l of the bacterial suspension were used to infect slugs (obtained from 2.5×10^7 cells) in each plate. At the stereo microscope (Leica M80), slugs were gently punctured with a sterile needle (23G \times 1^{1/4}) and 50 μ l of the bacterial suspension were layered on the injured slugs. This allows bacteria to gain entry into injured slugs. Plates were incubated in a dark, moist chamber with a unidirectional light source. Injured slugs reconstruct themselves and migrate towards the unidirectional light source (G. Chen, Zhuchenko, and Kuspa 2007). Migrating slugs were imaged under the microscope (SZX12 Olympus) 20 h post infection for *KpGFP* and 8 h post infection for *E. coli* DsRed.

3.31 Immunofluorescence microscopy

Blocking solution	0.1% (w/v) Porcine gelatine and 0.1% (v/v) Triton X-100 dissolved in 1X PBS
Washing solution	0.1% (v/v) Triton X-100 dissolved in 1X PBS
10X PBS	80 g NaCl, 2 g KCl, 26.8 g Na ₂ HPO ₄ .7H ₂ O (or 17.8 g Na ₂ HPO ₄ .2H ₂ O), and 2.4 g KH ₂ PO ₄ dissolved in 800 ml dH ₂ O. The pH 7.4 was adjusted with HCl, the volume was raised to 1L with dH ₂ O and autoclaved.

Paraformaldehyde	Paraformaldehyde was dissolved in SB at 37 °C to obtain a final concentration of 4% (w/v) and stored at -20 °C
Primary antibodies	Mouse anti-FLAG M2 and Mouse anti-PDI (Protein-disulfide isomerase, an endoplasmic reticulum [ER] marker), diluted 1:2,000 in blocking solution.
Secondary antibodies	Goat anti-mouse IgM, Alexa Fluor 488 conjugated and Goat anti-mouse IgG, Dylight 549 conjugated, diluted 1:5,000 in blocking solution.
Saturating antibody	Goat anti-mouse IgG, Horseradish peroxidase (HRP) conjugated, diluted 1:500 in blocking solution
Mounting solution	60% (v/v) Glycerol (87% stock) in 1X PBS and 1:1000 dilution Hoechst 33258 dye (10 mg/ml stock, in MeOH), stored at 4 °C

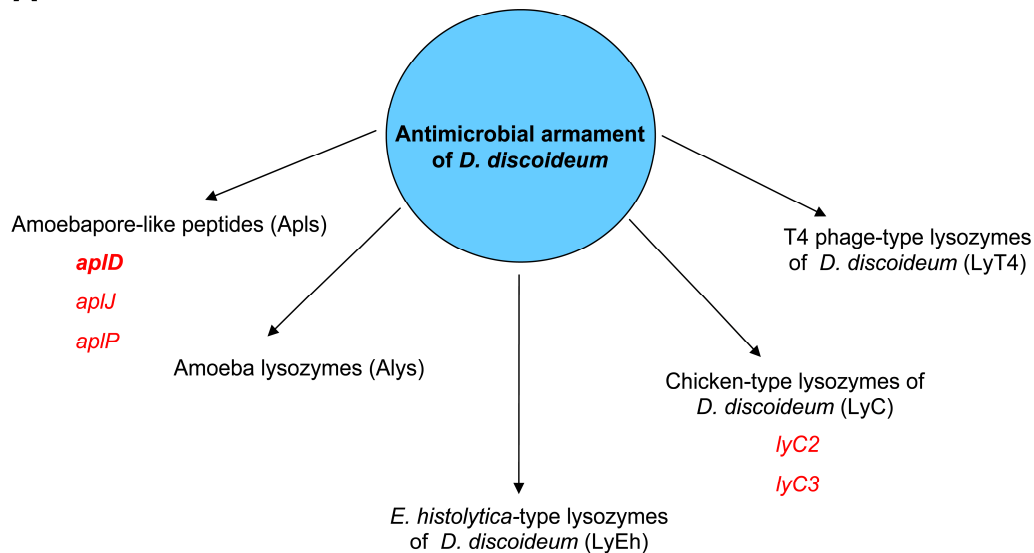
Immunostaining experiments were performed with the *ap1D*⁻ cells transfected with pDneo2a-3xFLAG[*act6/ap1D*] plasmid (**Appendix 8.2**) and *ap1D*⁻ cells were used as controls. The intra-cellular markers of interest include PDI (ER), comitin (Golgi complex), *vatA* (contractile vacuoles and endosomes) and vacuolin (post-lysosomes). As the secondary antibodies used to stain Ap1D-FLAG and PDI, both were from mouse, the sequential staining was performed. Three hundred microlitre of the cell suspension were dispensed on cover slips (#1, Thermo scientific), allowed to adhere on the cover slips at RT for 2 h. After 2 h, Maltose-HL5 medium on the cover slip was removed and the cells were fixed with 400 µl of 4% paraformaldehyde at 4 °C for 30 min. Cover slips were washed three times with excess for 1X PBS at RT, followed by blocking at RT for 15 min. Cells seeded side of the cover slip was filled with 85 µl-primary antibody (Mouse anti-FLAG) and incubated at RT for 1 h. Cover slips were washed five times with 1X PBS (Hagedorn, Neuhaus, and Soldati 2006) and incubated in blocking at RT for 15 min. Cover slips were incubated with 85 µl-secondary antibody (Goat anti-mouse, Alexa Fluor 488 conjugated) at RT for 1 h and subsequently washed five times with 1X PBS. After washing, the cover slips were incubated with 85 µl-saturation antibody (Goat anti-mouse, HRP conjugated) for 30 min at RT, followed by four sequential washes using washing solution. To remove unbound antibodies efficiently, sequential washing was

repeated five times and cover slips were incubated overnight in washing solution at 4 °C. This was followed by staining the cells for PDI marker, which was same as described above using appropriate antibodies. Finally, the cover slips were mounted on a glass slide with 7 µl of mounting solution. Sides of the cover slips were sealed with the sealant and stored in the dark at 4 °C until observed under the microscope.

4 RESULTS

4.1 Genes of interest

A



B

```

Ap-A -----GEI---LGNLCTGLINTLEN-LLTTKG-A 24
Ap-B ----MRAIIFVLI FAIFAATR-----EGAI---LGNLCKDTVKLVEN-LLTVDG-A 43
Ap-C -----ASQEKQQDR-----EIPV---LCPVCTSLVGKLLID-LVLGGA-V 34
Ap1D MYKINITYLLIFFTIILASLFATSKSLVVQKNVGEIDNNQCQICELLVKDIIIEGLTANQS-V 59
Ap1J ---MKLFILLILLNITILFSSNLFVKANNQVG-----CEICEMVTTFLEDKLANSNV-E 50
Ap1P MNKLIIALILIIICISISIFAQTTTPTNSPAPSPKVG--CDLCEFAVSVFGEFLVKNDNLTK 58
          * : *
          :

Ap-A DKVKDYISSLNKASGFIA TLCTKVLDFGIDKLIQLIEDKVDANAICAKIHAC----- 77
Ap-B QAVRQYIDNLCGKASGFLGTLCEKILSFGVDELVKLIENHVDPVVVCCKIHAC----- 96
Ap-C DKVTDYLETLCAKADGLVETLCTKIVSYGIDKLEKILEGGSAKLI CGLIHAC----- 87
Ap1D EVIEHGLNLI CDHIP-LHVRVCKQFVDSNFQKIVQFIENHDDPQETCEKCGVCGSSDEYN 118
Ap1J TNISEELMKLCNYIPSNYQTI CNNLIENNIDSIKSFENNETPTIICDQLGLCSQSSSSS 110
Ap1P AQLETDLKNI CTLVPSNITMECKFFMILAAPIIAGAISNGENPQTLCSDYKLC TTTTQQT 118
          : : * : * : : : : * *
          :

Ap-A -----
Ap-B -----
Ap-C -----
Ap1D -KIDTRYFPQHNQHKRHLKKQNSIKN----- 143
Ap1J SNFDTTIQTSSSSSSSSSSDLPSVGLICEFIVQKVESYIEVNATQSEIEYFLDQDCNKF 170
Ap1P PTTNNYSNQPNINIMKNKIKDIFVESTN-NIIEPKVKVTMRRNF----- 161

Ap-A -----
Ap-B -----
Ap-C -----
Ap1D -----
Ap1J GGGYAGECVVYVNQYVQLVNYLSYNQKPEKACSEIKACPSSSF 214
Ap1P -----

```

Fig. 17: A) Antimicrobial arsenal of *D. discoideum*. Amoebapore-like peptide coding genes (*apls*) and genes coding for lysozymes form the two major groups of antimicrobial genes of *D. discoideum*. Amoeba lysozymes, *E. histolytica*-type lysozymes, chicken-type lysozymes and T4-phage type lysozymes are categorised under lysozymes class. KO clones were generated for *ap1D*, *ap1J*, and *ap1P* from *apls* class and *lyC2* and *lyC3* from chicken-type lysozymes. Among all five KO clones functional and phenotypic characterisation was carried out for *ap1D*. **B)** Sequence similarity between the Amoebapore (Ap) A, B, and C and the Ap1 D, J, and P. One-letter code for amino acid residues is shown. Conserved cysteine residues are marked (red).

The genome of *D. discoideum* comprises two major groups of genes potentially involved in antimicrobial functions. The antimicrobial genes include amoebapore-like peptide coding genes or *apls* and lysozymes (**Fig. 17**). The lysozymes group constitutes four different classes of lysozymes. The amoeba lysozymes (*alys*), *E. histolytica* type lysozymes (*lyEh*), chicken-type lysozymes (*lyC*), and T4-phage type lysozymes (*lyT4*). Earlier work in our laboratory had found that recombinantly expressed ApID is antimicrobial against *Bacillus megaterium* and *E. coli* (unpublished data). Also through information from our collaborator (S. Bozzaro, pers. com.) that the transcripts of *apID*, *apIJ*, and *apIP* from *apls* family, and *lyC2* and *lyC3* from lysozymes family were up-regulated in *D. discoideum* cells upon confrontation with bacteria. For these reasons, the *apID*, *apIJ*, *apIP*, *lyC2*, and *lyC3* were chosen for the present phenotypic characterisation studies.

4.2 *ApID* gene ablation

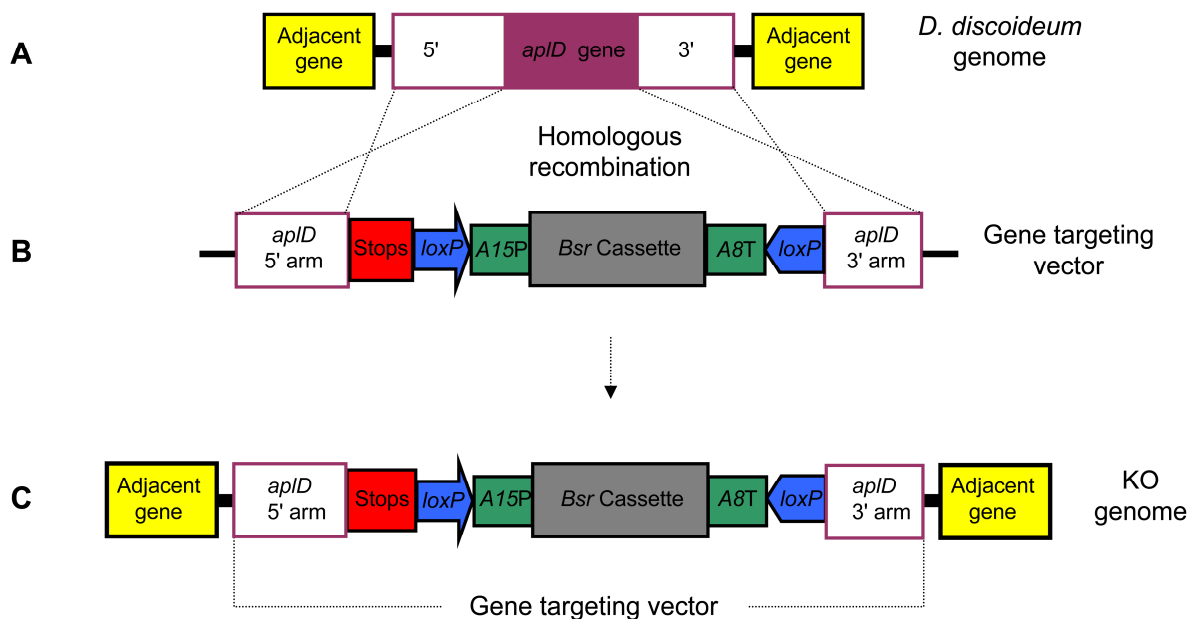


Fig. 18: Strategy followed to achieve *apID* ablation in Ax2 cells. **A)** *D. discoideum* genome: *apID* locus of Ax2 genome is shown. Marked 5' and 3' regions (open boxes) represent DNA fragments that are identical in *apID* gene and gene targeting vector that are crucial to achieve homologous recombination. **B)** Gene targeting vector: Linearised *apID* gene targeting vector possess a Blasticidin resistance gene (*Bsr*) which confers resistance to Blasticidin in the recombinant clonal isolates, the *Bsr* cassette is flanked on either sides by *loxP* sites which can be used to excise the *Bsr* cassette. Translation stop codon next to *loxP* prevents generation of truncated *apID*. **C)** KO genome: After homologous recombination, in the genome of KO clone, *apID* locus is replaced by *apID* gene targeting vector.

The *ap1D* gene targeting vector or the KO vector was constructed as described in the methods chapter (see **section 3.14**). The *ap1D* KO vector was transfected into the Ax2 cells by electroporation, which was followed by homologous recombination between the *ap1D* gene targeting vector and the *ap1D* gene (Chromosome 6) in the Ax2 genome (**Fig. 18**). The positive clones for homologous recombination were identified by antibiotic selection (Blasticidin). The clones that were resistant to 8 µg/ml Blasticidin were aspirated from the Petri dishes and the genomic DNA was isolated for the PCR analyses. Homologous recombination at the *ap1D* locus in these clonal isolates was confirmed by three different PCR analyses (J. Faix et al. 2004).

4.3 Identification of *ap1D*⁻ by PCR analyses

The Blasticidin resistant clonal isolates were examined by PCR to verify the KO vector insertion at the *ap1D* locus of their genome. Three different PCR analyses were performed to confirm the KO vector insertion in 5' to 3' orientation at the *ap1D* locus (**Fig. 19A**). Wild type (WT) Ax2 genomic DNA and the KO vector (VC) were used as controls for all the PCR analyses. The *ap1D* KO vector insertion in the *D. discoideum* genome at the 5' region of the *ap1D* gene was confirmed using the U1-FP and U1-RP primers. The U1-FP forward primer binds at the intergenic region that is present outside the *ap1D* gene and not included in the *ap1D* KO vector, whereas the U1-RP reverse primer binds at the Bsr cassette of the *ap1D* KO vector (**Fig. 19A**). As a result, with this primer combination only the clonal isolates that are positive for the *ap1D* KO vector insertion at the *ap1D* locus generates 1.4 kb amplicon. This PCR analysis showed several clones which were positive for KO vector insertion at the *ap1D* locus of their genome. (**Fig. 19B**). These clones were subjected to the second PCR analysis which includes U1-FP and D1-RP primers. This PCR strategy gave an advantage to verify whether the recombinant clones are homogenous without any WT contamination. Both, U1-FP and D1-RP binds at the intergenic sequence available at the 5' and 3' regions of the *ap1D* gene (**Fig. 19C**). Hence, both the WT and the recombinant clones create amplicons with this primer pair, but differ in the size of the amplicons. The recombinant clones were expected to produce 1.4 kb larger amplicon compared to WT. For this PCR the WT was considered as the positive control and the VC as negative control.

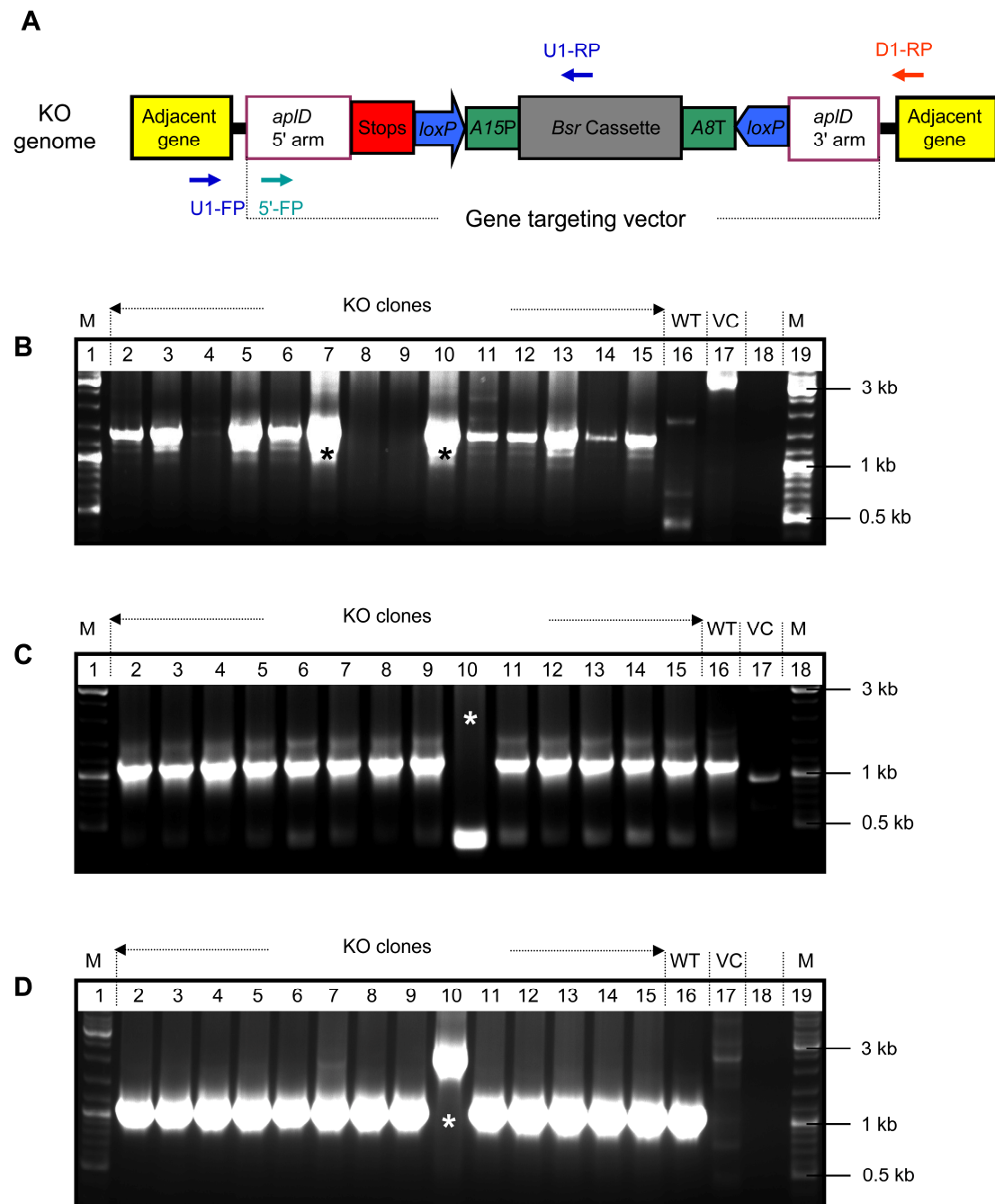


Fig. 19: PCR analysis of *apID* KO clones. **A)** Scheme of PCR screening strategy followed to examine *apID*⁻ clones. Arrows represent primers used for PCR analyses. **B)** *apID*⁻ clones PCR analysis using U1-FP and U1-RP primers. Ax2 genomic DNA (WT) and *apID* gene targeting vector (vector control; VC) was used as negative controls. Recombinants generated 1.4 kb amplicon, WT and VC produced no amplicon. **C)** *apID*⁻ clones PCR analysis with U1-FP and D1-RP primers. All clones produced positive signal for WT (1.1kb) except one clone (lane 10). **D)** *apID*⁻ clones PCR analysis using 5'-FP and D1-RP primers. Recombinant clone (lane 10) generated 1.3 kb larger amplicon than the WT. In B and C, WT was considered as positive control and VC as negative control. Asterisk symbols denote positive clones for *apID* gene ablation.

All the KO clones analysed by this PCR showed WT signal except one clone (**Fig. 19C**). This clone neither showed positive signal for recombination nor showed positive signal for WT. For this reason, all the recombinant clones were screened by

the third PCR scheme, using 5'-FP and D1-RP primers (J. Faix et al. 2004). The 5'-FP forward primer was designed in the *apID* region available both in the KO vector and the WT, whereas the D1-RP, as mentioned earlier, binds at the intergenic sequence available only at the 3' region of *apID* in the WT genome that is not available in the KO vector (**Fig. 19A**). For this primer pair, the recombinant clone generated an amplicon which was 1.3 kb larger than the WT positive control (**Fig. 19D**). Finally, all the three PCR examinations resulted in one positive clone that was positive for *apID* KO vector integration at the *apID* locus of the Ax2 genome. By following similar PCR schemes *apIJ*⁻, *apIP*⁻, *lyC2*⁻ and *lyC3*⁻ clones were isolated (see **Appendix 8.1**)

4.4 *ApID*⁻ growth analyses on *KpLM21* and *K*⁻

The growth ability of the *apID*⁻ was examined on several virulent and avirulent bacteria by performing the 24-well growth assays (Froquet et al. 2009). To understand the degree of bacterial virulence the growth assays were performed on two different growth media, the regular SM agar medium and the SM agar medium devoid of glucose (see Methods, section 3.27). The non-pathogenic bacterial strains used for the growth assays include Gram-positive bacteria *B. subtilis* (ATCC# 6051) and the Gram-negative, food bacterium for *D. discoideum*, *E. coli* B/r. Other Gram-negative bacterial strains tested include virulent and avirulent strains of *K. pneumoniae* and *P. aeruginosa* quorum sensing mutants. As the wild type *P. aeruginosa* strains do not permit *D. discoideum* growth (Pukatzki, Kessin, and Mekalanos 2002), (Benghezal et al. 2006) and (Alibaud et al. 2008) only the quorum sensing mutants were used for the growth assays. For detailed information about the bacterial strains refer Methods (**Tab. 6**). Growth ability of the *apID*⁻ is described in comparison with the Ax2 control. In general, all the bacterial strains grown on G+ medium were permissive for phagocytic growth plaque formation by *apID*⁻, but on the *K. pneumoniae* strains *Kp13883*, *Kp52145*, *K*⁻ and *KpLM21* the *apID*⁻ showed relatively slow growth. Unlike the Ax2 control, the *apID*⁻ was unable to form fruiting bodies on the *K. pneumoniae* strains (**Fig. 20**) deposited on G+ medium. In the case of G- medium, the *apID*⁻ was able to form plaques on *Kp13883* and *Kp52145* lawns,

but on K^- and $KpLM21$ the $apID^-$ created plaques only in the wells deposited with 10,000 amoebae. (Fig. 20).

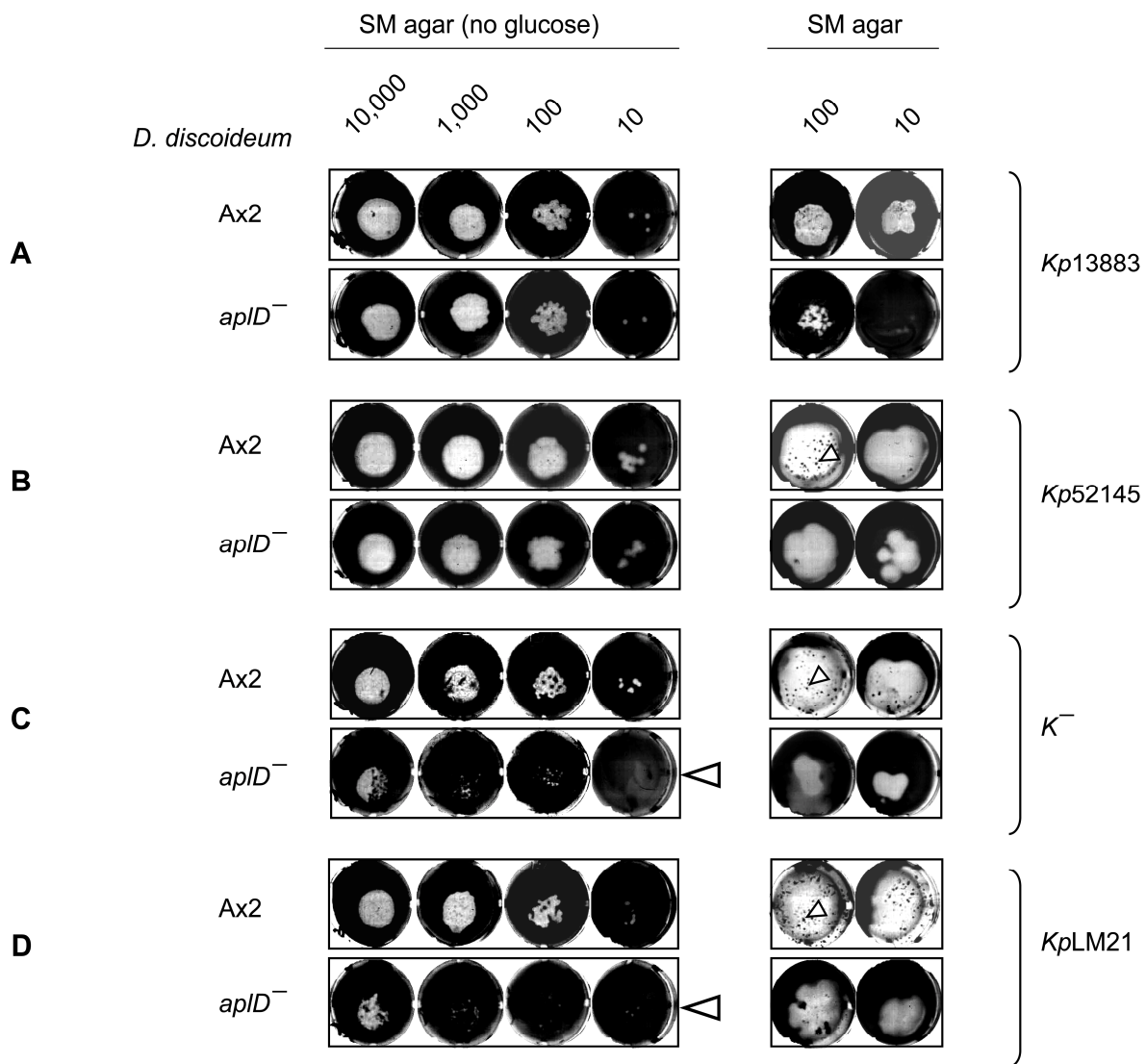


Fig. 20: *D. discoideum* growth assessed on *K. pneumoniae*. Growth assays were performed on regular SM agar medium (G+, right panels) and on regular SM agar medium devoid of glucose (G-, left panels). *D. discoideum* growth ability on bacteria was tested by depositing indicated number of amoebae with bacteria seeded on G+ and G- media. For G+ medium, only the results obtained with 100 and 10 amoebae are shown. *D. discoideum* amoebae fed with **A)** Non-pathogenic *K. pneumoniae* strain; $Kp13883$, **B)** Virulent *K. pneumoniae* strain; $Kp52145$, **C)** Mutant strain of $Kp52145$; K^- , and **D)** Wild isolate of *K. pneumoniae*; $KpLM21$. Arrowheads indicate absence of phagocytic growth plaques and arrows represent fruiting bodies. Scale bar, 1.5 cm

As a common observation, the growth plaques created by *D. discoideum* (Ax2 and $apID^-$) with *K. pneumoniae* strains grown on G+ medium were larger than those of G- medium. In $Kp52145$, K^- and $KpLM21$ even the plaques created by 10

amoebae on G+ medium was larger than those plaques observed on G- medium spotted with 10,000 amoebae (**Fig. 20B, C and D**)

4.5 Two-dimensional virulence array

The bacterial growth assays were also performed for *apIJ*⁻, *apIP*⁻, *lyC2*⁻ and *lyC3*⁻. In general, all the KO mutants grown with bacteria plated on G+ medium showed no growth defects. Likewise, all four KO mutants tested with bacterial strains grown on G- medium showed no growth defects, except *apIP*⁻ and *lyC2*⁻ plated on the *K. pneumoniae* strain *K*⁻. On *K*⁻ placed on G- medium, both the *apIP*⁻ and the *lyC2*⁻ created phagocytic growth plaques only in the wells deposited with 10,000 amoebae (data not shown). The virulence grades were designated to each bacterial strain tested based on the growth abilities of the KO mutants (Benghezal et al. 2006) and (Froquet et al. 2009) (see **Methods; Fig. 13**). The virulence grade was scored 0 if the bacterial strain was stringently non-permissive for plaque formation by the amoebae. Such bacterial strains could be lethal for *Dictyostelium*. When the growth plaque was visible in the wells deposited with 10,000 amoebae, the bacterial strain was designated as virulence grade 1. Virulence grade 2 was given to a bacterial strain if the phagocytic growth plaques were visible in wells with 10,000 and 1,000 amoebae. Accordingly, the virulence levels were graded up to 4 (Froquet et al. 2009). The *apID*⁻ grown with *Kp13883*, *Kp52145*, *K*⁻ and *KpLM21* seeded on G+ medium showed relatively slow growth compared to Ax2 cells. Nevertheless, the *apID*⁻ was able to form clearing plaques even in the wells loaded with 10 cells, but the plaque sizes were relatively small compared to Ax2 cells. Additionally, unlike Ax2 cells, the *apID*⁻ was unable to form fruiting bodies on these bacterial strains (**Fig. 20**). In the two-dimensional virulence array chart, these situations were categorised under virulence grade 4 and were represented by a different colour and marked with an asterisk to indicate this difference (**Fig. 21**).

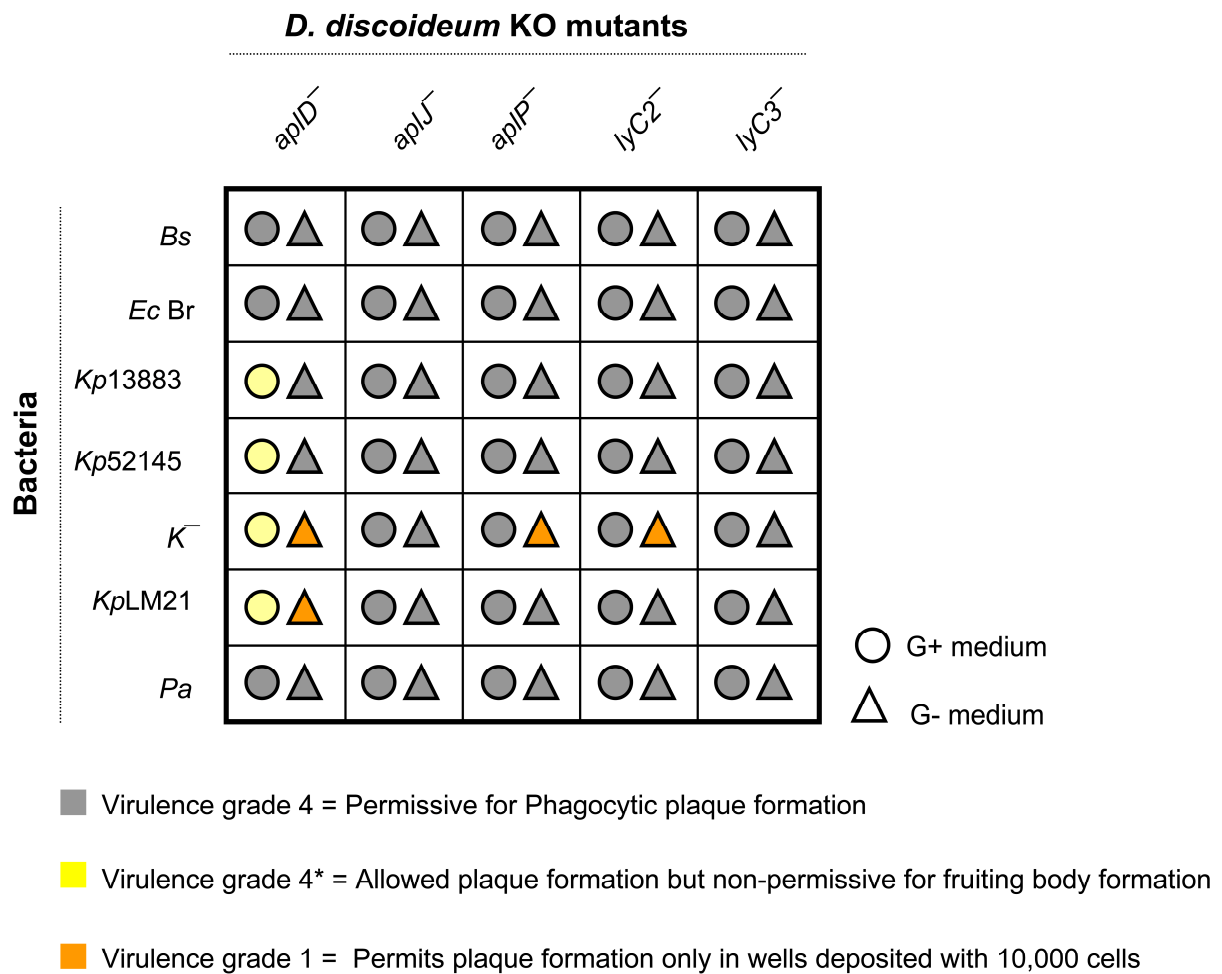


Fig. 21: *D. discoideum* KO mutants growth analyses on bacteria. Growth assays were performed on SM agar medium (G+; open circle) and SM agar medium devoid of glucose (G-; open triangle). *D. discoideum* mutants tested include *apID*⁻, *apIJ*⁻, *apIP*⁻, *lyC2*⁻ and *lyC3*⁻. Bacterial strains tested include *B. subtilis* (*Bs*), *P. aeruginosa* (*Pa*) quorum sensing mutant; PT531, an avirulent *K. pneumoniae* strain; *Kp13883*, a virulent encapsulated wild isolate of *K. pneumoniae*; *KpLM21*, a encapsulated *K. pneumoniae* strain with plasmid mediated virulence; *Kp52145*, a capsule defective mutant of *Kp52145*; *K*⁻ and a non-pathogenic, food bacterium for *D. discoideum*; *E. coli* B/r (*Ec B/r*). Based on growth abilities of KO mutants on bacteria the virulence grades were derived.

4.6 *ApID*⁻ plaques on *KpLM21* and *K*⁻

The *apID*⁻ amoebae plated with *KpLM21* and *K*⁻ on G+ agar plates formed relatively small plaques when compared with Ax2 cells. On *KpLM21*, the Ax2 cells formed phagocytic growth plaques of sizes 0.7 to 1.0 cm diameter, whereas the *apID*⁻ formed phagocytic growth plaques of sizes in between 0.4 to 0.7 cm diameter. In the case of *K*⁻ seeded on G+ medium, the Ax2 cells formed plaques of sizes in between 0.6 to 1.3 cm diameter and the *apID*⁻ formed phagocytic growth plaques of

sizes 0.2 to 0.3 cm diameter (**Fig. 22**). The *apID*⁻ grown with *KpLM21* and *K*⁻ on G-medium were unable to form any phagocytic plaques (data not shown).

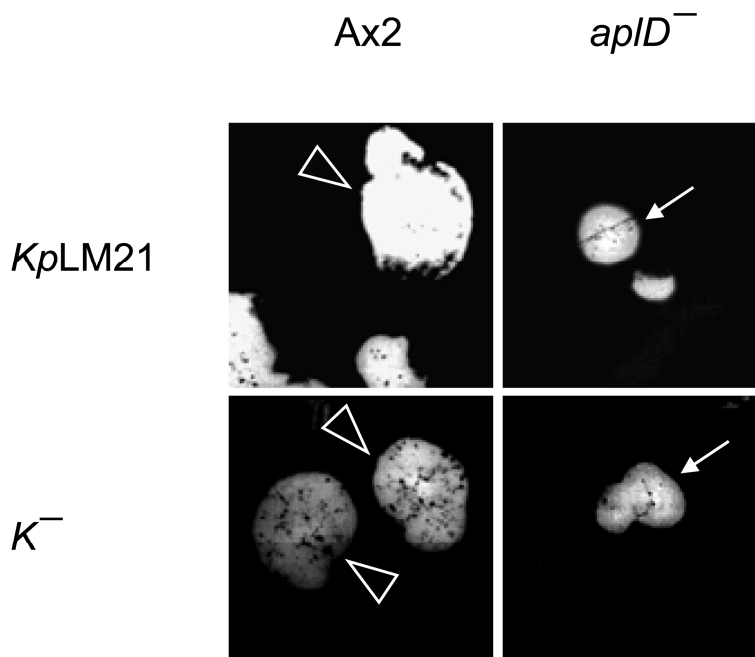


Fig. 22: *ApID*⁻ formed smaller growth plaques on *K. pneumoniae*. *D. discoideum* cells were mixed with overnight bacterial cultures and plated on SM agar plates (G+). The phagocytic growth plaques were observed after a week. *ApID*⁻ formed relatively smaller plaques on *K. pneumoniae* strains *KpLM21* and *K*⁻. Ax2 plaques (arrowheads); *apID*⁻ plaques (arrows)

4.7 Colony morphologies of avirulent and virulent *K. pneumoniae* strains

The frozen (-80 °C) stocks of *K. pneumoniae* were streaked on fresh LB agar plates and incubated overnight at 37 °C. The next day, the CFU were imaged under the stereo microscope (Leica M50) using a digital camera (Olympus 7.1, CAMEDIA, C-7070). The avirulent *K. pneumoniae* strain, *Kp13883* formed relatively large, globular and mucoid colonies of 4 mm diameter (**Fig. 23A**). When compared with *Kp13883*, the virulent and encapsulated *K. pneumoniae* strain, *Kp52145* formed relatively small, globular and mucoid colonies of 3 mm diameter (**Fig. 23B**), whereas the capsule defective mutant of *Kp52145*, *K*⁻ formed small, flat and non-mucoid colonies of about 2 mm diameter (**Fig. 23C**). The virulent and encapsulated wild isolate, *KpLM21* formed 2 mm diameter colonies that were non-mucoid, small and globular (**Fig. 23D**).

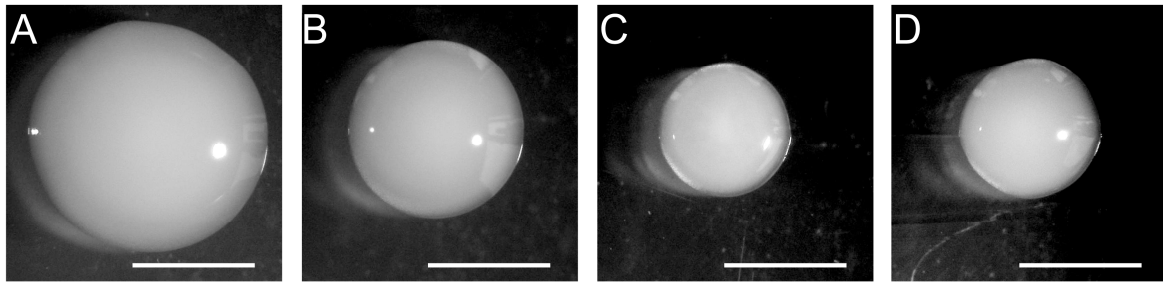


Fig. 23: Differential colony morphologies of *K. pneumoniae* strains on LB agar plates. **A)** Avirulent strain; *Kp13883*, **B)** Encapsulated virulent strain; *Kp52145*, **C)** Isogenic capsule defective mutant of *Kp52145*; K^- and **D)** Virulent wild isolate with huge capsule; *KpLM21*. Scale bars, 2 mm.

4.8 Phagocytosis and killing assays

Two different phagocytosis and killing assays, total and intracellular (**Fig. 24A**) were performed to measure the rate of bacterial killing by the *D. discoideum*. The *D. discoideum* cells, Ax2 and $apID^-$ were mixed with *B. subtilis* at a ratio of 100:1 and the rate of *B. subtilis* killing by the *D. discoideum* cells was measured at indicated time points (**Fig. 24B**). The rate of bacterial killing was measured by counting the total number of viable *B. subtilis* at each time point. Both, in the case of Ax2 cells and the $apID^-$, there was a gradual decrease in total number of viable *B. subtilis* observed over time. In particular, the $apID^-$ was relatively faster in phagocytosis and killing of *B. subtilis* when compared with the Ax2 cells. The differences observed were statistically ($p < 0.05$) significant only at time point 15 min ($p = 0.02448$). Similar assays were performed with the *K. pneumoniae* strain *KpLM21* (**Fig 24C**). In contrast to the phagocytosis and killing of *B. subtilis*, the $apID^-$ was less efficient in killing *KpLM21*. However, there was a gradual decrease in total number of viable *KpLM21* was observed at later time points. When compared with Ax2 cells, the total number of viable bacteria counted at each time point in the $apID^-$ was relatively more than that of the Ax2 cells and the differences were statistically ($p < 0.05$) significant only at 2 h time point ($p = 0.001084$).

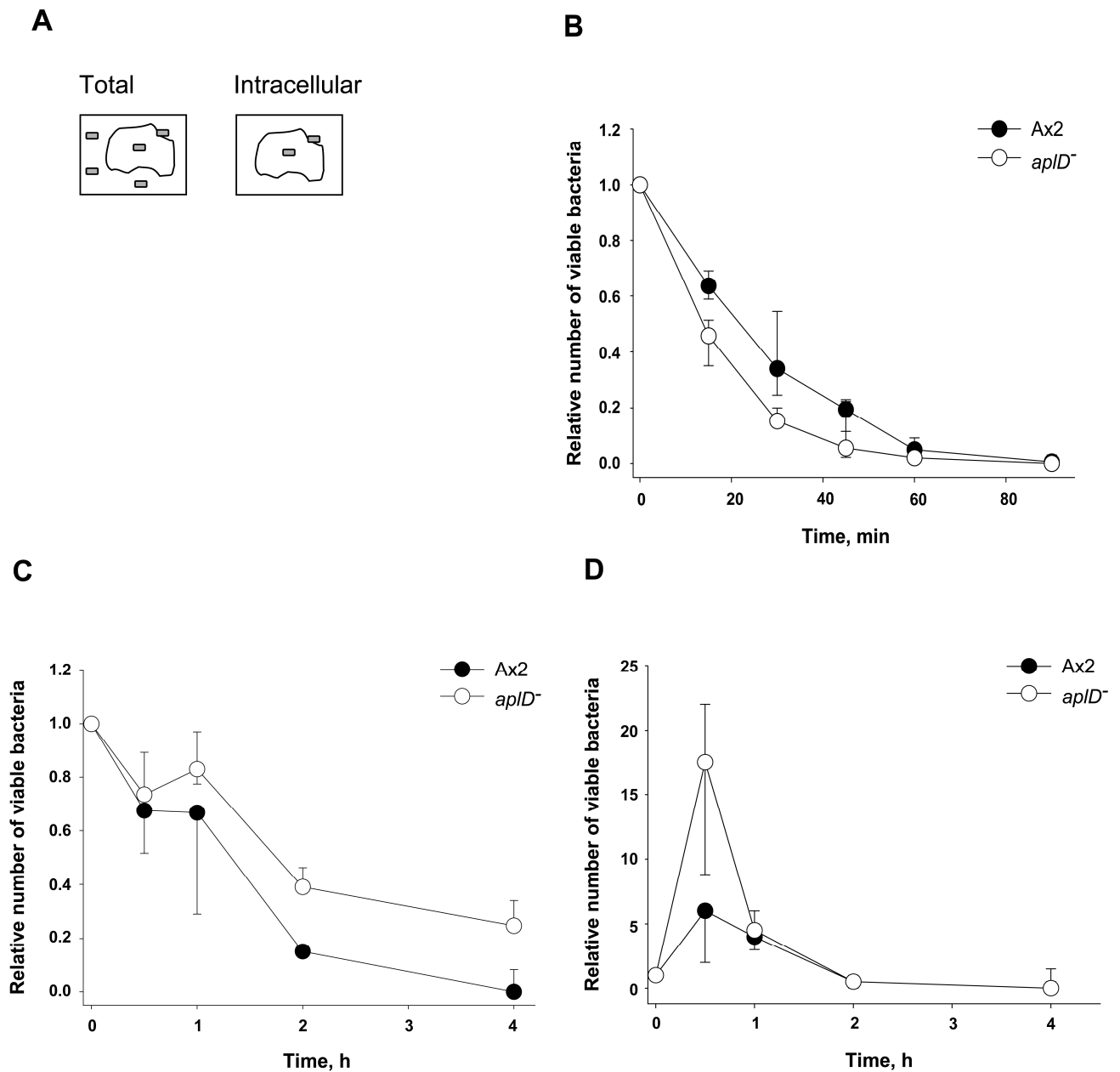


Fig. 24: Phagocytosis and killing assays with *B. subtilis* (ATCC# 6051) and *K. pneumoniae* (KpLM21). *D. discoideum* and bacteria were mixed at a ratio of 100:1 and incubated at 22 °C, 140 rpm. **A)** Killing assay cartoons: For killing assays total, the total number of viable bacteria at each time point was measured, for killing assays intracellular only the bacteria associated with *D. discoideum* at each time point is measured (Benghezal *et al.*, 2006). **B)** Killing assays with *B. subtilis* (total): At indicated times; aliquots were removed from the cell mixture, lysed, plated on LB agar plates and incubated overnight at 37 °C. Rate of bacterial killing was measured by counting the number of viable bacteria at each time point. **C)** Killing assays with *K. pneumoniae* (total): Performed and analysed the same way as the killing assays with *B. subtilis*. **D)** Phagocytosis and killing of KpLM21 (intracellular). At indicated times; aliquots were removed from the cell mixture, washed three times to remove extracellular bacteria, lysed and plated on LB agar plates. Rate of intracellular KpLM21 killing by *D. discoideum* cells was determined by counting the number of CFU on LB agar plates. Filled symbols represent Ax2 and open symbols represent *apD*⁻. Statistical analyses were performed for each time point using Shapiro-Wilk normality test, Brown-Forsythe Levene-type test and two sample *t*-test. For killing assays with *B. subtilis* (total), the differences were statistically significant ($p < 0.05$) at time point 15 min ($p = 0.02448$), for killing assays with *KpLM21* (total) the differences were statistically significant at time point 2 h ($p = 0.001084$) and killing assays with *KpLM21* (intracellular) the differences were statistical significance at time point 0.5 h ($p = 0.05247$).

Following this, to investigate whether the *apID*⁻ was defective in intracellular killing of *KpLM21*, the number of viable *KpLM21* associated with the *apID*⁻ at indicated time points was measured (**Fig. 24D**). In comparison to killing assays (total) with *KpLM21*, the *apID*⁻ was less efficient in intracellular killing of *KpLM21* and the differences were statistically ($p < 0.05$) significant at time point 0.5 h ($p = 0.05247$). All the killing assays explain that the *apID*⁻ is less efficient in killing *KpLM21*, but not *B. subtilis*.

4.9 *ApID* expression in axenic *D. discoideum* cultures

RNA was isolated from the axenic Ax2 and *apID*⁻ cells and the cDNA was synthesised. These cDNA samples were used for the qRT-PCR analysis to determine the *apID* regulation in the axenic *D. discoideum* cultures. The *apID* expression levels in the axenic cultures are defined based on the Ct (Cycle threshold) values obtained with three independent experiments. In a standard 38 cycle qRT-PCR programme the Ax2 cells showed positive signal for *apID* expression at the 26th cycle (Ct = 26), which implies that the *apID* is moderately expressed in Ax2 cells. In the case of *apID*⁻, no detectable positive signal for was observed. At the end of qRT-PCR, the samples were analysed by agarose gel electrophoresis and visualised under the UV-transilluminator to confirm the sizes of the DNA fragments. For both the *apID* and the housekeeping genes (*rnlA* and *GAPDH*) the expected amplicon sizes were about 170 bps, whereas upon genomic DNA contamination the *GAPDH* primers generate 250 bps amplicon. A typical example is shown below (**Fig. 25**).

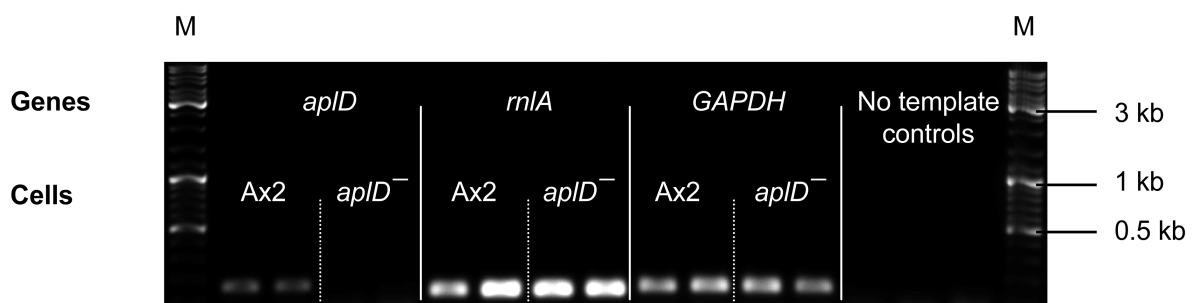


Fig. 25: *ApID* transcription profile in axenic *D. discoideum*. *ApID* transcript levels in Ax2 and *apID*⁻ were analysed by qRT-PCR. From left to right: qRT-PCR products of *apID*, of the house keeping genes *rnlA* and *GAPDH* on agarose gel. Ax2 cells were positive for *apID* expression, whereas *apID*⁻ was negative for *apID* expression. qRT-PCR reaction mixtures without any DNA template for *apID*, *rnlA*, and *GAPDH* primers (no template controls). M: 10 kb DNA ladder

4.10 *ApID* expression during Ax2 development

The Ax2 cells were subjected to development on the non-nutrient 1%-KK2 agar plates at a density of 5×10^5 cells/cm². RNA was isolated at different time points of development, which include 0 h; amoebae, 8 h; cell streams, 12 h; mounds, 16 h; slugs, and 24 h; fruiting bodies.

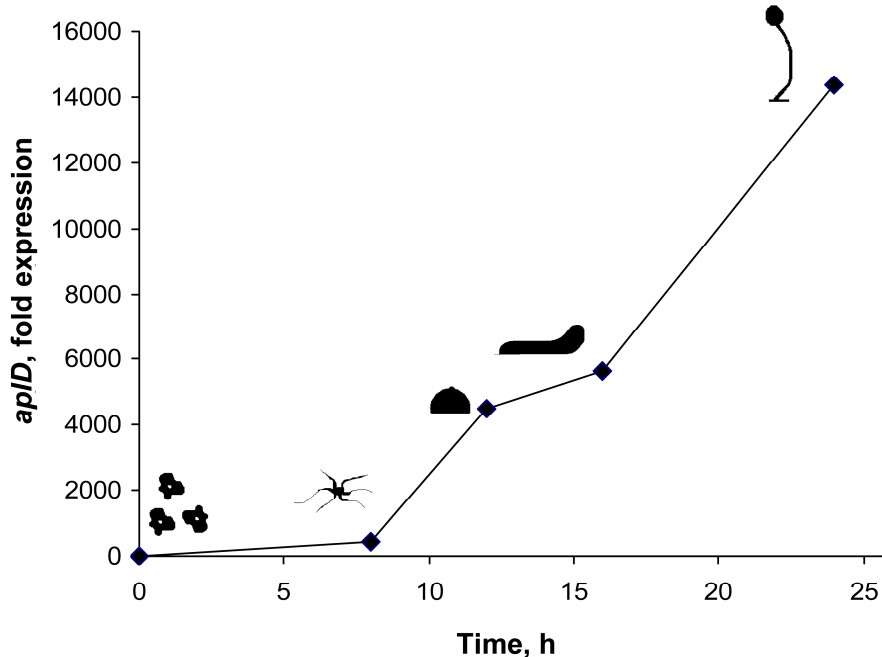


Fig. 26: *ApID* transcription profile during development. Axenically grown Ax2 cells were subjected to development on KK2 agar plates. RNA was isolated at indicated time points, cDNA was synthesised, and *apID* transcription at different stages of development was examined by qRT-PCR. *ApID* expression at time 0 was considered as reference to determine the *apID* fold expression at subsequent development times.

The cDNA samples were synthesised using the RNA templates and the qRT-PCR analyses were performed. The *apID* expression at 0 h was considered as reference to measure the *apID* fold expression at the later time points of Ax2 development (**Fig. 26**). The house keeping genes used for the qRT-PCR quantification includes *rnlA* and *GAPDH*. The qRT-PCR analyses of *apID* regulation during Ax2 development revealed that the *apID* gene is sturdily upregulated from 8 h until 24 h.

4.11 *ApID* regulation in xenic Ax2 cultures

The Ax2 cells were mixed with overnight bacterial cultures at 1:10 ratio and incubated at 22 °C, 140 rpm for 8 h. At the end of 8 h incubation, RNA was isolated, cDNA was synthesised and the *apID* expression was quantified by performing the qRT-PCR. The fold expression of *apID* in the xenic Ax2 cultures was quantified by considering the *apID* expression in the axenic Ax2 cultures as reference (**Fig. 27**).

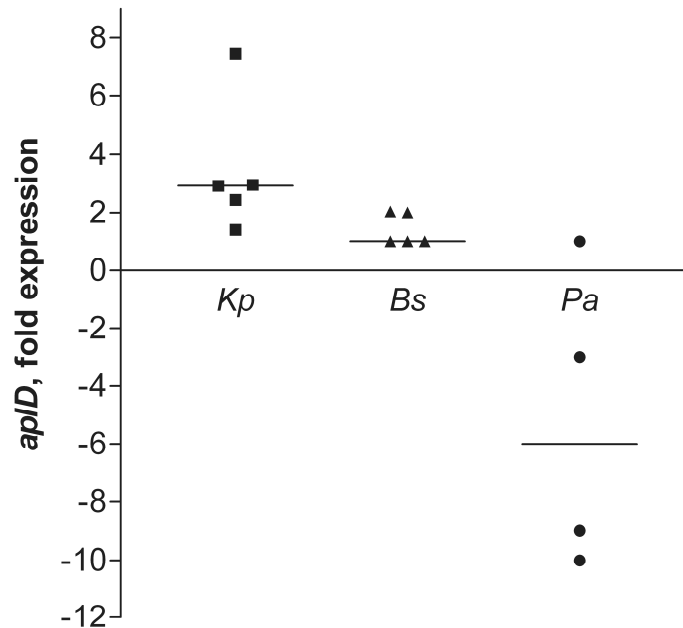


Fig. 27: *ApID* transcription profile in xenic Ax2 cultures. Ax2 cells were mixed with bacteria at 1:10 ratio and the cell suspensions were incubated at 22 °C, 140 rpm. After 8 h, Ax2 cells were collected and *apID* transcript levels were determined by qRT-PCR. *ApID* transcript levels in the axenic Ax2 cultures were considered as reference to determine *apID* fold expression in xenic Ax2 cultures. Bacterial strains tested include *Kp*; *K. pneumoniae* (*KpLM21*), *Bs*; *B. subtilis* (ATCC# 6051) and *Pa*; *P. aeruginosa* quorum sensing mutant (PT531). Each symbol denotes individual experiment and bar represents median.

The Ax2 cells confronted with *K. pneumoniae*, *KpLM21* (*Kp*) showed at least 3-fold up-regulation of *apID*, whereas the Ax2 cells challenged with *B. subtilis* (*Bs*) showed no *apID* regulation and in the Ax2 cells challenged with a quorum sensing mutant of *P. aeruginosa* (*Pa*), PT531, *apID* was at least 6-fold down-regulated.

4.12 *ApID*⁻ development on non-nutrient agar plates

The axenic *D. discoideum* cells were harvested, applied on 1%-KK2 agar plates at a density of 5×10^5 cells/cm² and incubated in the dark at 22 °C.

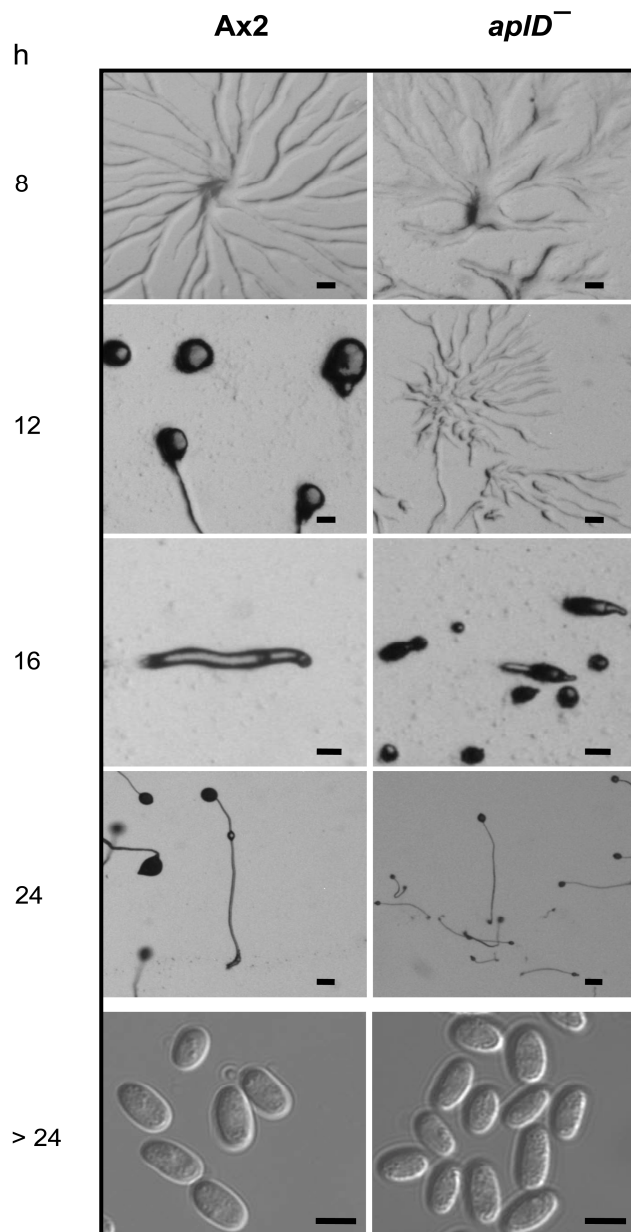


Fig. 28: *D. discoideum* development on agar plates. *D. discoideum* cells were applied on non-nutrient KK2 agar plates at a density of 5×10^5 cells/cm². Plates were incubated in the dark at 22 °C and images were taken at indicated time points. Differential interference contrast (DIC) images are shown; development from 8 to 24 h, scale bars 100 μ m and spores (> 24 h), scale bars 5 μ m.

The development structures were imaged under the microscope (SZX12 Olympus) at the time points indicated (**Fig. 28**). Unlike the Ax2 cells, the *apID*⁻ showed aberrant cell streaming at 8 h and late cell stream breaks at 12 h, which

subsequently resulted in relatively small and enormous number of slugs at ~20 h and fruiting bodies at 24 h of development. However, the spore morphology of the *apID*⁻ was comparable to that of the Ax2 spores (> 24 h) (**Fig. 28**).

4.13 Pre-stalk and pre-spore slug patterns in *apID*⁻

The pre-stalk and pre-spore specific promoter regulations in the *apID*⁻ slugs were analysed by performing the self-mixing experiments. The *apID*⁻ amoebae that were transfected with the *ecmAO*-RFP (pre-stalk reporter) plasmid were mixed with the untransfected *apID*⁻ amoebae at a ratio of 20:80 and subjected to development. When observed under the fluorescence microscope (SZX12 Olympus) the self-chimeric *apID*⁻ slugs showed red fluorescence at one-fifth of the slug front, the pre-stalk region (**Fig. 29C**), in comparison to control Ax2 slugs (**Fig. 29A**). Similar self mixing experiments were performed with the *apID*⁻ cells transfected with *pspA*-RFP (pre-spore reporter) plasmid, for which the slugs showed red fluorescence at four-fifth of the slug rear, the pre-spore region (**Fig. 29G**), similar to Ax2 control slugs (**Fig. 29E**)

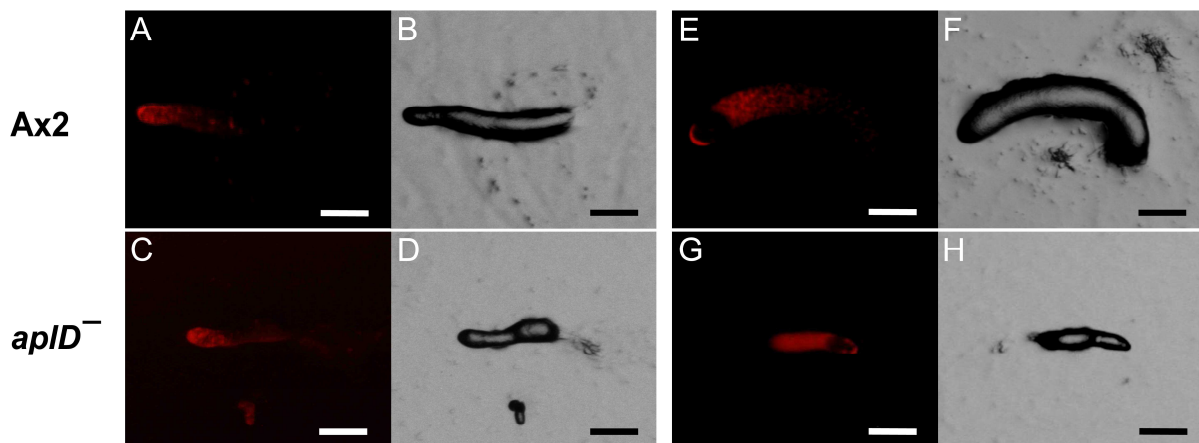


Fig. 29: Pre-stalk and pre-spore patterns of *D. discoideum* slugs. Left panels: *D. discoideum* cells carrying *ecmAO*-RFP plasmid (pre-stalk reporter) were mixed with *D. discoideum* cells. Cell mixture was plated on KK2 agar plates, incubated in dark at 22 °C and slugs were imaged 20 h after plating. Ax2 slug imaged under red filter and DIC (**A, B**) and *apID*⁻ slug imaged under red filter and DIC (**C, D**). Right panels: *D. discoideum* cells carrying *pspA*-RFP plasmid (pre-spore reporter) was mixed with *D. discoideum* cells, plated on KK2 agar plates and incubated in the dark at 22 °C. Slugs were imaged 20 h after plating. Ax2 slug imaged under red filter and DIC (**E, F**) and *apID*⁻ slug imaged under red filter and DIC (**G,H**). Scale bars, 100 μ m

4.14 Spore viability and spore formation efficiency (sfe)

The axenic cultures of *D. discoideum* were mixed with the overnight cultures of *E. coli* B/r and plated on non-nutrient KK2 agar plates. The spore viability was determined by counting the number of phagocytic growth plaques created by the germinated spores on the bacterial lawn.

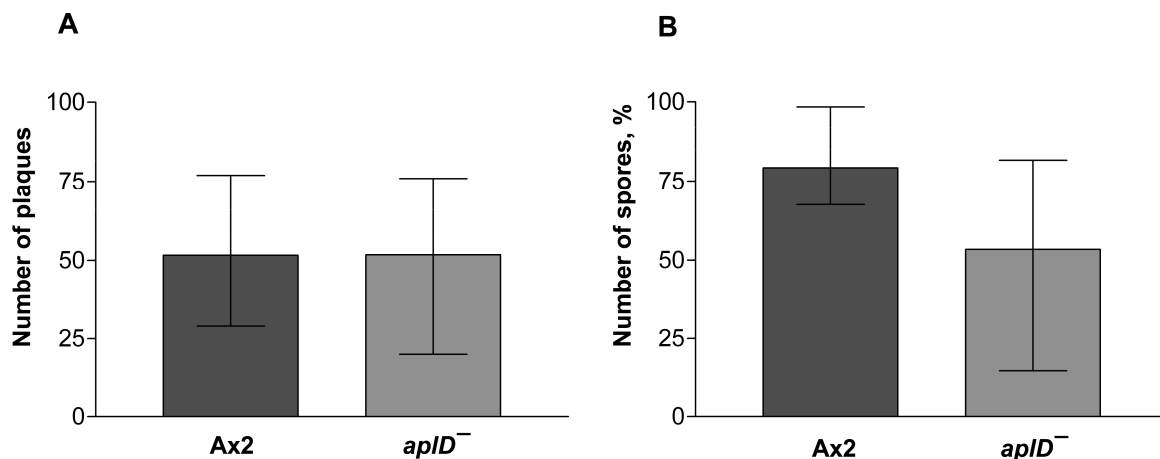


Fig. 30: Spore viability and spore formation efficiency (sfe) analyses in *apID*⁻. **A)** Spore viability: Mature fruiting bodies were harvested and spore densities were determined. A volume of spore suspension with 100 spores was mixed with *E. coli* B/r, plated on KK2 agar plates and incubated at 22 °C. Spore viability was scored by counting the number of phagocytic plaques (Cotter et al., 1966). Number of phagocytic growth plaques counted for Ax2 and *apID*⁻ is shown as median and range. Statistical significance ($p < 0.05$) was evaluated by performing the Mann Whitney test. Results obtained from two independent experiments carried out in triplicates are shown; $p = 0.9372$. **B)** Sfe: Mature fruiting bodies were harvested after 2 days, resuspended in KK2 buffer and spores were counted using a haemocytometer (Hashimoto et al., 1975). Sfe was measured in percentage and represented as median and range. Mann Whitney test was performed to examine the statistical significance ($p < 0.05$). Results are from three independent experiments performed in triplicates; $p = 0.0650$.

Two independent experiments were performed in triplicates to determine the spore viability of *apID*⁻ spores and the Ax2 spores were used as control. The results obtained imply that the viability of *apID*⁻ spores was comparable to that of the Ax2 spores (**Fig. 30A**) and the differences were statistically ($p < 0.05$) not significant ($p = 0.9372$). To measure the spore formation efficiency (sfe), the *D. discoideum* cells were subjected to development on non-nutrient agar plates and the number of spores obtained was counted. Three independent experiments were performed in triplicates and the statistical significance ($p < 0.05$) was analysed by Mann Whitney test. The results showed that the sfe of the *apID*⁻ was relatively reduced when compared with Ax2 cells ($p = 0.0650$) (**Fig. 30B**)

4.15 Examination of sentinel (S) cells in *aplD*⁻

The *aplD*⁻ slugs were allowed to migrate for 6 h on 1%-Sørensen's agar plates containing 3 $\mu\text{g/ml}$ EtBr and imaged under the fluorescence microscope (SZX12 Olympus) to examine the presence of S cells. Comparable to the Ax2 slugs (**Fig. 31B**), the *aplD*⁻ slugs showed EtBr filled S cell clumps in the slug interior and also in the slime sheath (**Fig. 31E**). Similar results were obtained for the slugs migrating on 10 $\mu\text{g/ml}$ EtBr agar plates (data not shown).

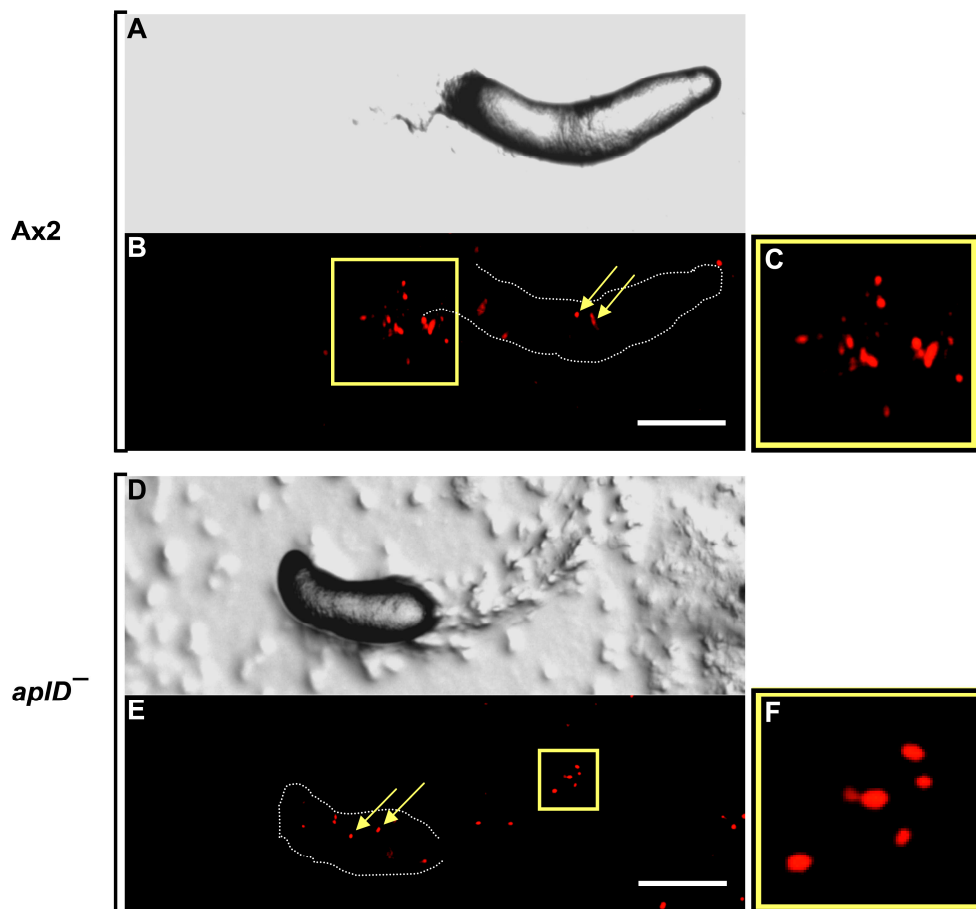


Fig. 31: Sentinel (S) cells examination in *D. discoideum* slugs. Axenic *D. discoideum* cells were applied on Sørensen's agar plates containing EtBr (3 $\mu\text{g/ml}$). Plates were incubated in a dark, moist chamber with a unidirectional light source. After 20 h, slugs of Ax2 and *aplD*⁻ were imaged under the microscope. (**A** and **D**) DIC images of *D. discoideum* slugs. (**B** and **E**) S cells in *D. discoideum* slugs are shown in red. S cells inside slugs (arrows) and in slime sheath (boxes in **B** and **E** were magnified: **C** and **F**). Scale bars, 100 μm .

4.16 *D. discoideum* slugs infection with *K. pneumoniae*

The *D. discoideum* slugs were infected with a *K. pneumoniae* strain expressing the GFP reporter (KpGFP) (Lee and Falkow 1998) and (Benghezal et al. 2006).

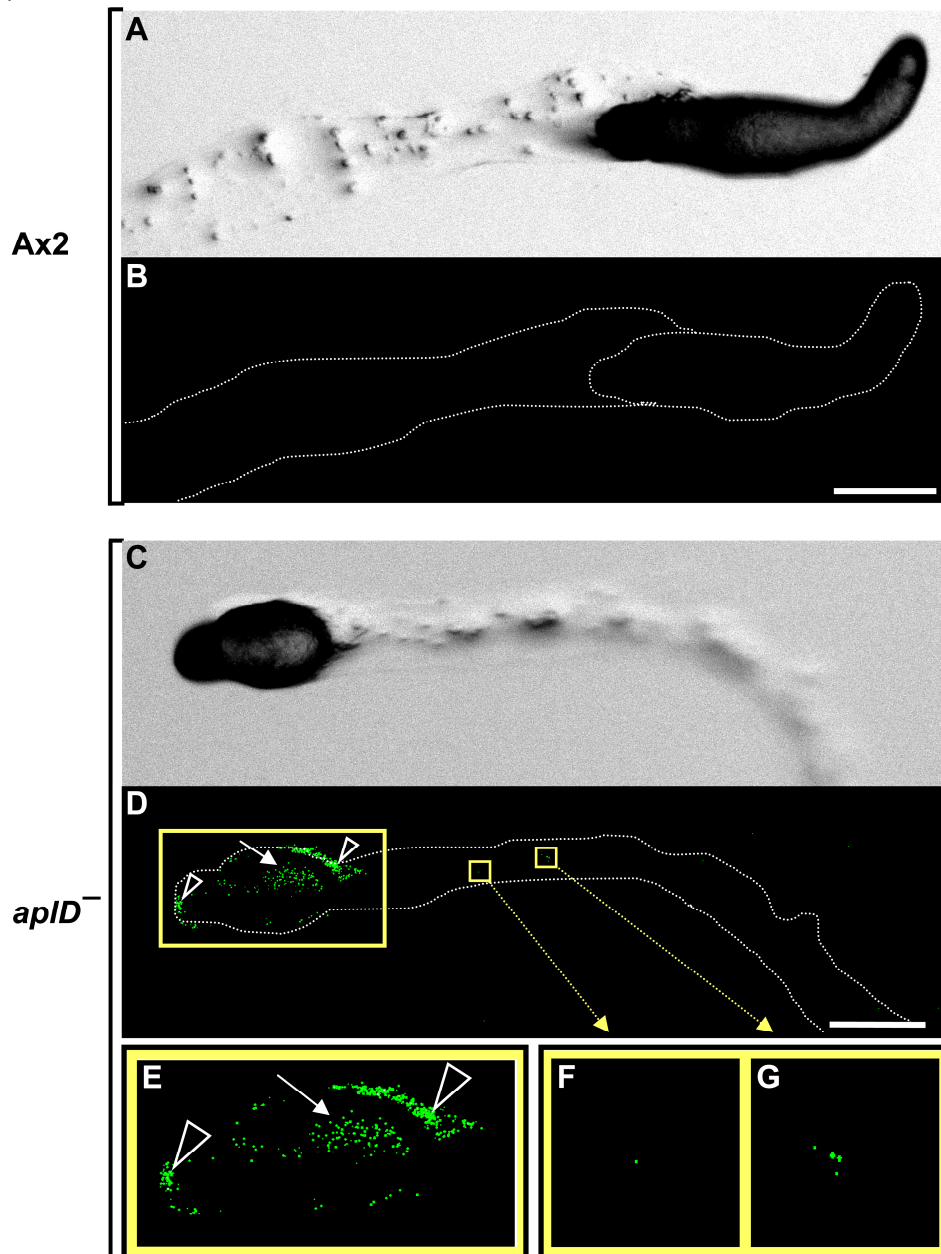


Fig. 32: *ApID*⁻ slugs infected with *KpGFP*. *D. discoideum* cells were deposited on Sørensen's agar plates and incubated in a dark, moist chamber with a unidirectional light source. After 20 h, under stereo microscope; slugs were gently punctured with a sterile needle. *KpGFP* bacteria of higher cell density were layered on injured slugs and plates were transferred to the incubation chamber. Slugs were imaged 24 h post infection. (A and C) DIC images of Ax2 and *apID*⁻ slugs. (B and D) *KpGFP* in *D. discoideum* slugs are shown in green. (E) Magnification of *apID*⁻ slug (D) showing *KpGFP* accumulation inside the slug (arrow) and *KpGFP* deposits on slug surface (arrowheads). (F and G) Magnifications of the slime sheath of *apID*⁻ slug (D) showing sloughed off *KpGFP* in the slime sheath. Scale bars, 100 μm

the slugs were imaged under the fluorescence microscope (SZX12 Olympus) 20 h post infection with *KpGFP*. In the case of Ax2 slugs, the slug interior, the slug surface and the slime sheath showed no *KpGFP* bacteria (**Fig. 32B**). In contrast, in the *ap1D*⁻ slug, both the slug surface and the slug interior were filled with *KpGFP*. Even after migrating for long distance as evidenced by a lengthy slime sheath, there was very less *KpGFP* visible in the slime sheath of the *ap1D*⁻ slug (**Fig. 32D**).

4.17 *KpGFP* bacterial clumps in *D. discoideum* slugs

The *D. discoideum* slugs were infected with *KpGFP* bacteria and observed under the fluorescence microscope (SZX12 Olympus) 24 h post infection.

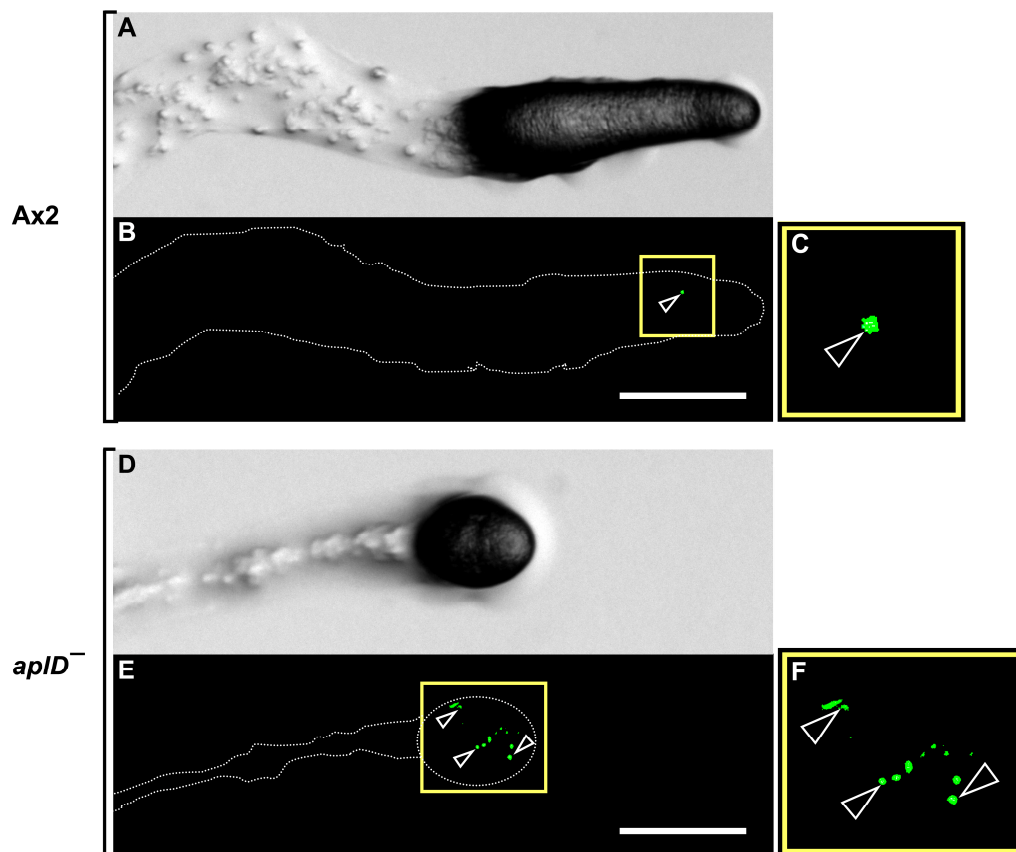


Fig. 33: *K. pneumoniae* (*KpGFP*) clumps visualised in *ap1D*⁻ slugs. *KpGFP* infected *D. discoideum* slugs were imaged 24 h post infection. (**A** and **D**) DIC images of Ax2 and *ap1D*⁻ slugs. (**B** and **E**) *KpGFP* clumps within *D. discoideum* slugs are shown in green. (**C** and **F**) Magnifications of the boxed areas in **B** and **E**. *KpGFP* clumps visible inside Ax2 and *ap1D*⁻ slugs (arrowheads). Scale bars, 100 μ m

The *KpGFP* bacterial clumps were visible both in the Ax2 slug and in the *ap1D*⁻ slug, but the number of *KpGFP* clumps observed within the *ap1D*⁻ slug was relatively more when compared with the *KpGFP* clump observed within the Ax2 slug (**Fig. 33**).

4.18 *D. discoideum* slugs infection with *E. coli* DsRed

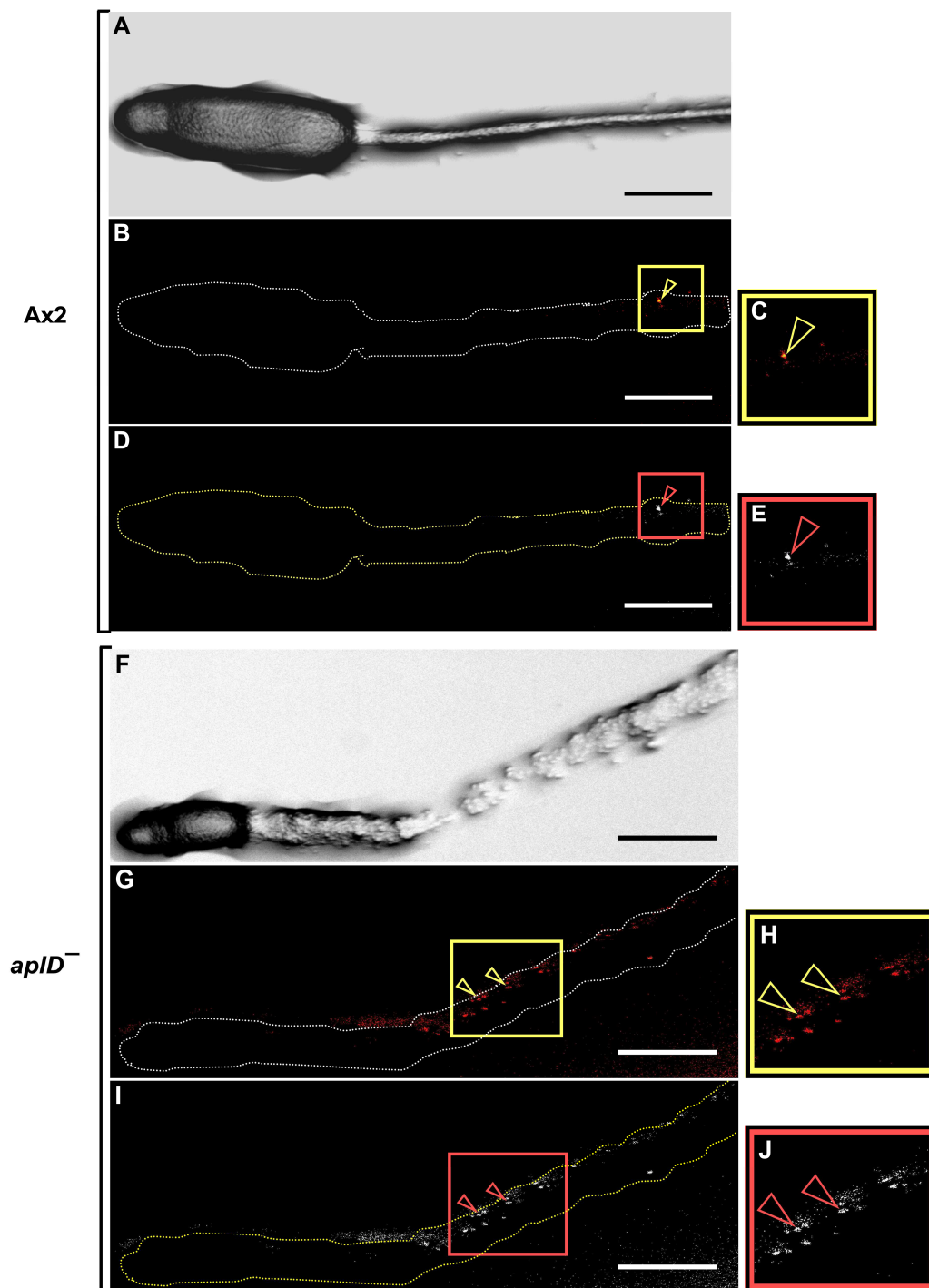


Fig. 34: *ApID⁻* slugs infected with *E. coli* DsRed. *D. discoideum* cells were deposited on Sørensen's agar plates and incubated in a dark, moist chamber with a unidirectional light source. After 20 h, under stereo microscope slugs were punctured with a sterile needle. *E. coli* DsRed bacteria of higher cell density were layered on injured slugs and slugs were imaged under microscope 8 h post infection. (A and F) DIC images of Ax2 and *apID⁻* slugs. *E. coli* DsRed clumps (arrowheads) in Ax2 (B and D) and *apID⁻* (G and I) slime sheath are shown in red and white. (C and E) magnifications of boxed areas in B and D. (H and J) magnified images of marked areas in G and I. Scale bars, 100 μ m

The *D. discoideum* slugs were infected with *E. coli* DsRed bacteria and observed under the fluorescence microscope (SZX12 Olympus) 8 h post infection. The Ax2 slug showed relatively less *E. coli* DsRed shedding in the slime sheath and the slug interior was totally free of any *E. coli* DsRed bacteria (**Fig. 34B** and **D**). In contrast, the *apID*⁻ slug infected with *E. coli* DsRed showed relatively substantial amount of *E. coli* DsRed clumps and depositions in the slime sheath, whereas the slug interior and the slug surface was comparable to that of the Ax2 slug, showed very less bacteria in the slug rear and on the slug surface (**Fig. 34G** and **I**).

4.19 Western blot analysis of ApID-FLAG protein

The *apID* cDNA was ligated into pDneo2a-3xFLAG expression vector (Dubin et al., 2010) for the synthesis of ApID protein with a C-terminal FLAG tag fusion.

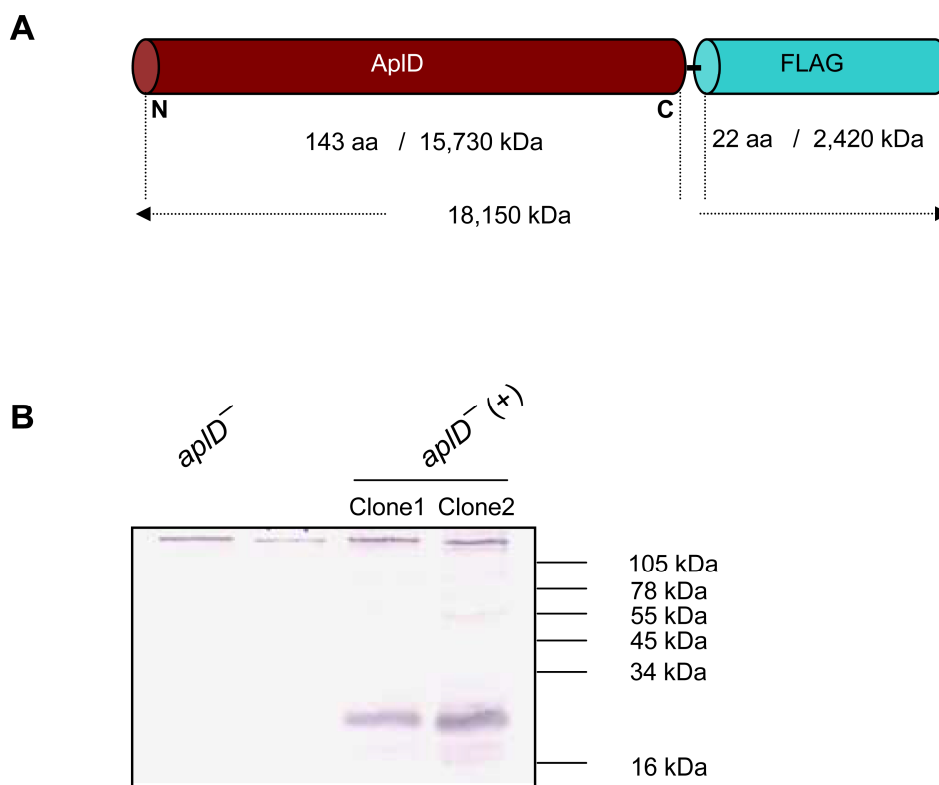


Fig. 35: Architecture and identification of ApID-FLAG tag protein produced in *apID*⁻ cells. **A)** ApID-FLAG tag protein: FLAG tag was fused at 3' region of *apID* cDNA to produce ApID protein with C-terminal FLAG tag. **B)** Western blot analysis: Cell lysates were prepared from *apID*⁻ (control) and *apID*⁻/[*act6*]:*apID*:FLAG [rescue strain: mentioned as *apID*⁻ (+)]. Two clones of the rescue strain were positive for ApID-FLAG fusion protein synthesis and no signal was observed in *apID*⁻. Molecular masses in kDa are shown at the right.

Cell lysates were prepared from the clonal isolates that overexpresses ApID-FLAG fusion protein in *apID*⁻ background and subjected to separation on a SDS gel, which was followed by western blot analysis. The cell lysate prepared from *apID*⁻ was used as negative control. Protein separation and western blot analysis was carried out as described in the Methods chapter (**section 3.19 to 3.21**). The expected size of the ApID-FLAG fusion protein was about 18.1 kDa (**Fig. 35A**). The western blot analysis confirmed two clones that were positive for ApID-FLAG fusion protein expression, whereas the *apID*⁻ was negative for the expression of ApID-FLAG fusion protein (**Fig. 35B**). The *apID*⁻/[*act6*]:*apID*:FLAG strain (clone 2) was used for the analysis of intra-cellular localisation of ApID protein and also for the phenotype rescue experiments (see **Appendix 8.2**)

4.20 Development experiment with rescue strain [*apID*⁻ (+)]

Axenic *D. discoideum* cultures were subjected to development on KK2 agar plates at a density of 5×10^5 cells/cm². The cell streams were imaged at 11 h of development and also the number of aggregation centres was determined (**Fig. 36 and 37**).

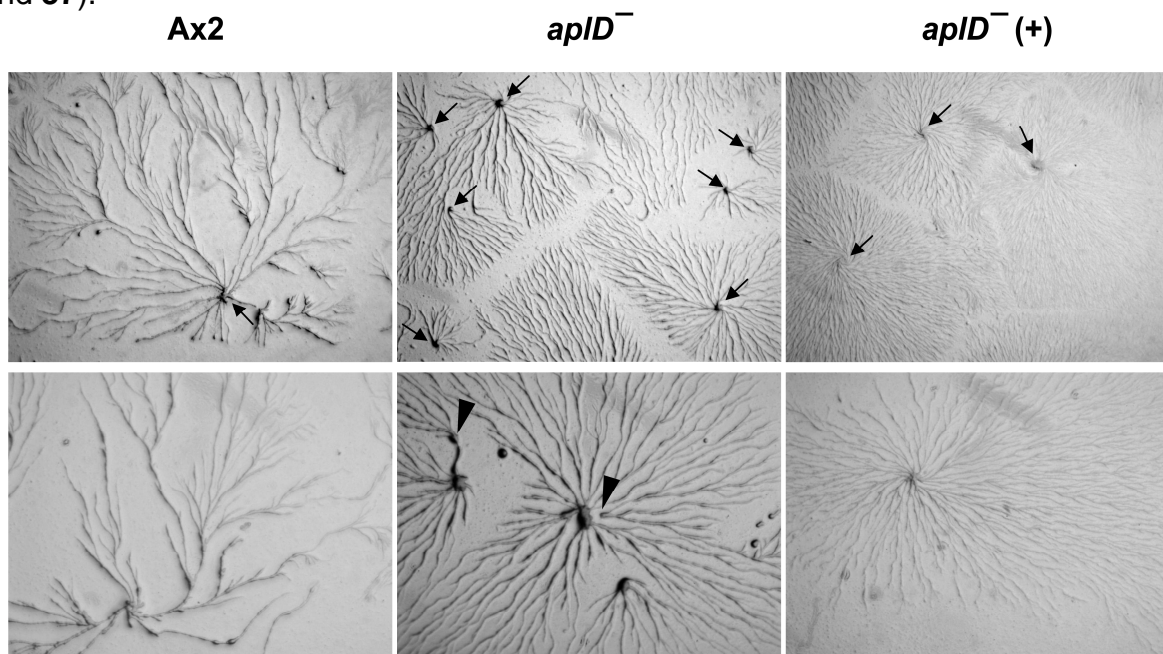


Fig. 36: Development experiment with rescue strain [*apID*⁻ (+)]. Axenically grown *D. discoideum* cells were applied on KK2 agar plates and imaged after 11 h. Right panels: *apID*⁻ (+); rescue strain expressing ApID-FLAG fusion protein under the control of *actin 6* promoter, in *apID*⁻ background. Arrows represent aggregation centres and the arrowheads denote stream breaks

As described earlier, the *apID*⁻ showed stream breaks during late streaming stage (11 h), whereas the *apID*⁻ (+), which expresses *apID* under *act6* promoter, in *apID*⁻ background, showed no stream breaks during late streaming (**Fig. 36**).

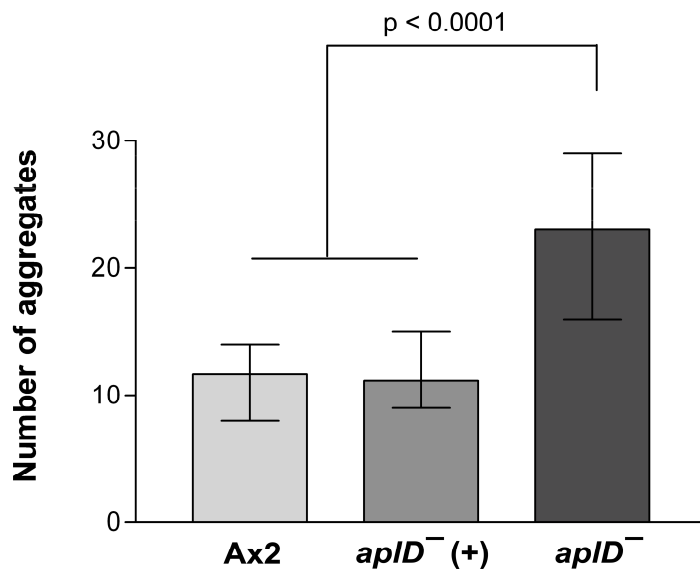


Fig. 37: Replacement of *apID* restores streaming defect. Indicated cell types were applied on KK2 agar plates and the number of aggregates was counted after 12 h. *apID*⁻ (+); rescue strain expressing ApID-FLAG fusion protein under actin 6 promoter, in *apID*⁻ background. Values represented are mean and bars denote range (n = 2, with triplicates). One-way-ANOVA was performed to determine the statistical (p < 0.05) significance and the differences are statistically significant (p < 0.0001). The difference between Ax2 and *apID*⁻ (+) is not significant (Dunnett's test) (Debra a Brock et al. 2006)

Unlike *apID*⁻, the pattern and the number of aggregates formed by *apID*⁻ (+) were comparable to that of Ax2 (**Fig. 36** and **37**). The difference in number of aggregates between *apID*⁻ (+) and *apID*⁻, including the technical control Ax2 was statistically significant (p = 0.0001). The statistical difference between *apID*⁻ (+) and Ax2 was not significant.

5 Discussion

D. discoideum genome comprises 17 apIs and at least 15 lysozyme genes (**Fig. 8** and **9**). *D. discoideum* ApIs belong to SAPLIP family, which is well known for its antimicrobial and cytolytic functions. In *D. discoideum* there are also SAPLIP domain containing proteins that remain as a part of large protein complex, as well as SAPLIP domain is found in multidomain protein. For instance, counting protein that possesses a SAPLIP domain is a part of a protein complex called counting factor and counting acts as an aggregate size sensor during development (D. A. Brock et al. 1996); (D. A. Brock and Gomer 1999); (D. A. Brock et al. 2006). Acyloxyacyl hydrolase possesses a SAPLIP domain and a hydrolase domain (Munford, Sheppard, and O'Hara 1995). The functions of both, counting factor complex and AOA in *D. discoideum* are unknown at present. As *D. discoideum* is a professional phagocyte it is not a surprise to evidence several SAPLIP members in its genome. Incidentally, the genome of *E. histolytica* possesses 15 SAPLIP, including three well characterised SAPLIP, amoebapore A, B, and C (H. Bruhn and Leippe 2001b). The amoebapores are persuasively proved for their pore-forming and antimicrobial activity, and are reported to be stored in the intracellular cytoplasmic granules. Upon exposure to bacteria, amoebapores are implicated in intracellular killing of bacteria (**Fig. 3**) (Andrä, Herbst, and Leippe 2003). Additionally, *E. histolytica* genome also possesses two lysozymes, which are described to be antimicrobial (Jacobs and Leippe 1995); (Nickel, Jacobs, and Leippe 1998). Many organisms analysed for lysozymes comprise only a specific class of lysozyme, but the *D. discoideum* genome constitutes different classes of lysozymes. Perhaps, in *D. discoideum*, apart from bacterial killing, lysozymes are also implicated in bacterial degradation processes (Prager 1996); (M. Leippe 1999); (Müller et al. 2005). It is also possible that the ApIs and lysozymes could play a synergistic role in bacterial killing and degradation. In the past, nothing was known about the functions of AMPs in *D. discoideum*, whereas concerning lysozymes, AlyA is the only lysozyme that had been characterised both, at gene and protein level. AlyA belongs to a unique class of lysozymes in *D. discoideum* and localise to cytoplasmic vesicles that are devoid of other lysozymes (Müller et al. 2005). My present study has focussed on three apIs, *apID*, *apIJ*, and *apIP* and two lysozyme genes, *lyC2* and *lyC3* (**Fig. 17A**). These

candidate genes are specifically chosen as they are suggested to be involved in bacterial killing and degradation processes (Bozzaro, pers. comm., 2008; (Sillo et al. 2008). Additionally, earlier work in our laboratory had found that recombinantly expressed ApIC and ApID were antimicrobial against *Bacillus megaterium* and *E. coli* (unpublished data). I generated single gene KO clones for *aplD*, *aplJ*, *aplP*, *lyC2*, and *lyC3* using the gene targeting vector (J. Faix et al. 2004) and tested their growth abilities on bacteria.

When plated on a lawn of non-pathogenic bacteria *D. discoideum* amoebae feed on bacteria, which result in the formation of phagocytic plaques, but the virulent bacteria remain non-permissive for phagocytic feeding by the amoebae. This phenomenon is widely used to examine the degree of bacterial virulence and their virulence factors, using *D. discoideum* as a model system (Cosson et al. 2002); (Pukatzki, Kessin, and Mekalanos 2002); (Benghezal et al. 2006). The degree of bacterial virulence mainly relies on the growth medium on which the bacteria are grown (Froquet et al. 2009). Likewise, the extent of pathogenicity varies depending on the number of host cells exposed to the bacterial pathogen and vice versa (Alibaud et al. 2008) (Froquet et al. 2009). For the precise understanding of virulence mechanism of a particular bacterial strain, it is crucial to consider both the above mentioned aspects. Therefore, I tested the growth abilities of the KO mutants with bacteria seeded on two different growth media (G+ and G-), by depositing varying number of *D. discoideum* amoebae on each bacterial strain (**Fig. 13**) (Froquet et al., 2009). Among all five KO mutants tested on various bacterial strains, the *aplD*⁻ showed growth defects on several strains of *K. pneumoniae*. The *K. pneumoniae* strains tested include a non-pathogenic laboratory strain (*Kp13883*), a clinical isolate with a plasmid mediated virulence that is characterised by a huge polysaccharide capsule (*Kp52145*) (Nassif et al. 1989); (Benghezal et al. 2006), an isogenic mutant of *Kp52145*, which is defective for capsule synthesis (*K*⁻) (Nassif et al. 1989) and, a wild isolate of *K. pneumoniae*, which is also characterised by a huge polysaccharide capsule (*KpLM21*) (Favre-Bonté et al. 1999). *K. pneumoniae* is a Gram-negative, rod shaped, and ubiquitous bacteria that is often described to cause nosocomial infections, such as urinary tract infection, pneumonia, surgical-wound infections, bacteraemia, and septicaemia (Podschun and Ullmann 1998). In general, the *D. discoideum* cells grown with *K. pneumoniae* plated on G+ medium were able to form larger growth plaques when compared with those plaques on G- plates

(**Fig. 20**). Moreover, the Ax2 cells were able to form fruiting bodies on G+ medium layered with *K. pneumoniae*, but not with *K. pneumoniae* plated on G- medium. Therefore, it can be hypothesised that the *K. pneumoniae* strains seeded on G+ medium were readily permissive for *D. discoideum* growth, unlike the *K. pneumoniae* strains grown on G- medium. These observations emphasise the fact that glucose may play a crucial role in determining the bacterial virulence. In other words, the *K. pneumoniae* virulence mechanism is suppressed in the presence of glucose. Notably, *Prevotella intermedia* and *P. nigrescens*, which are also Gram-negative rods, are known to produce cytotoxic end products only when grown in the absence of glucose, whereas in the growth medium containing glucose the production of cytotoxic end products is drastically reduced (Saito et al. 2001). Interestingly, the *apID*⁻, which was able to create plaques with *KpLM21* and *K*⁻ seeded on G+ medium, was unable to form plaques on the corresponding G- plates (**Fig. 20**). These observations were confirmed by three independent experiments performed with duplicates. Surprisingly, similar observations were reported for the laboratory mice infected with *KpLM21* and observed for the bacterial colonisation in their intestine (Favre-Bonté et al. 1999). The intestinal tract of the mice showed wide spread distribution of *KpLM21*, but not the capsule defective mutant of *KpLM21* (Favre-Bonté et al. 1999). These observations imply that the capsular polysaccharides protect the bacteria from the detrimental serum complements and to evade the harsh lysosomal environment of the professional phagocytes (Nassif et al. 1989); (Benghezal et al. 2006); (Alibaud et al. 2008). Additionally, the *KpLM21* strain used in this study was reported to produce autoinducer-2 (AI-2) to regulate the expression of its quorum sensing genes and the expression of AI-2 varies with the growth medium in which *KpLM21* was cultured (Balestrino et al. 2005). This finding corroborates with the growth defect phenotype of *apID*⁻ grown with *KpLM21* on G- plates and not on G+ plates. Probably, the bacterial virulence genes are highly expressed in *KpLM21* plated on G- medium than the *KpLM21* plated on G+ medium. However, Ax2 cells created plaques with *KpLM21* grown on both, G+ and G- media.

The *apID*⁻ also showed growth defect with the capsule defective mutant (*K*⁻) layered on G- medium, but not with its parent strain *Kp52145* (**Fig. 20**). Likewise, *apIP*⁻ and *lyC2*⁻ showed growth defects on *K*⁻, but not on *Kp52145* (data not shown). However, Ax2 was able to form phagocytic growth plaques on *Kp52145* and its isogenic mutant (*K*⁻). Apart from the capsular polysaccharides and

lipopolysaccharides, the virulence factors of *Kp52145* include pili which are implicated in adherence of *Kp52145* to the host cells and to other surfaces, and a 180 kb plasmid mediated production of aerobactin and the other factors that are crucial for mucoid phenotype (Riottot 1981); (Nassif et al. 1989). Hence, it is possible that the defect in capsule synthesis could be replaced by the regulation of other virulence factors, resulting in enhanced virulence of K^- when compared with the parent strain *Kp52145*. Supporting this notion, it had been shown that the human airway epithelial cells infected with a capsule defective mutant of *Kp52145* induced the expression of human β -defensins (hBD2 and hBD3), unlike the parent strain *Kp52145* (Moranta et al. 2010). This finding corroborates with the growth defect phenotype imposed by $apID^-$, $apIP^-$ and $lyC2^-$ with K^- , but not with its parent strain *Kp52145* (on G- medium). Presumably, ApID, ApIP and LyC2 may play a synergistic role in intracellular killing of K^- .

As an instant observation, the virulent *Kp52145* and its isogenic capsule defective mutant showed different colony morphologies on LB agar plates. The colonies of *Kp52145* were globular and mucoid with a viscid consistency (**Fig. 23B**). The mucoid phenotype serves as a confirmation for its plasmid mediated virulence. In contrast, the colonies of the isogenic capsule defective mutant of *Kp52145* (K^-) were relatively small, flat, non-mucoid, and non-viscous (**Fig. 23C**). Similar observation had been reported earlier by Nassif et al. (1989) while comparing the parent strain *Kp52145* and a plasmid cured variant of *Kp52145*. In comparison to K^- , the wild isolate, *KpLM21* also formed non-mucoid, small, but globular colonies (**Fig. 23D**). The colony sizes of K^- and *KpLM21* were comparable, whereas the colony morphologies of non-pathogenic *Kp13883* were comparable to that of *Kp52145*. The colonies of *Kp13883* were globular, mucoid and even larger than *Kp52145* (**Fig. 23A**). The colony morphologies of *K. pneumoniae* and their degree of permissiveness for *D. discoideum* growth explicitly demonstrate pathogenicity and virulence. The *K. pneumoniae* which formed large colonies were avirulent, whereas those which formed small colonies were virulent and non-permissive for the growth of $apID^-$. Notably, the multi-well growth assays remain as a promising approach to understand and to improvise our knowledge about bacterial virulence mechanisms and the host resistance factors.

Following the bacterial growth assays, I performed the bacterial phagocytosis and killing assays to analyse whether the $apID^-$ is also defective for killing *KpLM21*. I

performed the bacterial killing assays with non-pathogenic *B. subtilis* (ATCC #6051) and the virulent *K. pneumoniae* strain (*KpLM21*). The rate of bacterial killing by *D. discoideum* is inversely proportional to the number of viable bacteria counted during the course of experiment. When compared with Ax2, the *apID*⁻ was relatively more efficient in killing *B. subtilis*, whereas less efficient in killing *KpLM21*. On the other hand, the killing assays in which the number of viable *KpLM21* associated (intracellular) with *D. discoideum* was measured, the *apID*⁻ showed massive intracellular accumulation of viable *KpLM21* at time points in between 0.5 h to 1 h, but this was not the case with Ax2 (**Fig. 38B**). The mechanisms by which the bacterial pathogens evade the intracellular killing machinery of *D. discoideum* were well described. The bacterial pathogens entrapped within the phagosome may inhibit phagosome maturation and utilise the phagosomal niche for their replication, e.g., *Legionella pneumophila* (Bozzaro and Eichinger 2011), and *Mycobacterium marinum* and *M. tuberculosis* (Hagedorn et al. 2009). Soon, the phagosomes rupture releasing the bacteria into the cell cytosol. This was followed by necrotic cell lysis, delivering bacteria into the surrounding milieu. Another mechanism developed by the pathogenic bacteria is the spreading of bacterial pathogen from the infected amoebae to the neighbouring non-infected amoebae through the ejection, without destroying the *D. discoideum* amoebae (Hagedorn et al. 2009). This mechanism is termed as non-lytic spreading.

Additionally, *D. discoideum* is equipped with a sophisticated mechanism to liberate the undigested lysosomal cargo by efficient exocytosis (Müller et al. 2005). The former mechanism, intracellular replication of bacteria may not be the case observed in the killing assays of *apID*⁻ with *KpLM21*, because the number of viable bacteria counted at each time point was always less than the number of viable *KpLM21* at initial time point (0 h). Therefore, it is possible that the bacteria accumulated in the intracellular environment are cleared by exocytosis. In the following, the result obtained with killings assays total (**Fig. 38A**) and intracellular (**Fig. 38B**) are described from the perspective of phagocytosis scheme in *D. discoideum*. Generally, endocytic uptake of particle in *D. discoideum* begins at around 3 min, after exposure to the particles, followed by acidification of the phagosome at ~20 min by phago-lysosome fusion. Subsequently, neutralisation of the compartment at 45 min and finally the undigested materials are exocytosed at around 60 min (Maniak 2001); (Rupper and Cardelli 2001); (Müller et al. 2005). This

general endocytic pathway may be affected if the intracellular environment is manipulated by some pathogenic bacteria, e.g. *L. pneumophila* (Isberg, O'Connor, and Heidtman 2009); (Bozzaro and Eichinger 2011) and *Mycobacterium* species (Hagedorn et al. 2009). Ultimately, the killing assay results of *KpLM21* remain comparable with the general endocytic pathway of *D. discoideum*. In the case of killing assays where the total number of viable bacteria was counted, there was a gradual decrease in the number of viable *KpLM21* observed over time (**Fig. 38A**). However, in contrast with Ax2, the *apID*⁻ showed relatively high number of viable bacteria at later time points. The difference in number of viable *KpLM21* between the Ax2 and *apID*⁻ was apparent starting from 1 h up to 4 h time points (**Fig. 38A**). In the case of killing assays intracellular, there was a massive difference observed in the number of viable *KpLM21* between Ax2 and *apID*⁻ at time points 0 h up to 1 h, followed by no difference at later time points (**Fig. 38B**). The hypotheses derived from the killings assays with *KpLM21* (total [A] and intracellular [B]) are the following. The *apID*⁻ begins with *KpLM21* uptake (0 h) similar to the manner observed in Ax2, as the *apID*⁻ is defective for intracellular killing of *KpLM21*, it has gradually accumulated *KpLM21* (0.5 h to 1 h) that are efficiently exocytosed into the surrounding milieu at the end (1 h to 4 h) (**Fig. 38A and B**).

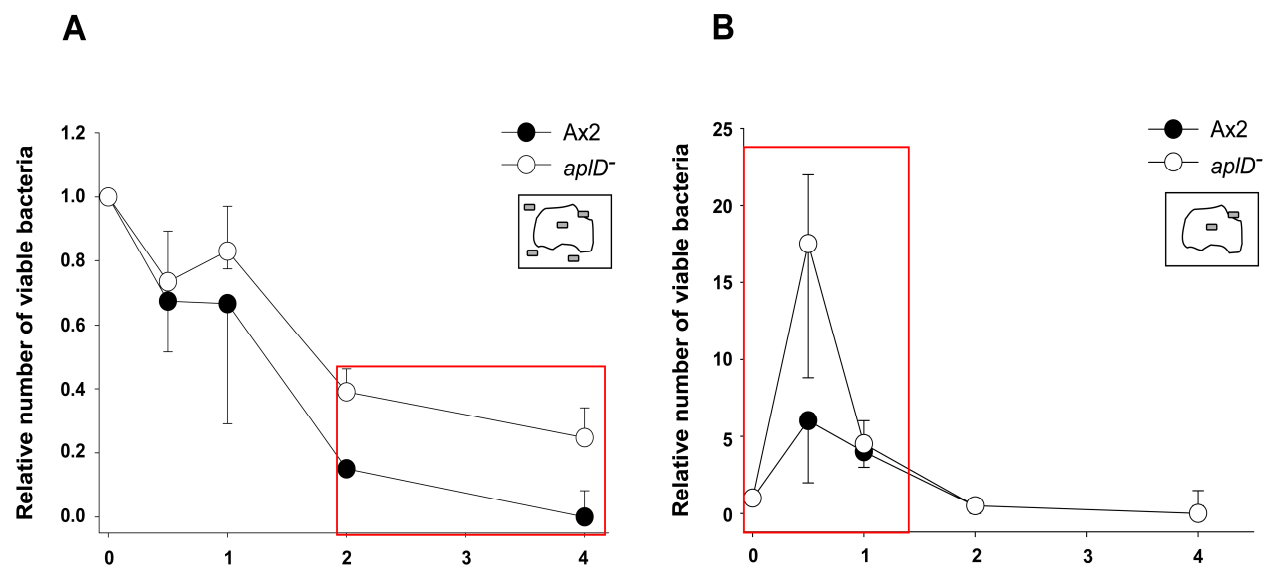


Fig. 38: *apID*⁻ is defective for intracellular killing of *KpLM21*. *D. discoideum* and *KpLM21* were mixed at a ratio of 100:1 and incubated at 22 °C, 140 rpm. At indicated time points, cell mixtures were removed and lysed to enumerate the total number of viable bacteria (A; see cartoon) and the number of viable bacteria associated with *D. discoideum* at each time point (B; see cartoon). The marked regions (red) represent the difference in number of viable bacteria between Ax2 (●) and *apID*⁻ (○).

To test whether the *apID*⁻ has any developmental defects, the *apID*⁻ cells were applied on non-nutrient KK2 agar plates and the development scheme was followed considering Ax2 as control. The morphogenetic stages investigated include 8 h cell streams, 12 h mounds, 16 h slugs, 24 h fruiting bodies, and the mature spores at 48 h (see **Fig. 28**). In comparison to Ax2, the *apID*⁻ cells were able to form early cell streams (8 h), but at 12 h of development the *apID*⁻ started showing stream breaks. As a consequence of stream breaks, the *apID*⁻ formed relatively smaller slugs and fruiting bodies, which were approximately half the size of Ax2 slugs and fruiting bodies. In addition, the morphogenetic time frame of *apID*⁻ was also affected because of the late stream breaks. Hence, the development stages proceeding after cell streaming, the mounds, slugs, and fruiting bodies showed at least 2 h delay. The *apID*⁻ formed mounds at about 15 h, slugs in between 18 h to 20 h and fruiting bodies at ~26 h (**Tab. 9**). Unlike the “Slugger” mutants (Sussman and Schindler 1978); (Gee, Russell, and Gross 1994), which migrate for 10 to 12 h, the *apID*⁻ slugs migrated for a short time, before progressing to culmination or fruiting body construction. Moreover, the pre-stalk and pre-spore slug patterns of the *apID*⁻ were comparable to that of the Ax2 slugs (see **Fig. 29**). The spore morphology and the spore viability (D. A. Cotter and Raper 1966); (D. A. Cotter and Raper 1968) of the *apID*⁻ were comparable to that of the Ax2 spores, but the spore formation efficiency (Y. Hashimoto, Cohen, and Biology 1975) of the *apID*⁻ was relatively reduced when compared with Ax2. Although the *apID*⁻ showed delayed development process, no signs of developmental arrest were evidenced. Usually, the stream break phenotype during *D. discoideum* development happens due to two reported reasons.

Tab. 9: Axenically grown *D. discoideum* cells were applied on non-nutrient KK2 agar plates and the development scheme was followed. (* delayed).

Time points	Ax2	<i>apID</i> ⁻
0 h	Starving amoebae	Starving amoebae
8 h	Early cell streaming	Early cell streaming
12 h	Late streams approaching to mounds	Stream breaks
14 h	Tipped mounds	Progressing to mounds*
16 h	Slugs	Tipped mounds*
20 h	Culmination	Slugs (18 h) *
24 h	Fruiting bodies	Migrating slugs and culmination*
26 h		Fruiting bodies*

The cell streams may break if the streaming cells are defective for the production of cell adhesion proteins, such as CsA (Contact site A) and LagC (Loose aggregate C). For instance, the *triA*⁻, which was defective for the synthesis of CSA (delayed production), followed by precocious production of LagC showed stream breaks during development (Mujumdar, Inouye, and Nanjundiah 2009). Moreover, the overexpression of *csA* was also described to cause cell stream breaks and subsequently, small fruiting bodies (J. Faix, Gerisch, and Noegel 1992). Also, cell stream breaks happen if the cells are defective for aggregation and/or if the cells are overproducing some extracellular factors that could act as cell size sensors during development. It is known in *D. discoideum* that during development the cells can both, produce and sense signals (Schaap 2011). For instance, the *smIA*⁻ of *D. discoideum* overproduces a 35 kDa protein, named as countin (CtnA). Countin is a hydrophilic protein that belongs to a polypeptide complex whose size is > 450 kDa. Overproduction of countin causes cell stream breaks in *smIA*⁻, resulting in the formation of small size aggregates and relatively smaller fruiting bodies. On the other hand, the *countin* mutant (*ctnA*⁻) was unable to sense the aggregate size, therefore form relatively larger aggregates and fruiting bodies, unlike Ax2 (D. A. Brock and Gomer 1999). Also, the mutants of signal transduction pathways were reported to show stream breaks and smaller aggregates. For instance, stream breaks were observed in mutants with hyperactivated extracellular phosphodiesterase that disrupts the cAMP waves required for chemotaxis (Riedel et al. 1973); (Faure et al. 1988), mutants with disrupted *mekA*, which encodes MAP kinase (Ma et al. 1997), and the mutants that overproduce modified *ras* signalling protein (Reymond et al. 1986). In many cases the formation of relatively smaller aggregates and subsequently, small fruiting bodies were the consequence of stream breaks that had occurred during early to late development. The early aggregation of *apID*⁻ was comparable to that of Ax2, which suggests that the *apID*⁻ is not defective for aggregation but may be producing some extracellular factors, which resulted in late stream breaks. The production of extracellular factors can be tested by performing development experiments in conditioned medium (D. A. Brock et al. 1996); (Okuwa et al. 2001); (Mujumdar et al. 2011) or by performing classical mixing experiments (Brown and Firtel 2000); (Jaiswal et al. 2006); (Mujumdar, Inouye, and Nanjundiah 2009). The possibility that the *apID*⁻ may produce some extracellular factors that cause cell stream breaks was examined by performing the mixing experiments. The

apID⁻ was mixed with Ax2 at different ratios and subjected to development on KK2 agar plates. The *apID*⁻:Ax2 mixing proportions 60:40% (**Fig. 39**), 40:60%, and 20:80% showed no cell stream breaks. Consequently, there was a gradual decrease in the number of slugs and fruiting bodies when compared with *apID*⁻.

At mixtures 80:20% and 90:10% (*apID*⁻:Ax2), stream breaks were apparent, which resulted in small aggregates and fruiting bodies (data not shown). It had been described that if a *D. discoideum* mutant is affected for the production of some extracellular factors, even a minor population of the mutant when mixed with Ax2 would result in the stream break phenotype. For instance, even 5% of *smIA*⁻ cells subjected to development with Ax2 (95%) showed stream break phenotype (D. A. Brock et al. 1996); (Brown and Firtel 2000). When majority of Ax2 cells (90%) were mixed with minor population of *triA*⁻ (10%) the resulting cell streams were broken (Mujumdar et al. 2011). In the case of *apID*⁻:Ax2 mixing experiments, although a major population of *apID*⁻ (60%) was mixed with minor population of Ax2 (40%), the stream break phenotype was not observed (**Fig. 39**) Therefore, the speculation that the *apID*⁻ is producing some extracellular factors, which are causing stream break, may be less plausible. Additionally, the phenotype rescue experiments were performed with the rescue strain [*apID*⁻ (+)] that overproduced ApID-FLAG fusion protein under the control of *actin 6* promoter (A6P), in *apID*⁻ background. The cell streams created by *apID*⁻ (+) were comparable to that of Ax2 cell streams and there was a drastic decrease in the number of aggregates when compared with *apID*⁻ (**Fig. 36 and 37**). Presumably, the replacement of *apID* is restoring the normal cell streaming phenotype. As ApID belongs to SAPLIP family, it could be possible that they are involved in some metabolism functions during the vegetative growth of *D. discoideum* amoebae. Therefore, the developmental defects observed in *apID*⁻ could be a consequence of disturbed metabolism that had occurred during vegetative growth phase. Accordingly, even in the bacterial growth assays the growth plaques formed by the *apID*⁻ were relatively smaller than the Ax2 growth plaques irrespective of the bacterial strains tested. SAPLIPs are known for their diverse cellular functions, including their metabolism functions. For example, in human, saposins A-D are involved in lipid metabolism and the absence of saposins result in lysosomal storage disease that is fatal (Wenger et al. 1989); (Vaccaro et al. 1999); (H. Bruhn 2005). Although SALPLIP members (e.g., Amoebapores) are known for their antimicrobial and cytolytic activities, the general characteristic of all the SAPLIP members is lipid

interaction (M. Leippe et al. 1991); (M. Leippe et al. 1992) (J. Andrä and Leippe 1994) (J. Andrä, Herbst, and Leippe 2003); (Gutsmann et al. 2003). However, *D. discoideum* possess a sophisticated mechanism to discharge the undigested cargo to the extracellular environment by exocytosis (Müller et al. 2005); (Charette and Cosson 2007); (Lima et al. 2012). At present, the reason for an antimicrobial peptide mutant (*apID*⁻) showing developmental defects appear profound. However, the more appealing speculation could be that the ApID is also crucial for metabolic functions, apart from its antimicrobial functions, which may determine the fitness and the nutrition status of the amoebae. The analyses of aspects, such as lysozyme activity, lysosomal pH, intracellular acidification and proteolytic activity in the growth phase *apID*⁻ may presumably elucidate the scenario of metabolism functions in *apID*⁻. Also, the examination of cell adhesion molecules (e.g., CsA and LagC) and the production of aggregate size regulator (countin) during *apID*⁻ development may explain the reasons for late stream breaks.

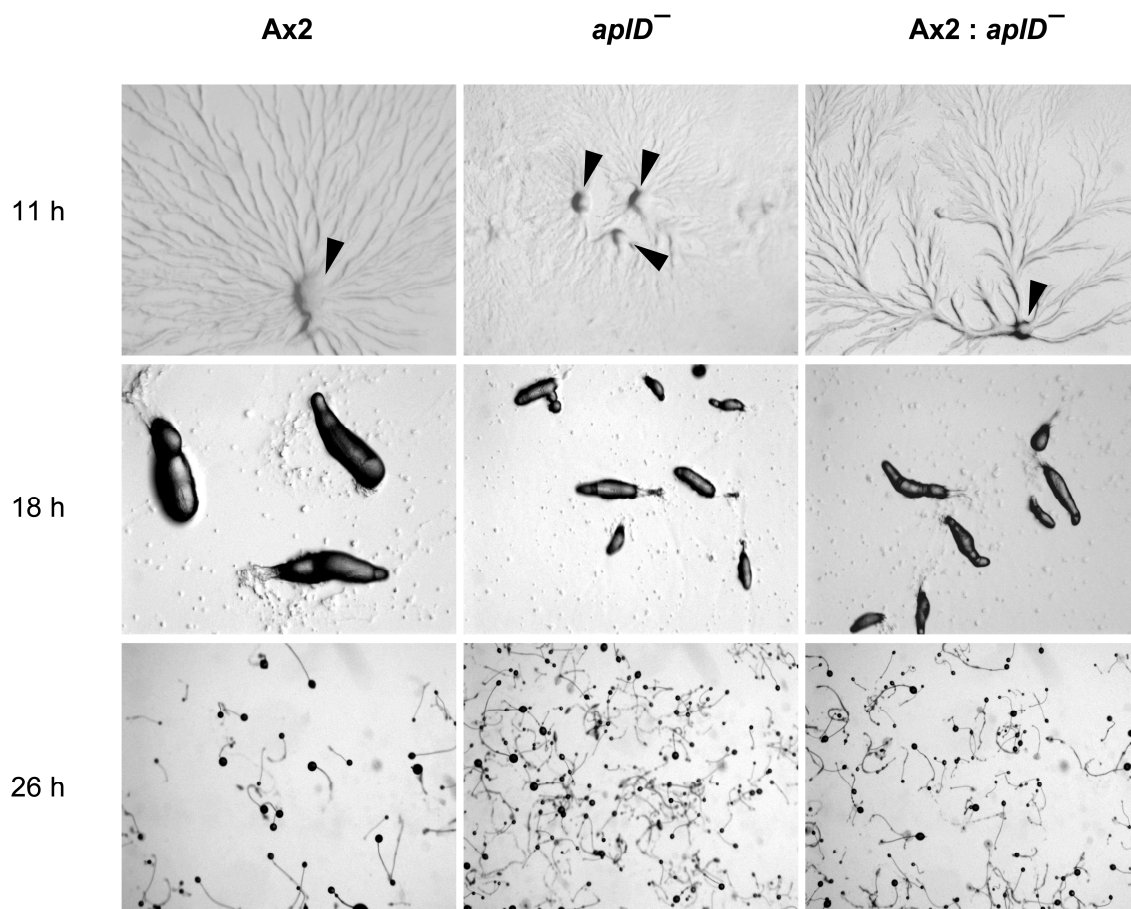


Fig. 39: Mixing experiments. Axenically grown *D. discoideum* cells were subjected to development on KK2 agar plates and imaged at time points, 11 h (aggregation centres), 18 h (slugs), and 26 h (fruiting bodies). Right panels: A minor proportion of Ax2 (40%) was mixed with a major proportion of *apID*⁻ (60%) and applied on KK2 agar plates for development. Arrowheads denote aggregation centres. All the images were obtained at same magnification.

apID transcriptional regulation during axenic growth, development and in xenic Ax2 cultures was examined by quantitative RT-PCR. The analyses of *apID* transcription profile in axenic Ax2 and *apID*⁻ cultures revealed that the *apID* transcript was moderately regulated in axenic Ax2, whereas no *apID* regulation was observed in *apID*⁻ (**Fig. 25**). This serves as an additional confirmation for the *apID* ablation in *apID*⁻. Presence of moderate levels of *apID* transcript in axenic Ax2 raises a speculation that ApID could be involved in some metabolism functions. Additionally, during vegetative growth ApID may also play a synergistic role with other members of antimicrobial arsenal to aid the *D. discoideum* amoebae in bacterial killing. The latter hypothesis was tested by confronting the axenic Ax2 with various bacteria and by analysing the *apID* transcription profile (qRT-PCR) in these xenic cultures.

apID expression in axenic Ax2 was considered as reference to calculate the *apID* fold expression ($2^{-\Delta\Delta CT}$) in xenic Ax2 cultures. The housekeeping genes used for qRT-PCR include *rnlA* and *GAPDH*. Notably, Ax2 confronted with *KpLM21* showed at least 3 fold up-regulation of *apID* transcript, whereas no *apID* regulation was observed in Ax2 co-cultured with *B. subtilis* and at least six fold down-regulation of *apID* transcript was observed in Ax2 challenged with a quorum sensing mutant of *P. aeruginosa* (PT531). As the toxins secreted by the wild type *P. aeruginosa* would kill the *D. discoideum* amoebae, a quorum sensing mutant of *P. aeruginosa* (PT531) was used for the xenic qRT-PCR experiments (Alibaud et al. 2008). Although *apID*⁻ was unaffected for its growth ability on PT531, the *apID* transcript was down-regulated in Ax2 confronted with PT531. Therefore, it can be hypothesised that even though the virulence genes are affected in PT531, this strain still retains the abilities that cause transcriptional changes in the amoeba host. However, these changes are not sufficient to inhibit the growth of the amoebae. Also, it is likely that ApID is not involved in killing PT531. Similarly, *apID* transcription profile during Ax2 development was analysed by qRT-PCR. The developmental stages (time points) tested include amoebae (0 h), cell streams (8 h), mounds (12 h), slugs (16 h), and fruiting bodies (24 h). *apID* expression at 0 h was considered as reference to calculate the *apID* fold expression ($2^{-\Delta\Delta CT}$) at subsequent time points. As mentioned earlier, *rnlA* and *GAPDH* were used as house keeping genes.

These experiments were performed to investigate the *apID* regulation pattern during Ax2 development in the total absence of bacteria. Surprisingly,

developing Ax2 cells showed massive up-regulation of *ap1D* transcript when compared with vegetative Ax2 amoebae. *ap1D* transcript was sturdily up-regulated starting from 12 h until 24 h, with peak expression at 16 h (slugs) of development. This observation implies that *ap1D* transcript is spontaneously up-regulated during Ax2 development even in the total absence of bacteria both, at growth and development phases. *ap1D* transcription profile in Ax4 cells (an axenic strain of *D. discoideum*) fed with *K. aerogenes* and subjected to development is available at dictybase. Additionally, the dictybase repository also provides information about the genes that show transcription patterns comparable to *ap1D* (**Fig. 40**). The data retrieved for *ap1D* coexpression network showed at least six genes whose transcription profiles are similar to that of *ap1D*. The DDB_G0270858 gene is implicated in regulation of G protein signalling pathway, *triA* is crucial for morphogenetic functions and is expressed in the pre-spore regions of the slugs, DDB_G0278655 is involved in metabolic functions, and DDB_G0275411 is expressed in a subtype of pre-stalk cells (*pstO*), but its function is unknown at present. Nothing is known concerning DDB_G0271510 and DDB_G0276989 (**Tab. 10**). As these data were obtained from the Ax4 amoebae fed with *K. aerogenes* and then subjected to development, it is possible that the food source provided during vegetative phase might have had some influence over the results described. For this reason, I analysed the *ap1D* transcription profile during the development of axenic Ax2 cells, in the total absence of bacteria. The results obtained from my experiments were comparable to the *ap1D* transcription profile available dictybase (for Ax4 cells). Additionally, my experimental results confirm that the *ap1D* is spontaneously up-regulated during Ax2 development even in the absence of bacterial influence. Although the transcription profile of *triA* is comparable to *ap1D*, the morphogenetic defects reported with *triA*⁻ is less comparable with *ap1D*⁻. In comparison to *triA*⁻, the *ap1D*⁻ also showed stream breaks and reduced sfe, but the cell fate commitment (pre-stalk and pre-spore), spore viability, spore and the fruiting body morphologies remain unaffected in *ap1D*⁻. Together, the results obtained for *ap1D* transcription profile indicates that *ap1D* transcript is moderately regulated in axenic Ax2, at least three fold up-regulated upon Ax2 exposure to *KpLM21*, whereas *ap1D* transcript is readily up-regulated during Ax2 development even in the total absence of bacteria. These observations prompted me to perform the slug infection

experiments, to scrutinise the fact whether *ApID* has been implicated in some immune functions to protect the developing structures from bacterial intruders.

Although development in *D. discoideum* has a defined time frame for each morphogenetic stage (Fey et al. 2007), in the context of infection experiments, the slug stage would be comparatively easier for microscopic observations. Indeed, the slug stage is the only migratory stage among the other developmental stages. Therefore, the migrating slugs are highly prone to pathogens compared to other stages of development. Additionally, a standard protocol for slug infection experiment was already established (G. Chen, Zhuchenko, and Kuspa 2007).

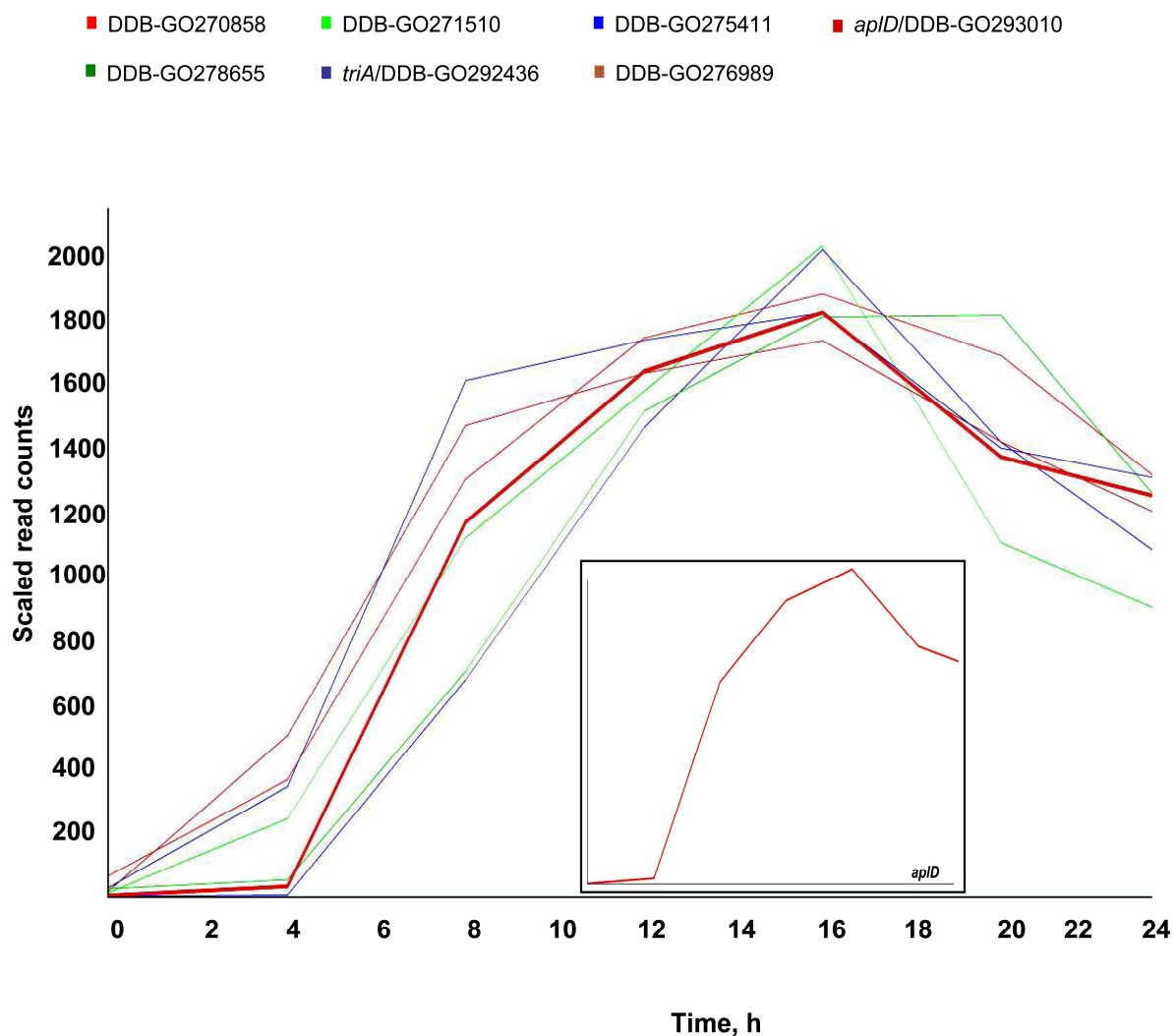


Fig. 40: *apID* coexpression network (dictybase). Transcriptome data obtained for *D. discoideum* (Ax4) amoebae fed with *K. aerogenes* and subjected to development. At indicated time points, RNA was isolated from the Ax4 amoebae to analyse the transcriptional regulation of several genes. Expression patterns of seven genes, including *apID* (red, see inset) is depicted (www.dictybase.org).

Apart from all these minor reasons, the major reason was that the axenic Ax2 cells subjected to development showed peak up-regulation of *ap1D* transcript at the slug stage (16 h). As the *ap1D*⁻ showed growth and killing defects with *K. pneumoniae*, a *K. pneumoniae* strain producing GFP protein (*KpGFP*) was prioritised to perform the slug infection experiments. The *KpGFP* used in this study is a virulent strain, which caused intracellular accumulation when fed to *phg1*⁻ (Benghezal et al. 2006). The overnight culture of *KpGFP* (OD₆₀₀ = 3.0) at a multiplicity of infection (MOI) of 1 was used to infect the *D. discoideum* slugs and the infected slugs were observed 20 and 24 h post infection. Similar to earlier reports with *L. pneumophila* (G. Chen, Zhuchenko, and Kuspa 2007), 24 h post infection with *KpGFP* the Ax2 slugs and their slime sheaths appeared completely free of any *KpGFP* infection.

Tab. 10: Members of *ap1D* coexpression network and their functions were retrieved from dictybase repository. No details (ND).

Genes	Functions
DDB_G0270858	Regulation of G protein signalling (RGS), RGS domain-containing protein. Molecular functions: Signal transduction
DDB_G0271510	ND
<i>triA</i> /DDB_G0292436	Prespore-specific gene that regulates cell sorting and morphogenesis; in mutants the spore mass is suspended halfway up the stalk. Molecular functions: Protein binding Biological processes: cell fate determination, calcium-independent cell-cell adhesion, sporulation resulting in the formation of a cellular spore, aggregation involved in sorocarp development, culmination involved in sorocarp development, and cell fate commitment Phenotype defects in <i>triA</i> ⁻ : Aberrant culminant morphology, aberrant streaming, aberrant upper cup formation, decreased cell fate commitment, decreased cell fate determination, decreased cell-cell adhesion, decreased spore size, decreased spore viability, increased number of aggregates, and increased stalk width.
DDB_G0275411	Expressed in <i>pstO</i> cells
DDB_G0276989	ND
DDB_G0278655	Short chain dehydrogenase/reductase (SDR) family protein glucose ribitol dehydrogenase family protein Molecular functions: Oxidoreductase activity Biological process: metabolic process

Interestingly, the *ap1D*⁻ slugs were highly vulnerable to *KpGFP* infection. Despite of this high load of *KpGFP* infection, the *ap1D*⁻ slugs were able to migrate, leaving long slime trails. The *ap1D*⁻ slugs observed 20 h post infection showed *KpGFP* deposits on the slug surface and in the slug interior, but the slime trail showed very rare incidence of *KpGFP* deposits (see *ap1D*⁻ slugs **Fig. 32** and **33**). However, the slime trails created by the *ap1D*⁻ slugs were comparable to that of the Ax2 slime trails. These observations exemplify the fact that the *ap1D*⁻ slugs were unaffected in their morphogenetic functions, such as slug formation, migration, and creating slime trails. When the *ap1D*⁻ slugs infected with *KpGFP* were observed 24 h post infection, several *KpGFP* clumps were visible within the slugs, but the presence of *KpGFP* clumps within the Ax2 slugs was a very rare observation. To investigate whether the *ap1D*⁻ slugs are specifically susceptible to *KpGFP*, similar slug infection experiments were performed with *E. coli* expressing DsRed (*E.coli* DsRed). The *ap1D*⁻ slugs infected with *E.coli* DsRed were able to reconstruct themselves and migrate towards the unidirectional light source 8 h post infection. In contrast, the *ap1D*⁻ slugs infected with *KpGFP* needed 20 h post infection to reconstruct and migrate towards the light source. Both, the Ax2 and *ap1D*⁻ slugs infected with *E.coli* DsRed formed fruiting bodies around 20 h post infection. Similar to Ax2 slugs infected with *E.coli* DsRed, the *ap1D*⁻ slugs surface and interior showed no *E.coli* DsRed deposits or clumps, but the slime sheaths of *ap1D*⁻ slugs showed heavy *E.coli* DsRed shedding unlike Ax2 slime sheaths (**Fig. 34**). This observation adds a fact that, although *ap1D*⁻ slugs were able to slough off *E. coli* DsRed in their slime sheaths, they were less efficient in sloughing of *E. coli* DsRed when compared with Ax2 slugs. To examine the reason why *ap1D*⁻ slugs are less efficient in recovering from bacterial infections, the immune-like phagocytic cells of the *ap1D*⁻ slugs were investigated.

The sentinel cells or S cells are the only specialised cells known so far to perform immune-like functions in *D. discoideum* slugs (G. Chen, Zhuchenko, and Kuspa 2007). The S cells are a minor population of cells, which move laterally forward and backward along the migrating slugs, and sequester the toxins or the microbial invaders. Finally, the S cells filled with toxins or bacteria are sloughed off in the slime sheath. To visualise the S cells, the *D. discoideum* slugs were allowed to migrate on EtBr agar plates and the S cells were observed under the fluorescence microscope. Similar to Ax2 slugs, the *ap1D*⁻ slugs that migrated on EtBr agar plates

showed S cells both in the slug interior and also in the slime sheath. Apart from the S cells mediated immune function, the mucoid layer covering the slugs may function as a physical barrier to prevent the spread of infection or the toxins to the slug interior. In the *ap/D⁻* slugs both, the slug surface and the slug interior showed high bacterial deposits and clumps. Presumably, the function of slime sheath is not only to slough off the S cells but also to immobilise or entrap the toxins or microbial intruders to a localised area, thereby preventing the spread of toxins or the microbial infection to the other slugs migrating in the surrounding vicinity.

6.A Summary

In *Entamoeba histolytica*, Amoebapores and lysozymes are known to confer antimicrobial functions. The structure and functions of Amoebapores and lysozymes are evolutionally conserved, as evidenced by their analogous in many other organisms. Amoebapores and its structural counterparts have five α -helices that are connected by disulfide bonds, involving cysteine residues. Any protein with this typical structure is categorised under the SAPLIP family (Saposin-like protein) and the domain is called SAPLIP domain. SAPLIPs are known for their diverse cellular functions. The Amoebapores (M Leippe 1997) from *E. histolytica* and their structural and functional analogues, NK-lysin (porcine) and granulysin (human) are known for their antimicrobial and cytolytic functions. By contrast, the name giving Saposins (human) are necessary for lipid metabolism. *Dictyostelium discoideum*, has a multi-protein complex in which one component, called countin has a SAPLIP domain. Countin is required for aggregate size determination during development. Earlier work in our laboratory has found that the *D. discoideum* genome harbours 17 genes, which encode for 33 putative Amoebapore-like peptides (Apls). In addition, the *D. discoideum* genome comprises 15 genes coding for four different classes of lysozymes. These classes are c-type lysozymes (LyC), phage-type lysozymes (LyT4), *Entamoeba*-type lysozymes (LyEh), and the amoeba lysozymes (Alys), which is a unique class of lysozymes found in *D. discoideum*. As *D. discoideum* amoebae feed on bacteria, they are at a risk to encounter pathogenic bacteria. Therefore, it has been postulated that the Apls and lysozymes may play a synergistic role to kill and degrade the bacteria. My study has focused on three *apl* genes (*aplD*, *aplJ*, and *aplP*) and two lysozyme genes (*lyC2* and *lyC3*), based on collaborator reports that these genes are implicated in bacterial destruction. The phenotypic characterisations were carried out with the single gene KO mutants for the corresponding genes. All the gene disruptions were performed in wild type Ax2 background. Among all five KO mutants tested for growth on bacteria, the *aplD*⁻ showed growth defects on several strains of *K. pneumoniae*. The *aplP*⁻ and *lyC2*⁻ were defective for growth only on the capsule defective mutant of *Kp52145* (*K*⁻). As the *aplD*⁻ was defective for growth on different *K. pneumoniae* strains, further phenotypic characterisations were carried out for the *aplD*⁻. In accordance with growth defects on *K. pneumoniae*, the *aplD*⁻ was

also defective for intracellular killing of *K. pneumoniae* (KpLM21). Moreover, the wild type Ax2 cells confronted with KpLM21 showed at least three fold up-regulation of the *apID* transcript (qRT-PCR). Similar qRT-PCR experiments with axenic Ax2 revealed that the transcription of *apID* is moderately up-regulated during axenic growth, whereas sturdily up-regulated during development and peaked at the slug stage. This spontaneous up-regulation of *apID* transcript during Ax2 development, which was performed totally in the absence of bacteria, prompted me to do the slug infection experiments with the *apID*⁻. As the *D. discoideum* cells stop feeding at the onset of development they may need an armament to protect their developing structures from foreign intruders. In fact, the migrating slugs are highly prone to infection when compared with the other stages of development. Following this, the slug infection experiments were performed with a GFP expressing strain of *K. pneumoniae* (KpGFP) and an *E. coli* strain that expressed DsRed (*E. coli* DsRed). The Ax2 slugs were used as controls. Unlike Ax2 slugs, the *apID*⁻ slugs infected with KpGFP showed massive KpGFP accumulation which corroborates with growth and killing defects of *apID*⁻ with *K. pneumoniae*. In contrast, the *apID*⁻ slugs infected with *E. coli* DsRed were able to slough off *E. coli* DsRed in their slime trail. However, I could show that the *apID*⁻ slugs were unaffected in their ability to form S cells and to sequester toxin (EtBr). Apart from their reduced ability to defend against *K. pneumoniae*, the *apID*⁻ also showed several morphogenetic defects during development. This includes late stream breaks (12 h), delayed formation of smaller slugs (18 h) and fruiting bodies (~ 26 h), and a relatively reduced spore formation efficiency (sfe). Nevertheless, the spore morphology and spore viability were unaffected in *apID*⁻. These observations may point to an additional role for *apID* during *D. discoideum* development. On the other hand, it is also possible that the *apID*⁻ is immunocompromised and therefore it is showing several developmental defects. In summary, this study shows that the *apID* is crucial for the growth of *D. discoideum* on *K. pneumoniae* and also for the intracellular killing of *K. pneumoniae*. Additionally, *apID* is required to prevent *K. pneumoniae* accumulation in the *D. discoideum* slugs.

6.B Zusammenfassung

In *Entamoeba histolytica* sind die Amoebapores und die Lysozyme dafür bekannt, antimikrobielle Funktionen zu übernehmen. Die Struktur und die Funktion sowohl der Amoebapores als auch der Lysozyme sind evolutionär konserviert, was durch das Vorhandensein analoger Proteine in einer Vielzahl anderer Organismen bewiesen ist. Die Amoebapores und deren strukturelle Verwandte sind durch fünf α -Helices charakterisiert, die über Disulfidbrücken zwischen Cysteinresten miteinander verbunden sind. Jedes Protein, das diese typische Struktur zeigt, wird der SAPLIP-Familie (Saposin-like protein), den Saposin-ähnlichen Proteinen, zugeordnet. Die entsprechende Domäne wird demnach SAPLIP-Domäne genannt. Die SAPLIPs sind für ihre vielfältigen Funktionen bekannt. Die Amoebapores aus *E. histolytica* und deren strukturell und funktionell analoge Proteine, das NK-lysin aus dem Schwein und das Granulysin aus dem Menschen, sind für ihre antimikrobiellen und cytolytischen Funktionen bekannt. Die namensgebenden Saposine des Menschen sind dagegen für den Lipidstoffwechsel wichtig. In *Dictyostelium discoideum* gibt es eine Komponente eines Multi-Protein-Komplexes, das countin, das ebenfalls eine SAPLIP-Domäne besitzt. Countin ist notwendig für die Bestimmung der Aggregatgröße während der Entwicklungsphase von *D. discoideum*. Als Ergebnis einer früheren Arbeit in diesem Labor konnte gezeigt werden, dass das Genom von *D. discoideum* 17 Gene aufweist, die für 33 putative Amoebapore-ähnliche Peptide (Apls) codieren. Zudem finden sich im Genom von *D. discoideum* 15 Gene, die für Lysozyme aus vier verschiedenen Klassen codieren. Dabei handelt es sich um die Klassen der c-Typ Lysozyme (LyC), T4 Phagen-Lysozyme (LyT4), Lysozyme des Entamoeba-Typs (LyEh) und die Amoeba-Lysozyme (Alys), eine ausschließlich in *D. discoideum* vorkommende Lysozym-Klasse. Da das Amöbenstadium von *D. discoideum* Bakterien als Nahrungsquelle nutzt, besteht für diese auch ein hohes Risiko, auf pathogene Bakterien zu treffen. Daher wurde angenommen, dass die Apls und die Lysozyme eine synergistische Rolle beim Töten und Degradieren von Bakterien spielen könnten. In meiner Arbeit habe ich mich auf die Untersuchung von drei Apl-Genen (*aplD*, *aplJ* und *aplP*) sowie zwei Lysozym-Genen (*lyC2* und *lyC3*) konzentriert, für die bereits von einer kooperierenden Arbeitsgruppe berichtet wurde, dass sie möglicherweise eine Rolle beim Abbau von Bakterien spielen. Die

phänotypischen Charakterisierungen wurden mithilfe von Deletionsmutanten für die einzelnen Gene durchgeführt. Als Ausgangsstamm für die Herstellung dieser Mutanten wurde jeweils der Wildtyp-Stamm Ax2 verwendet. Alle fünf Deletionsmutanten wurden bezüglich ihrer Fähigkeit, auf Bakterien zu wachsen, untersucht. Dabei zeigte die *apID*-Mutante Wachstumsdefekte auf den meisten der getesteten Stämme von *Klebsiella pneumoniae*, während die Mutanten *apIP* und *lyC2* nur einen Wachstumsdefekt auf dem *Klebsiella*-Stamm Kp52145 (*K*) zeigten, der sich wiederum dadurch auszeichnet, dass er eine veränderte Kapsel aufweist. Da das Wachstum der *apID*-Mutante auf verschiedenen Stämmen von *K. pneumoniae* gestört war, wurde diese Mutante im Folgenden genauer phänotypisch charakterisiert. In Übereinstimmung mit den Wachstumsdefekten auf *K. pneumoniae* zeigte sich, dass die *apID*-Mutante zudem in ihrer Fähigkeit beeinträchtigt war, intrazelluläre *K. pneumoniae* (KpLM21) zu töten. Des Weiteren zeigten Zellen des Wildtyps Ax2, die mit KpLM21 konfrontiert wurden, eine mindestens dreifache Hochregulierung des *apID*-Transkripts (qRT-PCR). Ähnliche qRT-PCR-Experimente mit axenischen Ax2-Zellen ergaben, dass die Transkription von *apID* während des axenischen Wachstums nur leicht hochreguliert wird, wohingegen dies während der Entwicklungsphase sehr stark der Fall ist, mit einem Maximum im sogenannten *Slug*-Stadium. Die spontane Hochregulierung der *apID*-Transkription während der Entwicklung von Ax2-Zellen passierte in der kompletten Abwesenheit von Bakterien. Diese Beobachtung veranlasste mich dazu, das Infektionsexperiment mit dem *Slug*-Stadium von *apID*-Mutanten durchzuführen. Da *D. discoideum* Zellen mit dem Beginn der Entwicklungsphase aufhören zu fressen, ist es anzunehmen, dass sie Abwehrmoleküle benötigen, um ihre sich entwickelnden Strukturen vor fremden Eindringlingen zu schützen. Tatsächlich sind wandernde *Slugs* im Vergleich zu den anderen Stadien der Entwicklungsphase hoch anfällig für Infektionen. Daraufhin wurden Infektionsexperimente mit *Slugs* mit einem GFP exprimierenden Stamm von *K. pneumoniae* (KpGFP) und einem DsRed exprimierenden Stamm von *E. coli* (*E. coli* DsRed) durchgeführt. *Slugs* des Wildtyps Ax2 wurden dabei als Kontrolle verwendet. Anders als der Wildtyp wiesen die mit KpGFP infizierten *apID*-*Slugs* eine massive Akkumulation der Bakterien auf, was mit den entsprechenden Wachstums- und Tötungsdefekten dieser Mutante übereinstimmt. Im Gegensatz dazu waren die mit *E. coli* DsRed infizierten *apID*-*Slugs* in der Lage, diese Bakterien in ihre Schleimspur mit abzugeben. Zudem

konnte ich zeigen, dass die *apID*⁻*Slugs* nicht in ihrer Fähigkeit beeinträchtigt waren, S-Zellen zu bilden und Giftstoffe (EtBr) abzusondern. Neben der verminderten Fähigkeit, sich gegen *K. pneumoniae* zu verteidigen, zeigte die *apID*⁻-Mutante außerdem einige morphogenetischen Defekte während der Entwicklungsphase. Hierzu gehörten Unterbrechungen in den Hyphen des späten Streaming-Stadiums (12 h), die verzögerte Bildung von kleineren *Slugs* (18 h) und Fruchtkörpern (~26 h) sowie eine etwas reduzierte Sporenbildungseffizienz. Gleichwohl waren die Morphologie und die Viabilität der Sporen in der *apID*⁻-Mutante nicht beeinträchtigt. Diese Beobachtungen könnten auf eine zusätzliche Rolle für ApID während der Entwicklungsphase hindeuten. Andererseits wäre es auch denkbar, dass die *apID*⁻-Mutante generell immunsupprimiert ist und somit mehrere Entwicklungsdefekte aufweist. Zusammenfassend konnte ich in dieser Arbeit zeigen, dass *apID* von entscheidender Bedeutung für das Wachstum von *D. discoideum* auf *K. pneumoniae* und auch für das intrazelluläre Töten dieser Bakterien ist. Außerdem ist *apID* notwendig, um die Akkumulation von *K. pneumoniae* in den *Slugs* von *D. discoideum* zu verhindern.

7 REFERENCES

- Alibaud, L, Köhler, T, Coudray, A, Prigent-Combaret, C, Bergeret, E, Perrin, J, Benghezal, M *et al.* 2008. "Pseudomonas aeruginosa Virulence Genes Identified in a Dictyostelium Host Model." *Cellular Microbiology* 10 (3) (March): 729–740.
- Andersson M, Gunne H, Agerberth B, Boman A, Bergman T, Olsson B, Dagerlind A, Wigzell H, Boman HG, Gudmundsson GH. 1996. "NK-lysin, Structure and Functions of a Novel Effector Molecule of Porcine T and NK Cells." *Veterinary Immunology and Immunopathology* 54 (1-4) (November): 123–126.
- Andrä, J, and Leippe, M. 1994. "Pore-forming Peptide of *Entamoeba histolytica*. Significance of Positively Charged Amino Acid Residues for Its Mode of Action." *FEBS Letters* 354 (1) (October 31): 97–102.
- Andrä, J, Herbst, R, and Leippe, M. 2003. "Amoebapores, Archaic Effector Peptides of Protozoan Origin, Are Discharged into Phagosomes and Kill Bacteria by Permeabilizing Their Membranes." *Developmental and Comparative Immunology* 27 (4) (April): 291–304.
- Andreu, D, and Rivas, L. 1998. "Animal Antimicrobial Peptides: An Overview." *Biopolymers* 47 (6) (January): 415–433.
- Arya, R, Bhattacharya, A, and Saini, K S. 2008. "Dictyostelium discoideum-a Promising Expression System for the Production of Eukaryotic Proteins." *FASEB Journal: Official Publication of the Federation of American Societies for Experimental Biology* 22 (12) (December): 4055–4066.
- Bader, S, Kortholt, A, and Van Haastert, P J. 2007. "Seven Dictyostelium discoideum Phosphodiesterases Degrade Three Pools of cAMP and cGMP." *The Biochemical Journal* 402 (1) (February 15): 153–161.
- Balestrino, D, Haagensen, A J, Rich, C, and Forestier, C. 2005. "Characterization of Type 2 Quorum Sensing in *Klebsiella pneumoniae* and Relationship with Biofilm Formation" 187 (8): 2870–2880.
- Barth, C, Fraser, D J, and Fisher, P R. 1998. "Co-insertional Replication Is Responsible for Tandem Multimer Formation During Plasmid Integration into the Dictyostelium Genome." *Plasmid* 39 (2) (January): 141–153.
- Belvin, M P, and Anderson, K V. 1996. "A Conserved Signaling Pathway: The Drosophila Toll-dorsal Ectopic I Pathway." *Annual Review of Cell and Developmental Biology* 12 (January): 393–416.
- Benghezal, M, Fauvarque, M O, Tournebize, R, Froquet, R, Marchetti, A, Bergeret, E, Lardy, B, *et al.* 2006. "Specific Host Genes Required for the Killing of Klebsiella Bacteria by Phagocytes." *Cellular Microbiology* 8 (1) (January): 139–148.

- Bertin, J, Nir, W J, Fischer, C M, Tayber, O V, Errada, P R, Grant, J R, Keilty, J J, et al. 1999. "Human CARD4 Protein Is a Novel CED-4/Apaf-1 Cell Death Family Member That Activates NF-kappaB." *The Journal of Biological Chemistry* 274 (19) (May 7): 12955–12958.
- Bierbaum, G, and Sahl, H G. 1987. "Autolytic System of *Staphylococcus Simulans* 22: Influence of Cationic Peptides on Activity of N-acetylmuramoyl-L-alanine Amidase." *Journal of Bacteriology* 169 (12) (December): 5452–5458.
- Boheim, G. 1974. "Statistical Analysis of Alamethicin Channels in Black Lipid Membranes." *The Journal of Membrane Biology* 19 (3) (January): 277–303.
- Boman, Hans G. 1995. "Peptide Antibiotics and their Role in Innate Immunity": 61–92. *Annual Reviews of Immunology*. 13: 61-92.
- Bonner, J T. 2003. "Evolution of Development in the Cellular Slime Molds." *Evolution & Development* 5 (3): 305–313.
- Bozzaro, S, and Eichinger, L. 2011. "The Professional Phagocyte *Dictyostelium discoideum* as a Model Host for Bacterial Pathogens." *Current Drug Targets* 12 (7) (June): 942–954.
- Brock, D A, and Gomer, R H. 1999. "A Cell-counting Factor Regulating Structure Size in *Dictyostelium*." *Genes & Development* 13 (15) (August 1): 1960–1969.
- Brock, D A, Buczynski, G, Spann, T P, Wood, S A, Cardelli, J, and Gomer, R H. 1996. "A *Dictyostelium* Mutant with Defective Aggregate Size Determination" 2578: 2569–2578.
- Brock, D A, Douglas, T E, Queller, D C, and Strassmann, J E. 2011. "Primitive Agriculture in a Social Amoeba." *Nature* 469 (7330) (January 20): 393–396.
- Brock, D A, van Egmond, W N, Shamo, Y, Hatton, R D, and Gomer, R H. 2006. "A 60-kilodalton Protein Component of the Counting Factor Complex Regulates Group Size in *Dictyostelium discoideum*." *Eukaryotic Cell* 5 (9) (September): 1532–1538.
- Brogden, K A, Ackermann, M, and Huttner, K M. 1998. "Detection of Anionic Antimicrobial Peptides in Ovine Bronchoalveolar Lavage Fluid and Respiratory Epithelium." *Infection and Immunity* 66 (12) (December): 5948–5954.
- Brogden, K A, De Lucca, A J, Bland, J, and Elliott, S. 1996. "Isolation of an Ovine Pulmonary Surfactant-associated Anionic Peptide Bactericidal for *Pasteurella haemolytica*." *Proceedings of the National Academy of Sciences of the United States of America*. 93 (1) (January 9): 412–416.
- Brogden, K A. 2005. "Antimicrobial Peptides: Pore formers or metabolic inhibitors in bacteria" *Nature Reviews Microbiology* .3 (3) (MARCH): 238–250.
- Brown, J M, and Firtel, R A. 2000. "Just the Right Size: Cell Counting in *Dictyostelium*." *Trends in Genetics*. 16 (5) (May): 191–193.

- Bruhn, H, and Leippe, M. 2001a. "Membrane-permeabilizing Polypeptides of Amoebae - Constituents of an Archaic Antimicrobial System." *Zoology (Jena, Germany)*. 104 (1) (January): 3–11.
- Bruhn, H, and Leippe, M. 2001b. "Novel Putative Saposin-like Proteins of *Entamoeba histolytica* Different from Amoebapores." *Biochimica Et Biophysica Acta*. 1514 (1) (September 3): 14–20.
- Bruhn, H. 2005. "A Short Guided Tour Through Functional and Structural Features of Saposin-like Proteins" *The Biochemical Journal*. 389 (Pt 2) (July): 249–257.
- Bruhn, H, Riekens, B, Berninghausen, O, and Leippe, M. 2003. "Amoebapores and NK-lysin, Members of a Class of Structurally Distinct Antimicrobial and Cytolytic Peptides from Protozoa and Mammals: a Comparative Functional Analysis." *The Biochemical Journal* 375 (Pt 3) (November 1): 737–744.
- Brötz, H, Bierbaum, G, Leopold, K, Reynolds, P E, and Sahl, H G. 1998. "The Lantibiotic Mersacidin Inhibits Peptidoglycan Synthesis by Targeting Lipid II." *Antimicrobial Agents and Chemotherapy* 42 (1) (January): 154–160.
- Cardelli, J. 2001. "Phagocytosis and Macropinocytosis in *Dictyostelium*: Phosphoinositide-based Processes, Biochemically Distinct." *Traffic (Copenhagen, Denmark)* 2 (5) (May): 311–320.
- Charette, S J, and Cosson, P. 2004. "Preparation of Genomic DNA from *Dictyostelium Discoideum* for PCR Analysis." *BioTechniques* 36 (4) (April): 574–575.
- Charette, S J, and Cosson, P. 2007. "A LYST/beige Homolog Is Involved in Biogenesis of *Dictyostelium* Secretory Lysosomes." *Journal of Cell Science* 120 (Pt 14) (July 15): 2338–2343.
- Chen, G, Zhuchenko, O, and Kuspa, A. 2007. "Immune-like Phagocyte Activity in the Social Amoeba." *Science (New York, N.Y.)* 317 (5838) (August 3): 678–681.
- Chen, J, Karim de Felipe, S, Clarke, M, Lu, H, Anderson, O R, Segal, G, and Shuman, H A. 2004. "*Legionella* Effectors That Promote Nonlytic Release from Protozoa." *Science (New York, N.Y.)* 303 (5662) (February 27): 1358–1361.
- Cho, J H, Fraser, I P, Fukase, K, Kusumoto, S, Fujimoto, Y, Stahl, G L, and Ezekowitz, R A. 2005. "Human Peptidoglycan Recognition Protein S Is an Effector of Neutrophil-mediated Innate Immunity." *Blood* 106 (7) (October 1): 2551–2558.
- Clarke, M, and Gomer, R H. 1995. "Early Development of *Dictyostelium*": 1124–1134.
- Cornillon, S, Foa, C, Davoust, J, Buonavista, N, Gross, J D, and Golstein, P. 1994. "Programmed Cell Death in *Dictyostelium*." *Journal of Cell Science* 107 (Pt 1) (October): 2691–2704.

- Cosson, P, Zulianello, L, Join-lambert, O, Faurisson, F, Gebbie, L, Benghezal, M, Van Delden, C, Curty, L K, Köhler, T, and Hôpital Bichat-claude Bernard. 2002. "Pseudomonas aeruginosa Virulence Analyzed in a *Dictyostelium discoideum* Host System" 184 (11): 3027–3033.
- Cotter, B Y, David A, and Raper, K B. 1966. "Synchronous Germination Is Essential for the Study of Enzymes Involved in Spore Germination. The Present Work Describes Some Properties of the Spores of *Dictyostelium discoideum*, and Methods That Have Been Developed to Induce Rapid and Synchronous Germination": 880–887.
- Cotter, D A, and Raper, K B. 1968. "Properties of Germinating Spores of *Dictyostelium discoideum*." *Journal of Bacteriology* 96 (5) (November): 1680–1689.
- David A C, and Raper, K B. 1968. "Factors Affecting the Rate of Heat-induced Spore Germination in *Dictyostelium discoideum*" *Journal of Bacteriology* 96 (1) 86-92.
- Deery, W J, and Gomer, R H. 1999. "A Putative Receptor Mediating Cell-density Sensing in *Dictyostelium*." *The Journal of Biological Chemistry* 274 (48) (November 26): 34476–34482.
- Eichinger, L, Pachebat, J A, Glöckner, G, Rajandream, M A, Sucgang, R, Berriman, M, Song, J, et al. 2005. "The Genome of the Social Amoeba *Dictyostelium discoideum*." *Nature* 435 (7038) (May 5): 43–57.
- Engström, Y, Sun, S C, Samakavlis, C, Mark, D H, and Faye, I.. 1993. "kB-like Motifs Regulate the Induction of Immune Genes in *Drosophila*." *Journal of Molecular Biology* 232(2) (July 20) 327-333.
- Faix, J, Gerisch, G, and Noegel, A A. 1992. "Overexpression of the csA Cell Adhesion Molecule Under Its Own cAMP-regulated Promoter Impairs Morphogenesis in *Dictyostelium*." *Journal of Cell Science* 102 (Pt 2 (June): 203–214.
- Faix, J, Kreppel, L, Shaulsky, G, Schleicher, M, and Kimmel, A R. 2004. "A Rapid and Efficient Method to Generate Multiple Gene Disruptions in *Dictyostelium discoideum* Using a Single Selectable Marker and the Cre-loxP System." *Nucleic Acids Research* 32 (19) (January): e143 (1-7).
- Faure, M, Podgorski, G J, Franke, J, and Kessin, R H. 1988. "Disruption of *Dictyostelium discoideum* Morphogenesis by Overproduction of cAMP Phosphodiesterase." *Proceedings of the National Academy of Sciences of the United States of America* 85 (21) (November): 8076–8080.
- Favre-Bonté, S, Licht, T R, Forestier, C, and Krogfelt, K A. 1999. "Klebsiella pneumoniae Capsule Expression Is Necessary for Colonization of Large Intestines of Streptomycin-treated Mice." *Infection and Immunity* 67 (11) (November): 6152–6156.

- Fehlbaum, P, Bulet, P, Michaut, L, Lagueux, M, Broekaert, W F, Hetru, C, and Hoffmann, J A. 1994. "Insect Immunity. Septic Injury of *Drosophila* Induces the Synthesis of a Potent Antifungal Peptide with Sequence Homology to Plant Antifungal Peptides." *The Journal of Biological Chemistry* 269 (52) (December 30): 33159–33163.
- Fey, P, Kowal, A S, Gaudet, P, Pilcher, K E, and Chisholm, R L. 2007. "Protocols for Growth and Development of *Dictyostelium discoideum*." *Nature Protocols* 2 (6) (January): 1307–1316.
- Fraser, I P, Koziel, H, and Ezekowitz, R A. 1998. "The Serum Mannose-binding Protein and the Macrophage Mannose Receptor Are Pattern Recognition Molecules That Link Innate and Adaptive Immunity." *Seminars in Immunology* 10 (5) (October): 363–372.
- Froquet, R, Lelong, E, Marchetti, A, and Cosson, P. 2009. "*Dictyostelium discoideum*: a Model Host to Measure Bacterial Virulence." *Nature Protocols* 4 (1) (January): 25–30.
- Ganz, T. 2003. "Defensins: Antimicrobial Peptides of Innate Immunity." *Nature Reviews. Immunology* 3 (9) (September): 710–720.
- Gazit, E, Boman, A, Boman, H G, and Shai, Y. 1995. "Interaction of the Mammalian Antibacterial Peptide Cecropin P1 with Phospholipid Vesicles." *Biochemistry* 34 (36) (September 12): 11479–11488.
- Gee, K, Russell, F, and Gross, J D. 1994. "Ammonia Hypersensitivity of Slugger Mutants of *D. Discoideum*." *Journal of Cell Science* 107 (Pt 2 (February): 701–708.
- Gennaro, R, and Zanetti, M. 2000. "Structural Features and Biological activities of Cathelicidin Derived Antimicrobial Peptides" *Biopolymers (Peptide Science)* 55. 31-49.
- Gerisch, G, Lüderitz, O, and Ruschmann, E. 1967. "Antibodies Promoting Phagocytosis of Bacteria by Amoebae" *Zeitschrift Für Naturforschung. Teil B: Chemie, Biochemie, Biophysik, Biologie* 22 (1) (January): 109.
- Gerisch, G, Benjak, A, Köhler, J, Weber, I, and Schneider, N. 2004. "GFP-golgesin Constructs to Study Golgi Tubulation and post-Golgi Vesicle Dynamics in Phagocytosis." *European Journal of Cell Biology* 83 (6) (July): 297–303.
- Gewurz, H, Mold, C, Siegel, J, Fiedel, B. 1982. "C-reactive Protein and the Acute Phase Response." *Advances in Internal Medicine* 27 (January): 345–372.
- Guina, T, Yi, E C, Wang, H, Hackett, M, and Miller, S I. 2000. "A PhoP-regulated Outer Membrane Protease of *Salmonella enterica* Serovar Typhimurium Promotes Resistance to Alpha-helical Antimicrobial Peptides." *Journal of Bacteriology* 182 (14) (July): 4077–4086.

- Gutsmann, T, Riekens, B, Bruhn, H, Wiese, A, Seydel, U, and Leippe, M. 2003. "Interaction of Amoebapores and NK-lysin with Symmetric Phospholipid and Asymmetric Lipopolysaccharide/phospholipid Bilayers." *Biochemistry* 42 (32) (August 19): 9804–9812.
- Hägele, S, Köhler, R, Merkert, H, Schleicher, M, Hacker, J, and Steinert, M. 2000. "*Dictyostelium discoideum*: a New Host Model System for Intracellular Pathogens of the Genus *Legionella*." *Cellular Microbiology* 2 (2) (April): 165–171.
- Hagedorn, M, Neuhaus, E M, and Soldati, T. 2006. "Optimized Fixation and Immunofluorescence Staining Methods for *Dictyostelium* Cells." *Methods in Molecular Biology* 346 (1) (January): 327–338.
- Hagedorn, M, Rohde, K H, Russell, D G, and Soldati, T. 2009. "Infection by Tubercular Mycobacteria Is Spread by Nonlytic Ejection from Their Amoeba Hosts." *Science (New York, N.Y.)* 323 (5922) (March 27): 1729–1733.
- Hammond-Kosack, K E., and Jones, D G. 1997. "Plant Disease Resistance Genes." *Annual Review of Plant Physiology and Plant Molecular Biology* 48 (June): 575–607.
- Hancock, R E, and Chapple, D S. 1997. "Peptide Antibiotics." *Antimicrobial Agents and Chemotherapy* 43 (6) (June): 1317–1323.
- Hashimoto, C, Hudson, K L, and Anderson, K V. 1988. "The Toll Gene of *Drosophila*, Required for Dorsal-ventral Embryonic Polarity, Appears to Encode a Transmembrane Protein." *Cell* 52 (2) (January 29): 269–279.
- Hashimoto, Y, Cohen, M H, and Robertson, A. Theoretical Biology. 1975. "Cell Density Dependence of the Aggregation Characteristics of Cellular Alime Mould" 229: 215–229.
- Hawn, T R, Verbon, A, Lettinga, K D, Zhao, L P, Li, S S, Laws, R J, Skerrett, S J et al. 2003. "A Common Dominant TLR5 Stop Codon Polymorphism Abolishes Flagellin Signaling and Is Associated with Susceptibility to Legionnaires' Disease." *The Journal of Experimental Medicine* 198 (10) (November 17): 1563–1572.
- Hecht, O, Van Nuland, N A, Schleinkofer, K, Dingley, A J, Bruhn, H, Leippe, M, and Grötzinger, J. 2004. "Solution Structure of the Pore-forming Protein of *Entamoeba histolytica*." *The Journal of Biological Chemistry* 279 (17) (April 23): 17834–17841.
- Hinas, A, Reimegård, J, Wagner, E G, Nellen, W, Ambros, V R, and Söderbom, F. 2007. "The Small RNA Repertoire of *Dictyostelium discoideum* and Its Regulation by Components of the RNAi Pathway." *Nucleic Acids Research* 35 (20) (January): 6714–6726.
- Hoffmann, J. A. 1999. "Phylogenetic Perspectives in Innate Immunity." *Science* 284 (5418) (May 21): 1313–1318.

- Hughes, J E, Ashtorab, H, and Welker, D L. 1988. "Nuclear Plasmids in the *Dictyostelium* Slime Molds." *Developmental Genetics* 9 (4-5) (January): 495–504.
- Inohara, N, Koseki, T, del Peso, L, Hu, Y, Yee, C, Chen, S, Carrio, R, et al. 1999. "Nod1, an Apaf-1-like Activator of Caspase-9 and Nuclear factor-kappaB." *The Journal of Biological Chemistry* 274 (21) (May 21): 14560–14567.
- Inohara, N, Ogura, Y, Chen, F F, Muto, A, and Nuñez, G. 2001. "Human Nod1 Confers Responsiveness to Bacterial Lipopolysaccharides." *The Journal of Biological Chemistry* 276 (4) (January 26): 2551–2554.
- Isberg, R R, O'Connor, T J, and Heidtman, M. 2009. "The *Legionella pneumophila* Replication Vacuole: Making a Cosy Niche Inside Host Cells." *Nature Reviews. Microbiology* 7 (1) (January): 13–24.
- Jacobs, T, and Leippe, M. 1995. "Purification and Molecular Cloning of a Major Antibacterial Protein of the Protozoan Parasite *Entamoeba histolytica* with Lysozyme-like Properties." *European Journal of Biochemistry / FEBS* 231 (3) (August 1): 831–838.
- Jaiswal, J K, Mujumdar, N, Macwilliams, H K, and Nanjundiah, V. 2006. "Trishanku, a Novel Regulator of Cell-type Stability and Morphogenesis in *Dictyostelium discoideum*." *Differentiation; Research in Biological Diversity* 74 (9-10) (December): 596–607.
- Janeway, C A, and Medzhitov, R. 2002. "Innate Immune Recognition." *Annual Review of Immunology* 20 (2) (January): 197–216.
- Jenssen, H, Hamill, P, and Hancock, R E W. 2006. "Peptide Antimicrobial Agents." *Clinical Microbiology Reviews* 19 (3) (July): 491–511.
- Kang, S J, and Cresswell, P. 2004. "Saposins Facilitate CD1d-restricted Presentation of an Exogenous Lipid Antigen to T Cells." *Nature Immunology* 5 (2) (February): 175–181.
- Kolter, T, Winau, F, Schaible, U E, Leippe, M, and Sandhoff, K. 2005. "Lipid-binding Proteins in Membrane Digestion, Antigen Presentation, and Antimicrobial Defense." *The Journal of Biological Chemistry* 280 (50) (December 16): 41125–41128.
- Krüger, A, Batsios, P, Baumann, O, Luckert, E, Schwarz, H, Stick, R, Meyer, I, and Gräf, R. 2012. "Characterization of NE81, the First Lamin-like Nucleoskeleton Protein in a Unicellular Organism." *Molecular Biology of the Cell* 23 (2) (January): 360–370.
- Lee, A K, and Falkow, S. 1998. "Constitutive and Inducible Green Fluorescent Protein Expression in *Bartonella henselae*." *Infection and Immunity* 66 (8) (August): 3964–3967.

- Lehrer, R I, and Ganz, T. 1990. "Antimicrobial Polypeptides of Human Neutrophils." *Blood* 76 (11) (December 1): 2169–2181.
- Leippe, M. 1997. "Amoebapores." *Parasitology Today (Personal Ed.)* 13 (5) (May): 178–183.
- Leippe, M. 1999. "Antimicrobial and Cytolytic Polypeptides of Amoeboid Protozoa--effector Molecules of Primitive Phagocytes." *Developmental and Comparative Immunology* 23 (4-5): 267–279.
- Leippe, M, Ebel, S, Schoenberger, O L, Horstmann, R D, and Müller-Eberhard, H J. 1991. "Pore-forming Peptide of Pathogenic *Entamoeba histolytica*." *Proceedings of the National Academy of Sciences of the United States of America* 88 (17) (September 1): 7659–7663.
- Leippe, M, Tannich, E, Nickel, R, van der Goot, G, Pattus, F, Horstmann, R D, and Müller-Eberhard, H J. 1992. "Primary and Secondary Structure of the Pore-forming Peptide of Pathogenic *Entamoeba histolytica*." *The EMBO Journal* 11 (10) (October): 3501–3506.
- Leippe, M, Bruhn, H, Hecht, O, and Grötzinger, J. 2005. "Ancient Weapons: The Three-dimensional Structure of Amoebapore A." *Trends in Parasitology* 21 (1) (January): 5–7.
- Lemaitre, B, Nicolas, E, Michaut, L, Reichhart, J M, and Hoffmann, J A. 1996. "The Dorsoventral Regulatory Gene Cassette *spätzle/Toll/cactus* Controls the Potent Antifungal Response in *Drosophila* Adults." *Cell* 86 (6) (September 20): 973–983.
- Lima, W C, Leuba, F, Soldati, T, and Cosson, P. 2012. "Mucolipin Controls Lysosome Exocytosis in *Dictyostelium*." *Journal of Cell Science* 125 (Pt 9) (May 1): 2315–2322.
- Lu, H, and Clarke, M. 2005. "Dynamic Properties of *Legionella*-containing Phagosomes in *Dictyostelium* Amoebae." *Cellular Microbiology* 7 (7) (July): 995–1007.
- Ludtke, S J, He, K, Heller, W T, Harroun, T A, Yang, L, and Huang, H W. 1996. "Membrane Pores Induced by Magainin." *Biochemistry* 35 (43) (October 29): 13723–13728.
- Ma, H, Gamper, M, Parent, C, and Firtel, R A. 1997. "The *Dictyostelium* MAP Kinase Kinase DdMEK1 Regulates Chemotaxis and Is Essential for Chemoattractant-mediated Activation of Guanylyl Cyclase." *The EMBO Journal* 16 (14) (July 16): 4317–4332.
- Maeda, M, Sakamoto, H, Iranfar, N, Fuller, D, Maruo, T, Ogihara, S, Morio, T, Urushihara, H, Tanaka, Y, and Loomis, W F. 2003. "Changing Patterns of Gene Expression in *Dictyostelium* Prestalk Cell Subtypes Recognized by in Situ Hybridization with Genes from Microarray Analyses." *Eukaryotic Cell* 2 (3) (June): 627–637.

- Maniak, M. 2001. "Fluid-phase Uptake and Transit in Axenic *Dictyostelium* Cells." *Biochimica Et Biophysica Acta* 1525 (3) (March 15): 197–204.
- Matsuzaki, K. 1998. "Magainins as Paradigm for the Mode of Action of Pore Forming Polypeptides." *Biochimica Et Biophysica Acta* 1376 (3) (November 10): 391–400.
- Medzhitov, R, and Janeway, C A. 1997. "Innate Immunity: The Virtues of a Nonclonal System of Recognition." *Cell* 91 (3) (October 31): 295–298.
- Mehdiabadi, N J, Jack, C N, Farnham, T T, Platt, T G, Kalla, S E, Shaulsky, G, Queller, D C, and Strassmann, J E. 2006. "Social Evolution: Kin Preference in a Social Microbe." *Nature* 442 (7105) (August 24): 881–882.
- Meima, M, and Schaap, P. 1999. "*Dictyostelium* Development-socializing Through cAMP." *Seminars in Cell & Developmental Biology* 10 (6) (December): 567–576.
- Moranta, D, Regueiro, V, March, C, Llobet, E, Margareto, J, Larrarte, E, Garmendia, J and Bengoechea, J A. 2010. "*Klebsiella pneumoniae* Capsule Polysaccharide Impedes the Expression of Beta-defensins by Airway Epithelial Cells." *Infection and Immunity* 78 (3) (March): 1135–1146.
- Mujumdar, N, Dubey, A K, Nandimath, K, and Nanjundiah, V. 2011. "Autonomous and Non-autonomous Traits Mediate Social Cooperation in *Dictyostelium discoideum*." *Journal of Biosciences* 36 (3) (July 23): 505–516.
- Mujumdar, N, Inouye, K, and Nanjundiah, V. 2009. "The Trishanku Gene and Terminal Morphogenesis in *Dictyostelium discoideum*." *Evolution & Development* 11 (6): 697–709.
- Munford, R S, and Hunter, J P. 1992. "Acyloxyacyl Hydrolase, a Leukocyte Enzyme That Deacylates Bacterial Lipopolysaccharides, Has Phospholipase, Lysophospholipase, Diacylglycerolipase, and Acyltransferase Activities in Vitro." *The Journal of Biological Chemistry* 267 (14) (May 15): 10116–10121.
- Munford, R S, Sheppard, P O, and O'Hara, P J. 1995. "Saposin-like Proteins (SAPLIP) Carry Out Diverse Functions on a Common Backbone Structure." *Journal of Lipid Research* 36 (8) (August): 1653–1663.
- Mysliwy, J, Dingley, A J, Stanisak, M, Jung, S, Lorenzen, I, Roeder, T, Leippe, M, and Grötzinger, J. 2010. "Caenopore-5: The Three-dimensional Structure of an Antimicrobial Protein from *Caenorhabditis elegans*." *Developmental and Comparative Immunology* 34 (3) (March): 323–330.
- Müller, I, Subert, N, Otto, H, Herbst, R, Rühling, H, Maniak, M, and Leippe, M. 2005. "A *Dictyostelium* Mutant with Reduced Lysozyme Levels Compensates by Increased Phagocytic Activity." *The Journal of Biological Chemistry* 280 (11) (March 18): 10435–10443.
- Nassif, X, Fournier, J M, Arondel, J, and Sansonetti, P J. 1989. "Mucoid Phenotype of *Klebsiella pneumoniae* Is Virulence Factor Plasmid-Encoded" 12 (2): 546–552.

- Neuhaus, E M, Almers, W, and Soldati, T. 2002. "Morphology and Dynamics of the Endocytic Pathway in *Dictyostelium discoideum*" *Mol. Biol. Cell* 13 (April 4): 1390–1407.
- Nickel, R, Jacobs, T, and Leippe, M. 1998. "Molecular Characterization of an Exceptionally Acidic Lysozyme-like Protein from the Protozoan *Entamoeba histolytica*." *FEBS Letters* 437 (1-2) (October 16): 153–157.
- Nürnberg, T, Brunner, F, Kemmerling, B, and Piater, L. 2004. "Innate Immunity in Plants and Animals: Striking Similarities and Obvious Differences." *Immunological Reviews* 198 (April): 249–266.
- Okuwa, T, Katayama, T, Takano, A, Kodaira, K, and Yasukawa, H. 2001. "Two Cell-counting Factors Regulate the Aggregate Size of the Cellular Slime Mold *Dictyostelium discoideum*." *Development, Growth & Differentiation* 43 (6) (December): 735–744.
- Otvos, L. 2002. "The Short Proline-rich Antibacterial Peptide Family." *Cellular and Molecular Life Sciences: CMLS* 59 (7) (July): 1138–1150.
- Pang, K M, Lynes, M A, and Knecht, D A. 1999. "Variables Controlling the Expression Level of Exogenous Genes in *Dictyostelium*." *Plasmid* 41 (3) (May): 187–197.
- Park, C B, Kim, H S, and Kim, S C. 1998. "Mechanism of Action of the Antimicrobial Peptide Buforin II: Buforin II Kills Microorganisms by Penetrating the Cell Membrane and Inhibiting Cellular Functions." *Biochemical and Biophysical Research Communications* 244 (1) (March 6): 253–257.
- Parkinson, K, Bolourani, P, Traynor, D, Aldren, N L, Kay, R R, Weeks, G, and Thompson, C R. 2009. "Regulation of Rap1 Activity Is Required for Differential Adhesion, Cell-type Patterning and Morphogenesis in *Dictyostelium*." *Journal of Cell Science* 122 (Pt 3) (February 1): 335–344.
- Patrzykat, A, Friedrich, C L, Zhang, L, Mendoza, V, and Hancock, R E. 2002. "Sublethal Concentrations of Pleurocidin-Derived Antimicrobial Peptides Inhibit Macromolecular Synthesis in *Escherichia coli*" 46 (3): 605–614.
- Peschel, A, and Sahl, H G. 2006. "The Co-evolution of Host Cationic Antimicrobial Peptides and Microbial Resistance." *Nature Reviews. Microbiology* 4 (7) (July): 529–536.
- Podschun, R, and Ullmann, U. 1998. "*Klebsiella* Spp. as Nosocomial Pathogens: Epidemiology, Taxonomy, Typing Methods, and Pathogenicity Factors." *Clinical Microbiology Reviews* 11 (4) (October): 589–603.
- Ponting, C P. 1994. "Acid Sphingomyelinase Possesses a Domain Homologous to Its Activator Proteins: Saposins B and D." *Protein Science: a Publication of the Protein Society* 3 (2) (February): 359–361.

- Prager, E M. 1996. "Adaptive Evolution of Lysozyme: Changes in Amino Acid Sequence, Regulation of Expression and Gene Number." *EXS* 75 (January): 323–345.
- Pukatzki, S, Kessin, R H, and Mekalanos, J J. 2002. "The Human Pathogen *Pseudomonas aeruginosa* Utilizes Conserved Virulence Pathways to Infect the Social Amoeba *Dictyostelium discoideum*." *Proceedings of the National Academy of Sciences of the United States of America* 99 (5) (March 5): 3159–3164.
- Regué, M, Climent, N, Abitiu, N, Coderch, N, Merino, S, Izquierdo, L, Altarriba, M, and Tomás, J M. 2001. "Genetic Characterization of the *Klebsiella pneumoniae* Waa Gene Cluster, Involved in Core Lipopolysaccharide Biosynthesis." *Journal of Bacteriology* 183 (12) (June): 3564–3573.
- Reymond, C D, Nellen, W, Gomer, R H, and Firtel, R A. 1986. "Regulation of the *Dictyostelium* Ras Gene During Development and in Transformants." *Progress in Clinical and Biological Research* 217A (January): 17–21.
- Riedel, V, Gerisch, G, Müller, E, and Beua, H. 1973. "Regulation in Morphogenetic Mutants of *Dictyostelium discoideum*." *Journal of Molecular Biology* 74 (4) (March): 573–585.
- Riottot, MM, Fournier, J M, Jouin, H. 1981. "Direct Evidence for the Involvement of Capsular Polysaccharide in the Immuno Protective Activity of *Klebsiella pneumoniae* Ribosomal Preparations." *Infection and Immunity* 31 (1) (January): 71–77.
- Rupper, A, and Cardelli, J. 2001. "Regulation of Phagocytosis and Endo-phagosomal Trafficking Pathways in *Dictyostelium discoideum*." *Biochimica Et Biophysica Acta* 1525 (3) (March 15): 205–216.
- Sahl, H G, Jack, R W, and Bierbaum, G. 1995. "Biosynthesis and Biological Activities of Lantibiotics with Unique Post-translational Modifications." *European Journal of Biochemistry* 230 (3) (June 15): 827–853.
- Saito, K, Takahashi, N, Horiuchi, H, and Yamada, T. 2001. "Effects of Glucose on Formation of Cytotoxic End-products and Proteolytic Activity of *Prevotella intermedia*, *Prevotella nigrescens* and *Porphyromonas gingivalis*." *Journal of Periodontal Research* 36 (6) (December): 355–360.
- Schaap, P. 2011. "Evolutionary Crossroads in Developmental Biology: *Dictyostelium discoideum*." *Development (Cambridge, England)* 138 (3) (February): 387–396.
- Schlatterer, C, Knoll, G, and Malchow, D. 1992. "Intracellular Calcium During Chemotaxis of *Dictyostelium discoideum*: a New Fura-2 Derivative Avoids Sequestration of the Indicator and Allows Long-term Calcium Measurements." *European Journal of Cell Biology* 58 (1) (June): 172–181.

- Schägger, H, and von Jagow, G. 1987. "Tricine-sodium Dodecyl Sulfate-polyacrylamide Gel Electrophoresis for the Separation of Proteins in the Range from 1 to 100 kDa." *Analytical Biochemistry* 166 (2) (November 1): 368–379.
- Shi, J, Ross, C R, Chengappa, M M, Sylte, M J, McVey, D S, and Blecha, F. 1996. "Antibacterial Activity of a Synthetic Peptide (PR-26) Derived from PR-39, a Proline-arginine-rich Neutrophil Antimicrobial Peptide." *Antimicrobial Agents and Chemotherapy* 40 (1) (January): 115–121.
- Siegert, F, and C J Weijer. 1995. "Spiral and Concentric Waves Organize Multicellular *Dictyostelium* Mounds." *Current Biology: CB* 5 (8) (August 1): 937–943.
- Sieprawska-lupa, M, Mydel, P, Wójcik, K, Puklo, M, Lupa, B, Suder, P, Silberring, J, et al. 2004. "Degradation of Human Antimicrobial Peptide LL-37 by *Staphylococcus aureus* Degradation of Human Antimicrobial Peptide LL-37 by *Staphylococcus aureus*-Derived Proteinases."
- Sillo, A, Bloomfield, G, Balest, A, Balbo, A, Pergolizzi, B, Peracino, B, Skelton, J, Ivens, A, and Bozzaro, S. 2008. "Genome-wide Transcriptional Changes Induced by Phagocytosis or Growth on Bacteria in *Dictyostelium*." *BMC Genomics* 9 (January): 291.
- Solomon, J M, Rupper, A, Cardelli, J A, and Isberg, R R. 2000. "Intracellular Growth of *Legionella Pneumophila* in *Dictyostelium discoideum*, a System for Genetic Analysis of Host-pathogen Interactions." *Infection and Immunity* 68 (5) (May): 2939–2947.
- Sodergren E, Weinstock GM, Davidson EH, Cameron RA, Gibbs RA, Angerer RC, Angerer LM, Arnone MI, Burgess DR, Burke RD, Coffman JA, Dean M, Elphick MR, Etensohn CA, Foltz KR, Hamdoun A, Hynes RO, Klein WH, Marzluff W, McClay DR, Morris RL, Mushegian A, Rast JP, Smith LC, Thorndyke MC, Vacquier VD, Wessel GM, Wray G, Zhang L, Elisk CG, Ermolaeva O, Hlavina W, Hofmann G, Kitts P, Landrum MJ, Mackey AJ, Maglott D, Panopoulou G, Poustka AJ, Pruitt K, Sapojnikov V, Song X, Souvorov A, Solovyev V, Wei Z, Whittaker CA, Worley K, Durbin KJ, Shen Y, Fedrigo O, Garfield D, Haygood R, Primus A, Satija R, Severson T, Gonzalez-Garay ML, Jackson AR, Milosavljevic A, Tong M, Killian CE, Livingston BT, Wilt FH, Adams N, Bellé R, Carbonneau S, Cheung R, Cormier P, Cosson B, Croce J, Fernandez-Guerra A, Genevière AM, Goel M, Kelkar H, Morales J, Mulner-Lorillon O, Robertson AJ, Goldstone JV, Cole B, Epel D, Gold B, Hahn ME, Howard-Ashby M, Scally M, Stegeman JJ, Allgood EL, Cool J, Judkins KM, McCafferty SS, Musante AM, Obar RA, Rawson AP, Rossetti BJ, Gibbons IR, Hoffman MP, Leone A, Istrail S, Materna SC, Samanta MP, Stolc V, Tongprasit W, Tu Q, Bergeron KF, Brandhorst BP, Whittle J, Berney K, Bottjer DJ, Calestani C, Peterson K, Chow E, Yuan QA, Elhaik E, Graur D, Reese JT, Bosdet I, Heesun S, Marra MA, Schein J, Anderson MK, Brockton V, Buckley KM, Cohen AH, Fugmann SD, Hibino T, Loza-Coll M, Majeske AJ, Messier C, Nair SV, Pancer Z, Terwilliger DP, Agca C, Arboleda E, Chen N, Churcher AM, Hallböök F, Humphrey GW, Idris MM, Kiyama T, Liang S, Mellott D, Mu X, Murray G, Olinski RP, Raible F, Rowe M, Taylor JS, Tessmar-Raible K, Wang D, Wilson KH, Yaguchi S, Gaasterland T, Galindo BE, Gunaratne HJ, Juliano C, Kinukawa M,

- Moy GW, Neill AT, Nomura M, Raisch M, Reade A, Roux MM, Song JL, Su YH, Townley IK, Voronina E, Wong JL, Amore G, Branno M, Brown ER, Cavalieri V, Duboc V, Duloquin L, Flytzanis C, Gache C, Lapraz F, Lepage T, Locascio A, Martinez P, Matassi G, Matranga V, Range R, Rizzo F, Röttinger E, Beane W, Bradham C, Byrum C, Glenn T, Hussain S, Manning G, Miranda E, Thomason R, Walton K, Wikramanayake A, Wu SY, Xu R, Brown CT, Chen L, Gray RF, Lee PY, Nam J, Oliveri P, Smith J, Muzny D, Bell S, Chacko J, Cree A, Curry S, Davis C, Dinh H, Dugan-Rocha S, Fowler J, Gill R, Hamilton C, Hernandez J, Hines S, Hume J, Jackson L, Jolivet A, Kovar C, Lee S, Lewis L, Miner G, Morgan M, Nazareth LV, Okwuonu G, Parker D, Pu LL, Thorn R, Wright R. 2006. "Sea Urchin Genome Sequencing Consortium." *Science*. 314(5801) (November 10): 941-52.
- Stenger, S, Hanson, D A, Teitelbaum, R, Dewan, P, Niazi, K R, Froelich, C J, and Gan, T. 1998. "An Antimicrobial Activity of Cytolytic T Cells Mediated by Granulysin." *Science* 282 (5386) (October 2): 121–125.
- Sternfeld, J. 1998. "The Anterior-like Cells in Dictyostelium Are Required for the Elevation of the Spores During Culmination." *Development Genes and Evolution* 208 (9) (November): 487–494.
- Strassmann, J E, Gilbert, O M, and Queller, D C. 2011. "Kin Discrimination and Cooperation in Microbes." *Annual Review of Microbiology* 65 (January): 349–367.
- Su, X Z, Wu, Y, Sifri, C D, and Wellems, T E. 1996. "Reduced Extension Temperatures Required for PCR Amplification of Extremely A+T-rich DNA." *Nucleic Acids Research* 24 (8) (April 15): 1574–1575.
- Sultana, H, Neelakanta, G, Eichinger, L, Rivero, F, and Noegel, A A. 2009. "Microarray Phenotyping Places Cyclase Associated Protein CAP at the Crossroad of Signaling Pathways Reorganizing the Actin Cytoskeleton in *Dictyostelium*." *Experimental Cell Research* 315 (2) (January 15): 127–140.
- Sussman, M, and Schindler, J. 1978. "A New Class of Morphogenetic Mutants in *D. discoideum*, Alternate Morphogenetic Pathways Are Open to the Newly Formed Cell Aggregate: Either It Can Immediately Construct a Fruiting Body Directly at the Site of Aggregation or It Can Transform into a Mi" 116: 217–227.
- Thompson, A J, and Locarnini, S A. 2007. "Toll-like Receptors, RIG-I-like RNA Helicases and the Antiviral Innate Immune Response." *Immunology and Cell Biology* 85 (6): 435–445.
- Tjabringa, G S, Rabe, K F, and Hiemstra, P S. 2005. "The Human Cathelicidin LL-37: a Multifunctional Peptide Involved in Infection and Inflammation in the Lung." *Pulmonary Pharmacology & Therapeutics* 18 (5) (January): 321–327.
- Turvey, S E, and Broide, D H. 2010. "Innate Immunity." *The Journal of Allergy and Clinical Immunology* 125 (2 Suppl 2) (February): S24–32.

- Tydell, C C, Yuan, J, Tran, P, and Selsted, M E. 2006. "Bovine Peptidoglycan Recognition protein-S: Antimicrobial Activity, Localization, Secretion, and Binding Properties." *Journal of Immunology (Baltimore, Md.: 1950)* 176 (2) (January 15): 1154–1162.
- Vaccaro, A M, Salvioli, R, Tatti, M, and Ciaffoni, F. 1999. "Saposins and Their Interaction with Lipids." *Neurochemical Research* 24 (2) (February): 307–314.
- Vizioli, J and Salzet, M. 2002. "Antimicrobial Peptides from Animals: Focus on Invertebrates." *Trends in Pharmacological Sciences* 23 (11) (November): 494–496
- Wang, Y, Knoop, F C, Jouet, I R, Delarue, C, Vaudry, H, and Conlon, J M. 1998. "Antimicrobial Peptides of the Brevinin-2 Family Isolated from Gastric Tissue of the Frog, *Rana esculenta*." *Biochemical and Biophysical Research Communications* 253 (3) (December 30): 600–603.
- Wenger, D A, DeGala, G, Williams, C, Taylor, H A, Stevenson, R E, Pruitt, J R, Miller, J, Garen, P D, and Balentine, J D. 1989. "Clinical, Pathological, and Biochemical Studies on an Infantile Case of sulfatide/GM1 Activator Protein Deficiency." *American Journal of Medical Genetics* 33 (2) (June): 255–265.
- Williams, J G. 2006. "Transcriptional Regulation of *Dictyostelium* Pattern Formation." *EMBO Reports* 7 (7) (July): 694–698.
- Williams, J G. 2010. "*Dictyostelium* Finds New Roles to Model." *Genetics* 185 (3) (July): 717–726.
- Winau, F, Schwierzeck, V, Hurwitz, R, Rimmel, N, Sieling, P A, Modlin, R L, Porcelli, S A, et al. 2004. "Saposin C Is Required for Lipid Presentation by Human CD1b." *Nature Immunology* 5 (2) (February): 169–174.
- Yamada, Y, Kay, R R, Bloomfield, G, Ross, S, Ivens, A, and Williams, J G. 2010. "A New *Dictyostelium* Prestalk Cell Sub-type." *Developmental Biology* 339 (2) (March 15): 390–397.
- Zasloff, M. 2002. "Antimicrobial Peptides of Multicellular Organisms" *Nature* 415 (6870) (January): 389–395.
- Zhou, D, Cantu, C, Sagiv, Y, Schrantz, N, Kulkarni, A B, Qi, X, Mahuran, D J, et al. 2004. "Editing of CD1d-bound Lipid Antigens by Endosomal Lipid Transfer Proteins." *Science (New York, N.Y.)* 303 (5657) (January 23): 523–527.

8 APPENDIX

8.1 Identification of KO clones by PCR

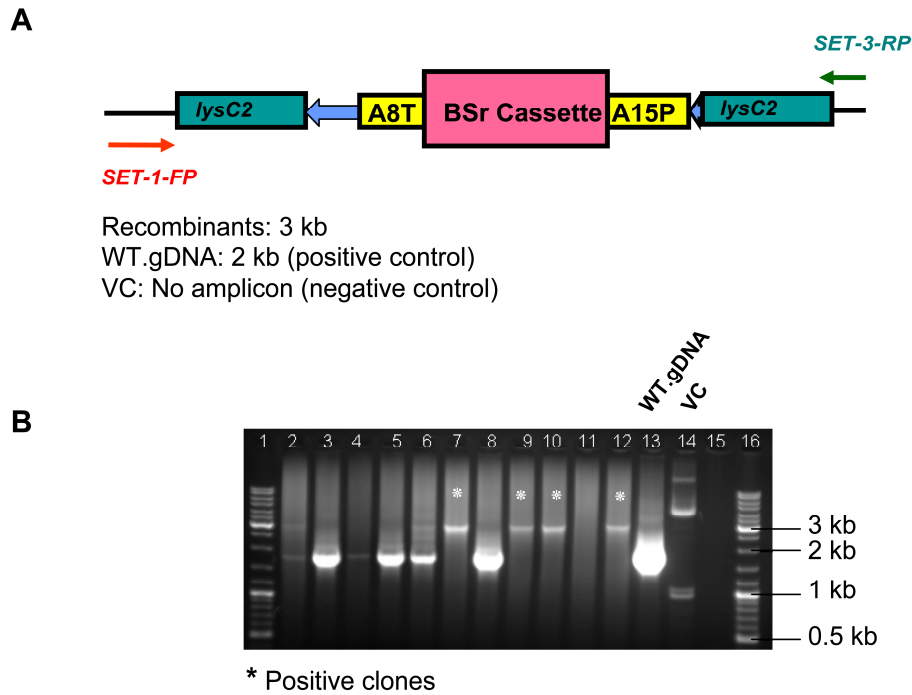


Fig. 41: *lysC2*⁻ identification by PCR analysis. **A)** After transfecting the *lysC2* gene targeting vector into Ax2 cells, the positive clones for recombination were selected by antibiotic selection, using Blasticidin (Bsr) and these positive clones were subjected to PCR scheme described above. **B)** Both the primers bind in regions outside the *lysC2* gene, therefore both Wild type (WT.gDNA) and the positive clones for *lysC2* ablation produce PCR amplicons, but of varying sizes. The amplicon generated by *lysC2* ablated clones were ~1 kb larger than the amplicon produced by WT. However, *lysC2* targeting vector used as vector control (VC) produced no amplicon. Among several clones examined, four clones were found to be positive for *lysC2* ablation (*).

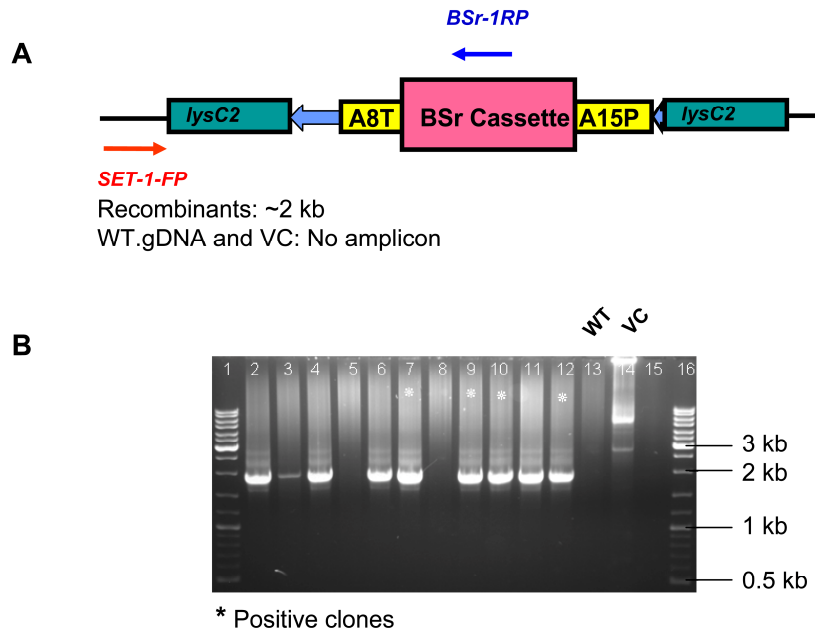


Fig. 42: *lysC2*⁻ analyses for Bsr cassette insertion **A)** *lysC2* ablation was also investigated for Bsr cassette insertion at required orientation in the *lysC2* gene of the Ax2 genome by performing the PCR scheme described above. **B)** With this primer combination only the recombinant clones generated PCR amplicons of size ~2 kb, whereas the WT and VC produced no amplicons. Positive clones for Bsr cassette insertion are marked (*).

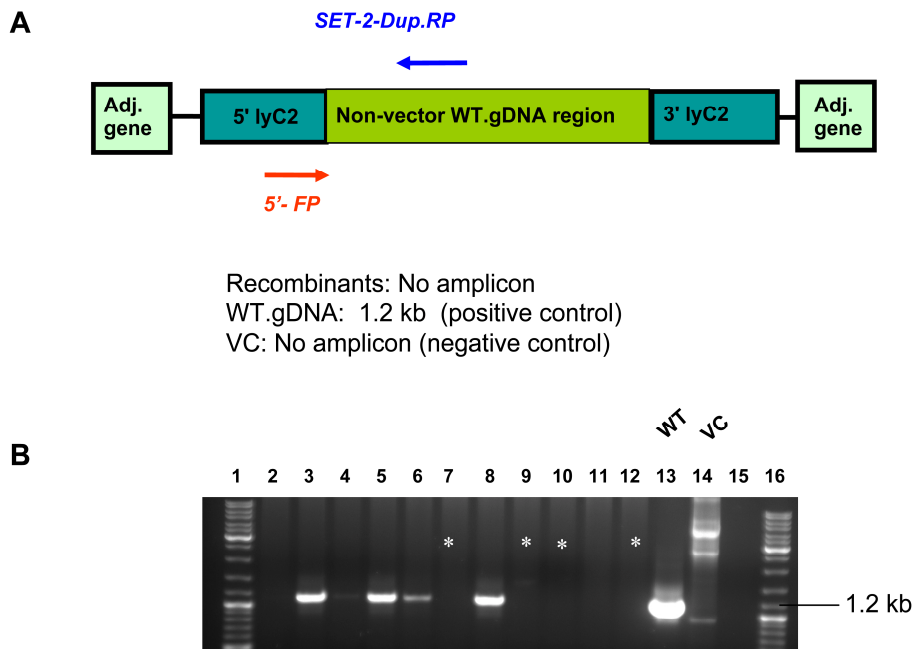


Fig. 43: *lysC2*⁻ analyses for WT contamination. **A)** All *lysC2*⁻ clones identified by earlier described PCR were examined for WT contamination. PCR scheme described above generated amplicon only with the WT *lysC2* gene, **B)** because the SET-2-Dup.RP (reverse primer) can bind only to the WT *lysC2*. The recombinant clones for *lysC2* and VC generated no amplicons. Positive clones for *lysC2* ablation are denoted by asterisks (*).

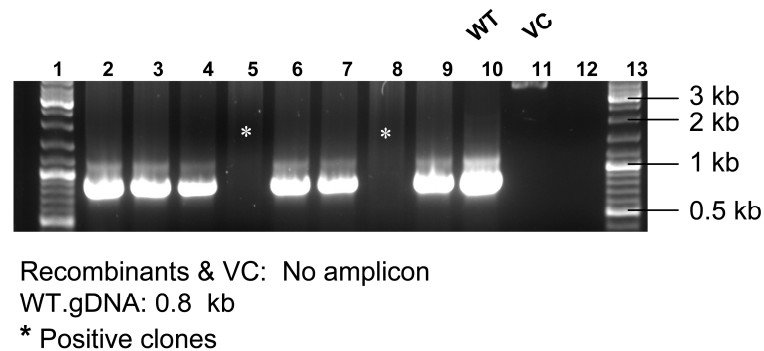
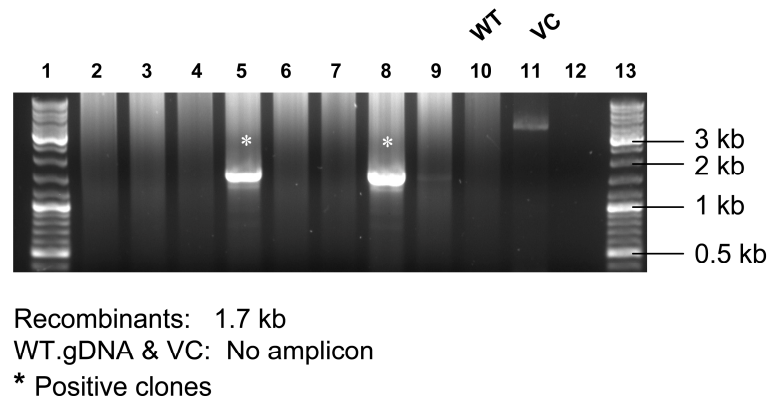


Fig. 44: Identification of *lyC3* ablation. **Top panel:** PCR scheme followed for analysing Bsr cassette insertion with *lyC2*⁻ (Fig. 42) was also followed to analyse *lyC3*⁻. WT and VC were used as negative controls to confirm Bsr cassette insertion in the recombinant clones that generated 1.7 kb amplicons (*). **Bottom panel:** Further these positive clones for *lyC3*⁻ ablation was analysed for WT contamination. WT was used as positive control and VC was used as negative control to verify the *lyC3*⁻ clones for their homogeneity.

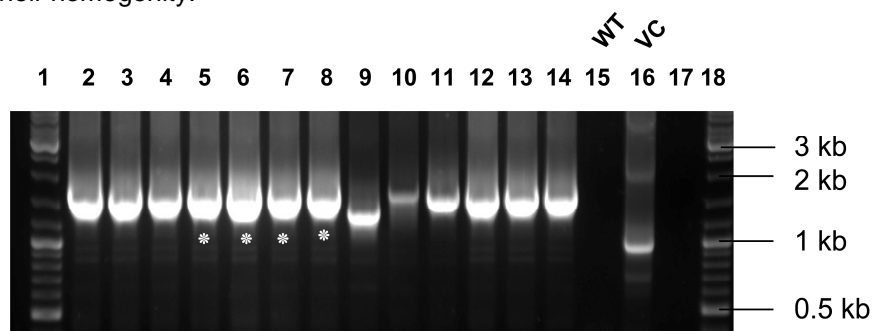


Fig. 45: Identification of *aplJ* ablation. *AplJ*⁻ clones were analysed for Bsr cassette insertion by performing the PCR scheme described earlier to analyse the Bsr cassette insertion. Among clones analysed for *aplJ* ablation many were positive for recombination at *aplJ* locus for the insertion of *aplJ* targeting vector, only those clones marked (*) were free of any WT contamination.

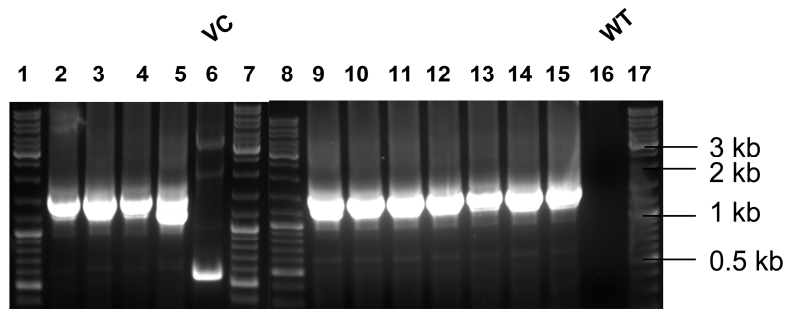


Fig. 46: Identification of *apIP* ablation. *ApIP*⁻ clones analysed for Bsr cassette insertion showed many clones that were positive for *apIP* ablation. Further these clones were also analysed for PCR that confirmed clones that were free of WT contamination (data not shown)

8.2 Intracellular localisation of ApID-FLAG fusion protein

As mentioned earlier, a strain that produces ApID-FLAG fusion protein in *apID*⁻ background was generated [*apID*⁻ (+)] and ApID-FLAG protein production in this strain was confirmed by western blot analyses (**Fig. 35**). These clones were subjected to immunofluorescence microscopy to identify the intracellular localisation of ApID-FLAG protein. The confocal microscopic images obtained for ApID-FLAG protein and vacuolin staining is shown below. Sequential staining of ApID-FLAG and vacuolin (post-lysosomal marker) was performed to analyse whether ApID-FLAG colocalises with vacuolin. As the Primary antibodies against ApID-FLAG and vacuolin were from mouse, corresponding controls experiments were also performed in parallel to confirm the absence of false positive results due to cross reaction between the secondary antibodies.

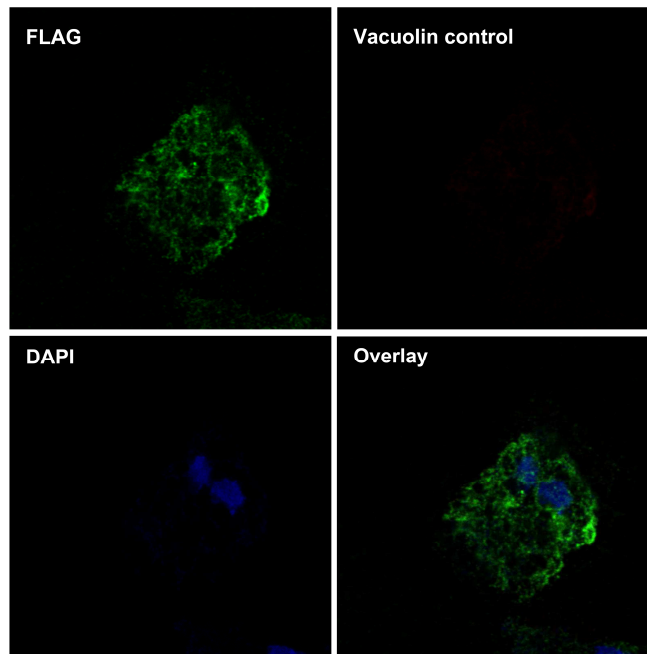
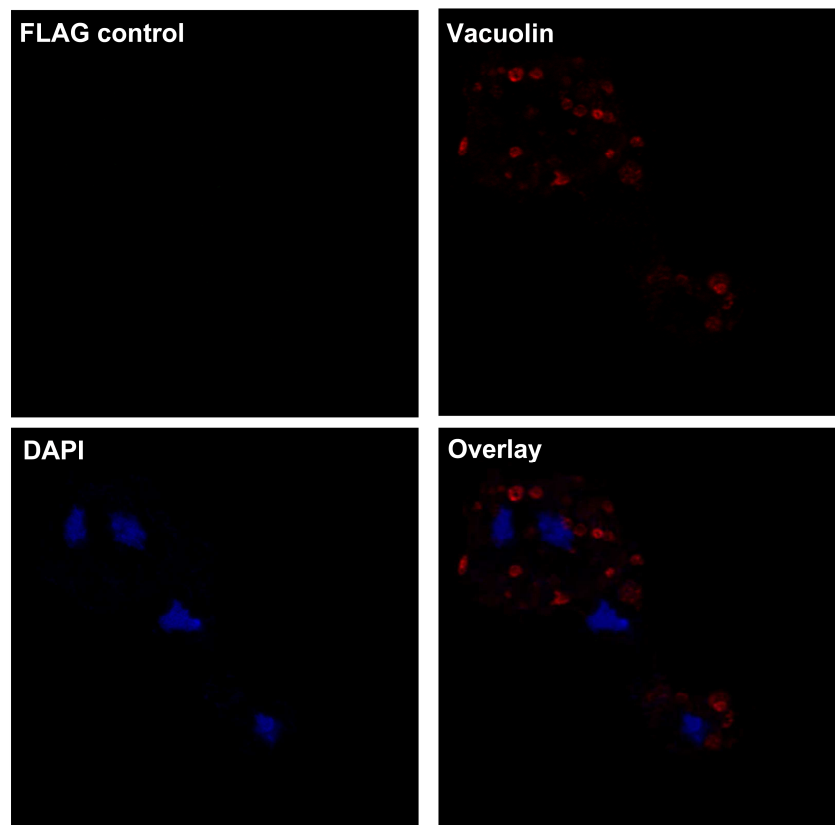


Fig. 46: ApID-FLAG staining. The details of each panel are described at the top of all images. Top left panel (vacuolin control) confirms that there is no cross reaction between antibodies. The image shown was obtained from a *apID*⁻ (+) amoeba exposed to primary antibody for ApID-FLAG (mouse anti-FLAG), secondary antibody against FLAG (anti-mouse-IgG, green) and then exposed to another secondary antibody (anti-mouse-IgG, red) is shown. The second secondary antibody (anti-mouse, red) is the one used for staining vacuolin in the double staining immunofluorescence methods. Similar staining was also performed for vacuolin and the results obtained are shown below



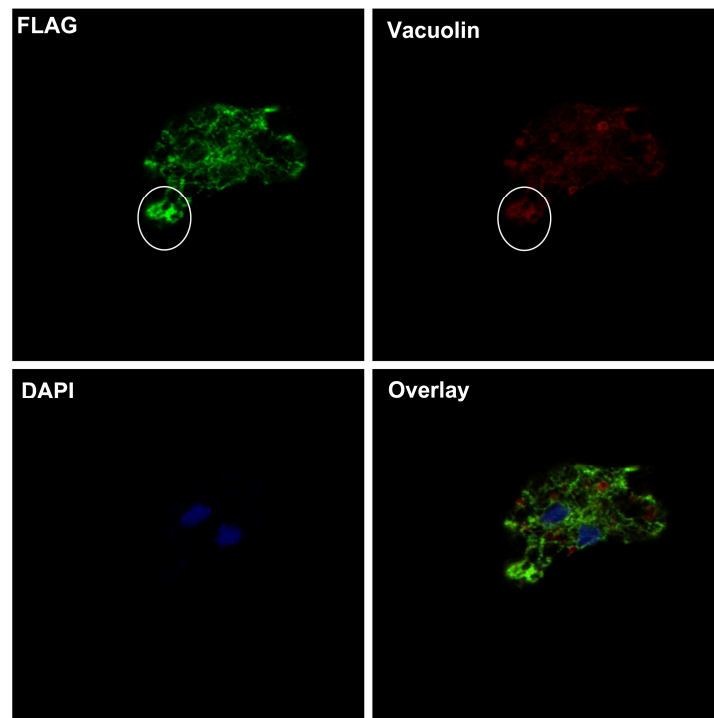


Fig. 47: ApID-FLAG and vacuolin sequential staining. An *apID*⁻ (+) amoeba stained for ApID-FLAG (green) and vacuolin (red) is shown. The region of ApID-FLAG (green) and vacuolin (red) colocalisation is marked by circles.

Declaration

I hereby declare that, the work reported in this thesis titled “Molecular Characterisation of Antimicrobial Arsenal of *Dictyostelium discoideum*” is the result of investigations carried out by me at the Zoological Institute, Christian Albrechts University of Kiel, Germany, under the guidance of Prof. Dr. Matthias Leippe. I further declare that this work has not formed the basis for the award of any degree, diploma or fellowship in any other Institution.

Kiel, October 2011

Ranjani Dhakshinamoorthy

Date, Signature

Acknowledgements

I am extremely grateful to my Doctoral father, Prof. Dr. Matthias Leippe, for giving me an opportunity to carry out my doctoral research in his laboratory. I would like to thank him also for his valuable suggestions and ideas. I thank Dr. Thierry Soldati (University of Geneva, Switzerland) for his suggestions and for teaching me the *D. discoideum* gene ablation technique and for providing space in his laboratory for the same work. I would like to thank Prof. Dr. Pierre Cosson (University of Geneva, Switzerland) for teaching me the growth and killing assays. I would thank Prof. Dr. Angelika A. Noegel (University of Cologne) and Prof. Dr. Markus Maniak (Universität Kassel, Germany) for providing me the antibodies for immunofluorescence microscopy. I would extend my thanks also for providing us the bacterial strains as a kind gift. I wish to thank Prof. Dr. Thomas Roeder for allowing me to use his laboratory equipments during the course of my PhD. research. I greatly appreciate Dr. Christoph Gelhaus for providing me insights about the antimicrobial protein related information of *D. discoideum*. I would like to thank Dr. Christine Desel for helping me with confocal microscopy. I am grateful to Dr. Henning Fedders for his constant scientific and moral support and for his intriguing questions about my experiments. I am grateful to Dr. Monica Hagedorn for her suggestions for my immunofluorescence microscopy experiments. I would like to extend my gratitude to Dr. Huajiang Xiong for proof reading my Thesis and for her generous support. I would like to thank Heidrun Wegner for making all my official work very smooth and at right time. Special thanks to Heidrun Liesegang for her courteous and clever technical support during all my experiments. I am thankful to Stephanie Neunzig for her technical support to characterize the *D. discoideum* knock-out clones. I extend my thanks to Christiane Sandberg for her technical supports whenever possible. I am grateful to Miriam (Thierry Soldati's student) for teaching me the knock-out clones isolation and Margot (Monica's student) for her contribution in immunofluorescence microscopy. I would like to thank my colleagues Silja, Saskia, Aylin, Stephan, Moritz, Tasja, Ahmed, Flora, Tinky, Renja, Julia, and Li for all their scientific support, general guidance and for making the laboratory environment pleasant both, for research and fun throughout the course of my Doctoral Thesis. I would like to render my soulful thanks to my parents, Mr. P. Dhakshinamoorthy and Mrs. D. Neela, my sisters,

Malini, Deepa and my brother, Saravana Kumar for their encouragement and constant support throughout my PhD. work and personal life. I would like to thank my in-laws for their patience and support. I would like to thank my Husband, Arunkumar for his patience and being the source of energy during the end of my Doctoral thesis. Beyond all, I would like to extend my whole hearted thanks to *Dictyostelium discoideum* for cooperating and reciprocating my scientific thirst. Last but not least I would like to surrender myself and thank Nature for its love and care for me.

Biodata

Name: Ranjani Dhakshinamoorthy

Date of Birth: 04.12.1981

Birth place: Tamilnadu

Marital status: Married

Country: India

Doctoral study:	03/2008 – at present	Christian Albrechts University of Kiel Dept. of Zoologie, Zoophysiology, c/o Prof. Dr. Matthias Leippe
Research and Development Assistant	04/2006 – 02/2008	Jawaharlal Nehru Centre for Advanced Scientific Research (JNCASR) c/o Prof. V. Nanjundiah, MRDG, Indian Institute of Science
Teaching Assistant	08/2004 – 03/2006	Madurai Kamaraj University, School of Biological Sciences, c/o Dr. G. S. Selvam
Master's degree:	04/2002 – 04/2004	MSc. Biochemical technology, Madurai Kamaraj University, School of biological sciences, c/o Prof. C. Rajamanickam
Bachelor's degree	04/1997 – 03/2002	BSc. Microbiology, Shrimathi Indira Gandhi College
School	1991 – 1997	Boiler Plant Girls Higher Secondary School
	1984 – 1991	RSK Primary School